Chapter 13

GEOTECHNICAL SEISMIC HAZARDS

FINAL

SCDOT GEOTECHNICAL DESIGN MANUAL

June 2010

Table of Contents

List of Tables

List of Figures

CHAPTER 13

GEOTECHNICAL SEISMIC HAZARDS

13.1 INTRODUCTION

The screening, identification, and evaluation of geotechnical seismic hazards at a project site are an integral part of geotechnical earthquake engineering. The effects of these hazards must be taken into consideration during the design of geotechnical structures such as bridge foundations, retaining walls, and roadway embankments. Geotechnical seismic hazards can generally be divided into those that are associated with losses in soil shear strength and stiffness, seismic ground shaking (i.e. accelerations), and seismic induced lateral ground movements and settlement. Losses in the soil shear strength in South Carolina are primarily due to cyclic liquefaction of loose cohesionless soils and secondarily due to cyclic softening of cohesive soils. Seismic accelerations can create instability due to increased driving forces as a result of increased static active soil pressures. Seismic induced lateral ground movement can occur in sloping ground conditions where the increased driving forces exceed the soil shear strength. Seismic settlement can be either the result of cyclic liquefaction of cohesionless soils, densification/compression of unsaturated soils, or compacted fill materials.

The procedures for analyzing soil Shear Strength Loss (SSL) and associated geotechnical seismic hazards such as flow slide failure, lateral spread, and seismic slope instability are provided in this Chapter. Methods of computing horizontal seismic accelerations based on peak horizontal ground accelerations (PHGA = PGA) and seismic displacements are also provided in this Chapter. Methods of computing seismic active and passive soil pressures on earth retaining structures (ERS) are provided in Chapter 14. Procedures for evaluating seismic settlement due to either cyclic liquefaction or densification/compression of unsaturated soils are presented in this Chapter.

SCDOT recognizes that the methods presented in this Manual may not be the only methods available, particularly since geotechnical earthquake engineering is developing at a very rapid pace as earthquakes around the world contribute to the study and enhancement of analytical methods for geotechnical seismic hazard evaluation. Because geotechnical earthquake engineering in South Carolina (and CEUS) is at the very early stages of development, the overall goal of this Chapter is to establish a state-of-practice that can evolve and be enhanced as methodologies improve and regional (CEUS) experience develops. Methods other than those indicated in this Manual may be brought to the attention of the Pre-construction Support - Geotechnical Design Section (PCS/GDS) for consideration on a specific project or for consideration in future updates of this Manual.

Geotechnical seismic hazards such as fault rupturing and flooding (tsunami, seiche, etc.) are not addressed in this Chapter since current views suggest that the potential for these types of hazards in the Eastern United States is very low. If there is any evidence of faults traversing a project site that have been active within the Holocene epoch (10 thousand years ago to present day) it should be brought to the attention of the PCS/GDS.

South Carolina geology and seismicity, discussed in Chapter 11, will have a major impact on the evaluation of soil SSL and should be well understood when evaluating geotechnical seismic hazards. Earthquake shaking parameters will have a direct effect on the magnitude and extent of the deformations caused by geotechnical seismic hazards. Earthquake shaking parameters such as the moment magnitude (M_W), site-to-source distance (R), duration (D), and peak horizontal ground accelerations (PGHA or PGA) must be determined based on the design earthquake (FEE or SEE) under evaluation as described in Chapter 12. Geotechnical seismic hazards that may affect the design of transportation structures are described in the following Sections and analytical methods are presented to evaluate their potential and magnitude. The effects of geotechnical seismic hazards on the geotechnical design of bridge foundations, abutment walls, earth retaining systems, and other miscellaneous structures are discussed in Chapter 14.

13.2 GEOTECHNICAL SEISMIC HAZARD FAILURE MODES

In order to evaluate the potential for the various geotechnical seismic hazards at a project site, it is important to understand the various modes of failure that have been documented through case histories. Geotechnical seismic hazard modes of failure can be generally categorized as: Global Hazards, Localized Hazards, or Seismic Acceleration Hazards. These geotechnical seismic hazard categories are discussed in the following Sections.

13.2.1 Global Hazards

Global hazards are those failures that result in large-scale site instability in the form of translational/rotational instability and/or flow sliding. These hazards may begin as translational/rotational instability and then trigger a flow slide. Displacements associated with global hazards are the result of soil SSL combined with seismic inertial and/or gravitational driving forces. Displacements associated with translational/rotational instability can be the result of any of the following three instability cases that have also been summarized in Table 13-1.

Case 1. Instability due to soil SSL and static gravitational driving forces (Post-Earthquake condition).

Case 2. Instability due to soil SSL, static gravitational driving forces, and seismic inertial driving forces.

Case 3. Instability due to static gravitational driving forces and seismic inertial driving forces with no loss in soil shear strength

Table 13-1, Global Hazard Instability Cases

Contributors to Instability	Instability Types		
	Case 1	**Case 2**	**Case 3**
Soil SSL	X	X	
Static Gravitational Driving Forces	X	X	X
Seismic Inertial Driving Forces		X	X

A common example of Case 1 instability is a flow slide failure that occurs after the earthquake (post-earthquake). Flow slide failures are the most catastrophic form of ground failures. Sites susceptible to flow failure typically have ground slopes greater than 5 percent grade and are continuous over large areas of soils that are contractive and susceptible to cyclic liquefaction (Section 13.6.1 – Sand-Like Soil). These failures result from post-earthquake instability when the soil shear strength resisting force required for post-earthquake static equilibrium of the soil mass is less than the static gravitational driving force. Flow slide failure is typically confirmed by screening for contractive soils that are susceptible to soil SSL, evaluating triggering of soil SSL, and then evaluating instability by using conventional limit-equilibrium static slope stability methods.

Lateral spread is an example of Case 2 instability that results in lateral ground displacements. Lateral spread typically occurs on gently sloping sites (< 5 degrees) where large blocks of soil displace towards the free-face of a channel or incised river. The displacements result from losses in soil shear strength due to cyclic liquefaction of cohesionless soils combined with static shear stresses and inertial forces induced by the earthquake. Large displacements up to 30 feet have been reported from case studies. Lateral spread can damage bridge foundations and utilities that are located on or across the failure path. Bridge foundations and abutments are particularly susceptible to damage because of their location being near the free-face of a water-way boundary and consequently the large soil pressure loads from the displaced soil mass are applied to the bridge structure and foundation components.

Cases 2 and 3 are typically seismic instability failures that are characterized by translational or rotational slope failure that occurs during earthquake shaking. Translational/rotational instability are typically evaluated by screening for soils susceptible to SSL, evaluating triggering of soil SSL (if applicable), and evaluating instability by using conventional limit-equilibrium pseudo-seismic slope stability methods with appropriate soil shear strengths (accounting for soil SSL) and seismic acceleration coefficients. Deformations are typically evaluated by using Newmark's rigid sliding block displacements methods.

13.2.2 Localized Hazards

Localized hazards include those hazards that occur in isolated areas of failure such as loss of foundation capacity, excessive ground settlement, and lateral displacements.

Foundation capacity failure is the result of SSL of the soils that support either shallow or deep foundations. Shallow foundations are susceptible to bearing capacity failure. Deep foundations are susceptible to vertical foundation movements due to reduced pile capacity to support the structure loads plus any downdrag loads, lateral movements due to loss of lateral support, and pile damage from displacement induced stresses. These hazards are typically evaluated by screening for soils susceptible to soil SSL and using the residual soil shear strengths to compute the resulting margin of safety and estimate the performance of the structure.

Ground settlement is due to volumetric strain (consolidation) (Section 13.18) that results from the earthquake shaking. The settlement can be due to either seismic densification/compression of unsaturated soils or fills and/or seismic consolidation resulting from excess pore water pressure relief of cohesionless soils that have undergone cyclic liquefaction. There may be ground surface manifestations in the form of sand-boils as excess pore water pressure dissipates to the ground surface during cyclic liquefaction. Alternatively, water may get trapped

under non-liquefiable capping soil layers above the cyclic liquefiable soils that will affect the rate of soil subsidence and may trigger other hazards due to loss in soil shear strength at these interfaces.

Localized lateral ground displacements can be the result of ground oscillation. Ground oscillation generally occurs on level ground with liquefied soils at a depth that causes a de-coupling of the soils from the ground surface to the top of the liquefied soils. The de-coupling of the surface soils allows permanent displacements at the ground surface that are usually small and disordered in magnitude and direction. Cyclic liquefaction of the subsurface cohesionless soils has been linked to larger amplitude oscillations that in-turn affect the spectral response accelerations used for design by increasing the spectral accelerations for periods greater than one second (Youd and Carter, 2005). `

13.2.3 Seismic Acceleration Hazards

ERSs such as bridge abutments, gravity walls, cantilever walls, etc. (Chapter 18) are the most susceptible to damage resulting from seismic accelerations that induce inertial loads. Seismic inertial loads can cause damage to the structure as described below:

1. Static active earth pressures plus seismic inertial loads can increase lateral earth pressures on ERSs which can result in failure due to deformations that exceed the performance limits or structural capacity of the ERS. Failure may manifest itself in the form of lateral translations, rotations, overturning, or structural failure. Failure of tie-back systems may jeopardize the integrity of the whole structure. Increased bearing loads at the toe of shallow foundations may exceed the bearing capacity of the soil causing rotational displacement or bearing failure.

2. Static passive earth pressure resistance to lateral loads can be reduced due to seismic inertial loads that can result in failure of the ERS by allowing forces from either seismic active soil pressures or inertial forces from the structure to cause large translational displacements.

3. Global limit-equilibrium instability of the structure resulting in rotational or translational deformations that may exceed the ERS performance limits or structural capacity.

13.3 GEOTECHNICAL SEISMIC HAZARD EVALUATION PROCESS

The effects of geotechnical seismic hazards must be considered in the design of all bridges, ERSs, roadway embankments, and other transportation structures where poor performance could endanger the lives and safety of the traveling public. The effectiveness of state highways in South Carolina depends on proper evaluation of the geotechnical seismic hazard and design to meet the performance requirements established in Chapter 10 for bridges, roadway embankments, ERSs and other transportation structures.

The geotechnical seismic hazard evaluation begins with an evaluation of the earthquake shaking parameters that are used to define the intensity and duration of the earthquake at the project site. A summary of the earthquake shaking parameters that will be used during the geotechnical seismic hazard evaluation is presented in Section 13.3.1. The geotechnical seismic hazard evaluation process then proceeds to the screening and identifying of the

subsurface soils that have the potential to experience soil SSL. The soil SSL evaluation process is presented in Section 13.3.2. Once the potential for soil SSL has been identified, the potential failure modes of the geotechnical seismic hazards presented in Section 13.2 can be evaluated. For purposes of evaluating the different geotechnical seismic hazard failure modes, the site conditions of *level ground sites* (or gentle sloping, < 5 degrees) and *steeply sloped ground sites* (≥ 5 degrees) are used. Detailed criteria for defining *level ground sites* and *steeply sloped ground sites* are provided in Sections 13.7 and 13.9, respectively.

The effects of the geotechnical seismic hazards on the stability and performance of project sites, embankments and slopes are addressed in this Chapter. The seismic design of bridge foundations, bridge abutments, and ERSs is addressed in Chapter 14.

Provided in Figure 13-1 is a flow chart of the overall geotechnical seismic hazard evaluation process described previously. The processes presented in this Manual are meant to serve as a guide in the evaluation and assessment of geotechnical seismic hazards. It is by no means the only approach that can be used; as a minimum, it should serve as a point of reference to understanding the layout of the following Sections in this Chapter.

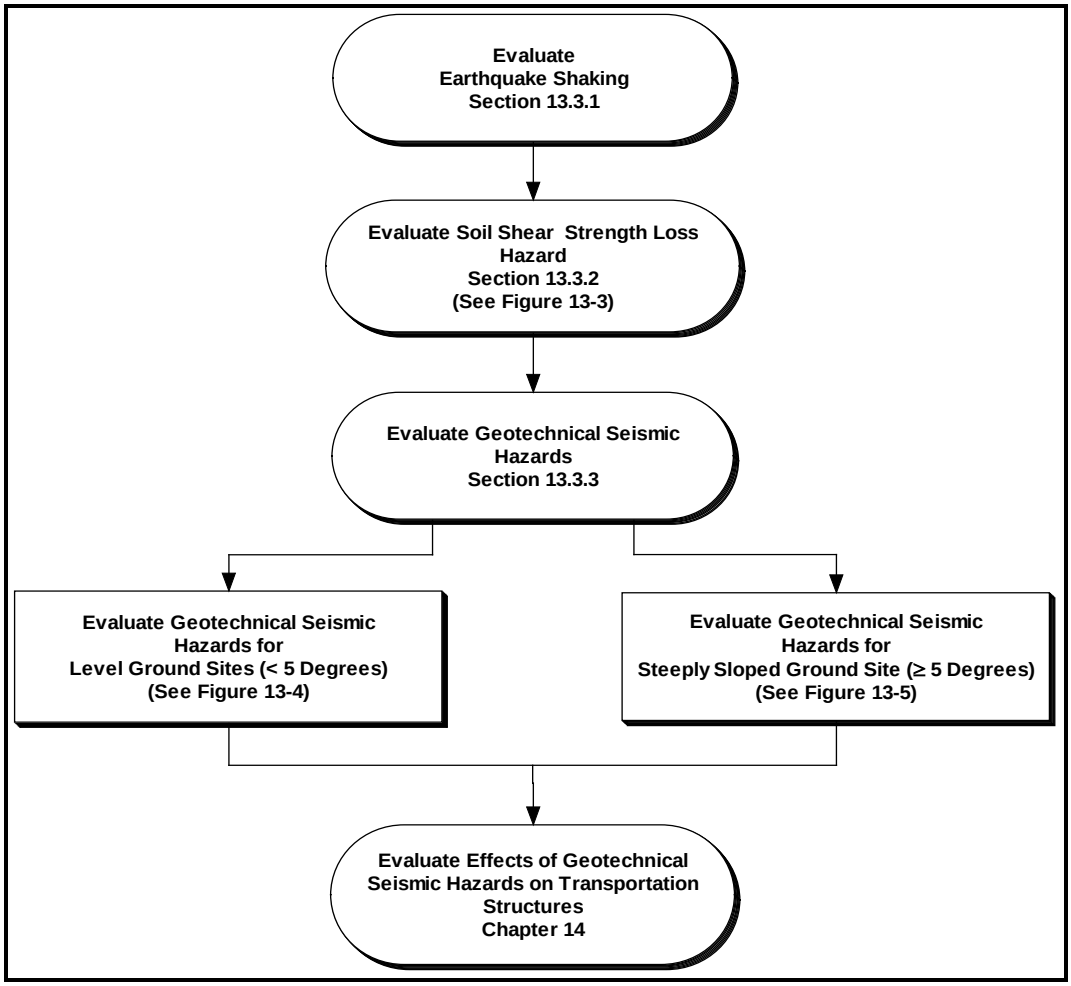

Figure 13-1, Geotechnical Seismic Hazard Evaluation Process

13.3.1 Earthquake Shaking Evaluation Process

Geotechnical seismic hazards are triggered by the intensity and duration of the earthquake shaking at the project site. The intensity and duration of the earthquake shaking is primarily dependent on the size and location of the earthquake and the characteristics of the site. Chapter 12 - Geotechnical Earthquake Engineering provides the methodology for the assessment of the earthquake shaking at a project site. The earthquake shaking can be quantitatively assessed by the moment magnitude of the earthquake (M_W), site-to-source distance (R), peak horizontal ground acceleration at the ground surface (PHGA = PGA), the duration of the earthquake (D), and design spectral acceleration at 1 second (S_{D1}). The level of shaking at the project site is directly proportional to the potential for geotechnical seismic hazard damage. Project sites that are closer to the earthquake source experience higher levels of shaking; therefore, more damage can occur from geotechnical seismic hazards when compared to project sites further away.

13.3.2 Soil Shear Strength Loss Hazard Evaluation Process

Soil SSL that is induced by the earthquake shaking can produce severe damage as a result of the various geotechnical seismic hazard failure mechanisms as described in Section 13.2. The soil SSL hazard evaluation process has three components: (1) Evaluating soil SSL susceptibility at the project site; (2) Evaluating soil SSL triggering potential of the earthquake shaking; and (3) Evaluating the effects of soil SSL on the design parameters used to evaluate the geotechnical seismic hazard.

The soil SSL evaluation process begins with the screening for soils that are susceptible to soil SSL for the design earthquake (FEE or SEE) under evaluation. The screening criteria (Section 13.6) consist of three soil categories that are susceptible to soil SSL: Sand-Like soils, Normally Sensitive (NS) Clay-Like soils, and Highly Sensitive (HS) Clay-Like soils. The screening criteria uses standard laboratory soil shear strength testing, in-situ testing, index testing, and site conditions (i.e. water table) to determine if soils are susceptible to SSL. If soils are found not to be susceptible to soil SSL during the screening process, then no further analysis is required of the triggering of soil SSL and an evaluation of geotechnical seismic hazard evaluation can proceed.

The main contributor to catastrophic damage and poor performance of structures has in past case histories been attributed to cyclic liquefaction-induced seismic geotechnical hazards shown in Figure 13-2. Soil SSL due to cyclic liquefaction of Sand-Like soils (Section 13.6.1) has the potential to cause the most damage in the Coastal Plain of South Carolina as evident from the historical cyclic liquefaction case histories presented in Section 13.5.3.

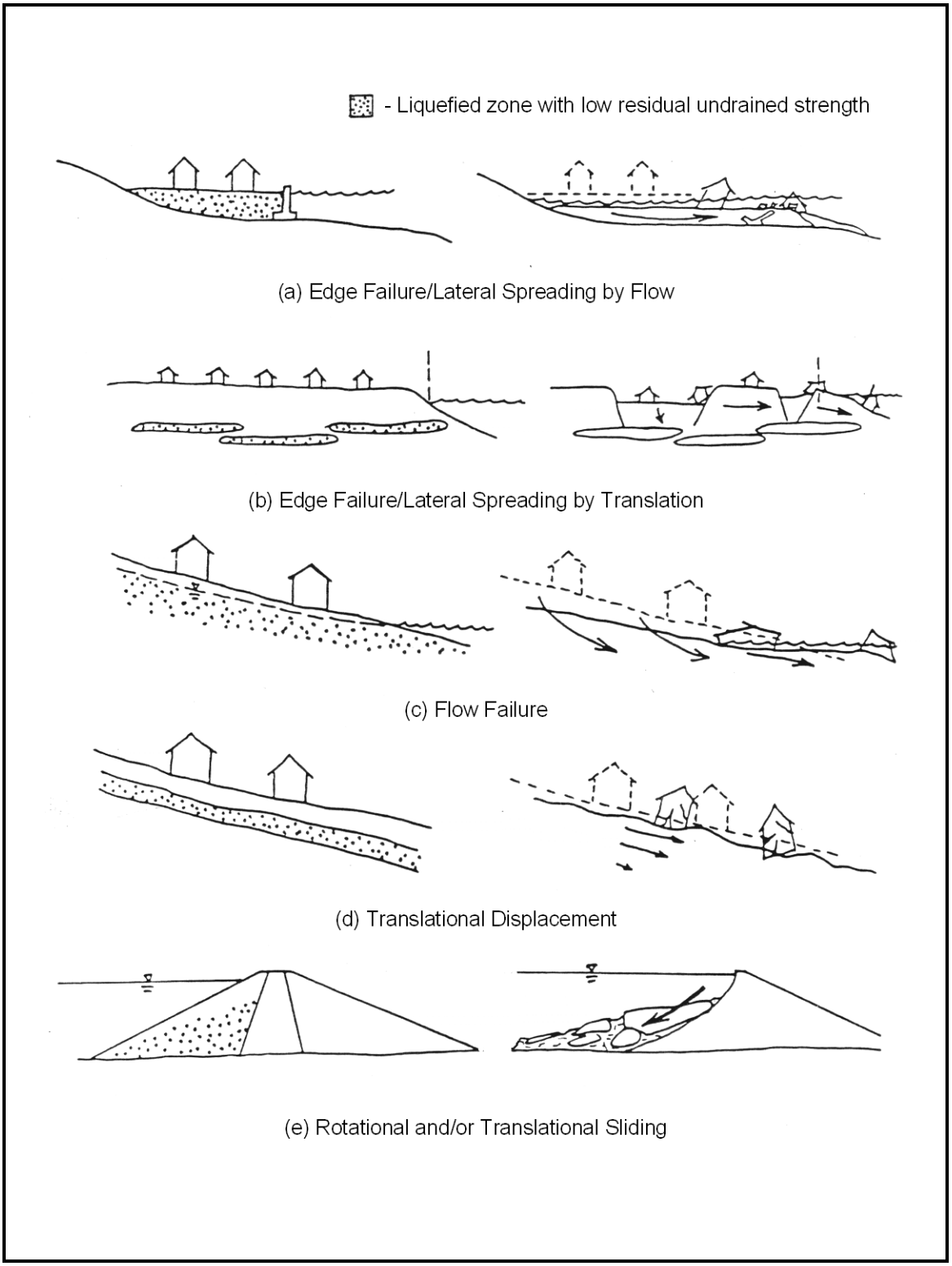

Figure 13-2, Cyclic Liquefaction-Induced Seismic Geotechnical Hazards (Seed et al., 2003)

Soils that are identified as being susceptible to losses in soil shear strength need to be evaluated to determine if the earthquake shaking can trigger (or initiate) the soil SSL. Soil SSL triggering for Sand-Like soils and Clay-Like soils is dependent on the site conditions of level ground or steeply sloped ground. The soil SSL triggering of Clay-Like soils is applicable to both NS Clay-Like soils and HS Clay-Like soils. The overall method for analyzing the triggering of soil SSL for Sand-Like soils and Clay-Like soils consists of determining if the cyclic stresses induced by design earthquake (FEE or SEE) and any initial static shear stresses in the soil (Demand, D) are greater than the soil's cyclic resistance (Capacity, C) based on a specified margin of safety (on-set of soil SSL resistance factor, φ_{SL}). If the soil SSL resistance ratio, $(D/C)_{SL}$, is greater than φ_{SL}, the soil under evaluation has the potential for soil SSL and a reduced shear strength should be used in the evaluation of geotechnical seismic hazards.

The triggering of soil SSL at *Level Ground Sites* (or gently sloping, < 5 degrees) is based on an evaluation of the cyclic stress ratio (CSR = Demand) and the cyclic resistance ratio (CRR = Capacity) of the soils as described in Section 13.7. These sites are assumed to have no initial static shear stresses (τ_{Static}) that would reduce the soil's cyclic resistance capacity (C).

The triggering of soil SSL at *Steeply Sloped Ground Sites* (≥ 5 degrees) is more complex because the initial static shear stress (τ_{Static}) reduces the soil's capacity (C) to resist the soil SSL. The triggering of soil SSL at steeply sloped ground sites consists of first screening for flow failure as described in Section 13.8. If the screening indicates that the soil is contractive and flow failure resistance ratio, $(D/C)_{Flow}$ is greater than φ_{Flow}, then a soil SSL triggering analysis is required as described in Section 13.9. If screening indicates that the site does not have the potential for flow failure within a margin of safety (on-set of flow failure resistance factor, φ_{Flow}) then a soil SSL triggering analysis is not required and soil SSL is less likely to happen. The triggering of soil SSL in Clay-Like soils (NS and HS) can also occur in steeply sloped ground sites due to an increase in static shear stresses that occurs when Sand-Like soils experience cyclic liquefaction. Soil SSL in NS Clay-Like soils causes the soils to have cyclic softening residual shear strength (τ_{rs}) and in HS Clay-Like soils causes the soils to have remolded soil shear strength ($\tau_{remolded}$).

The selection of soil shear strength properties for soils with and without the potential for soil SSL is performed during the geotechnical seismic hazard evaluation. The overall process for evaluating soil SSL is shown in Figure 13-3.

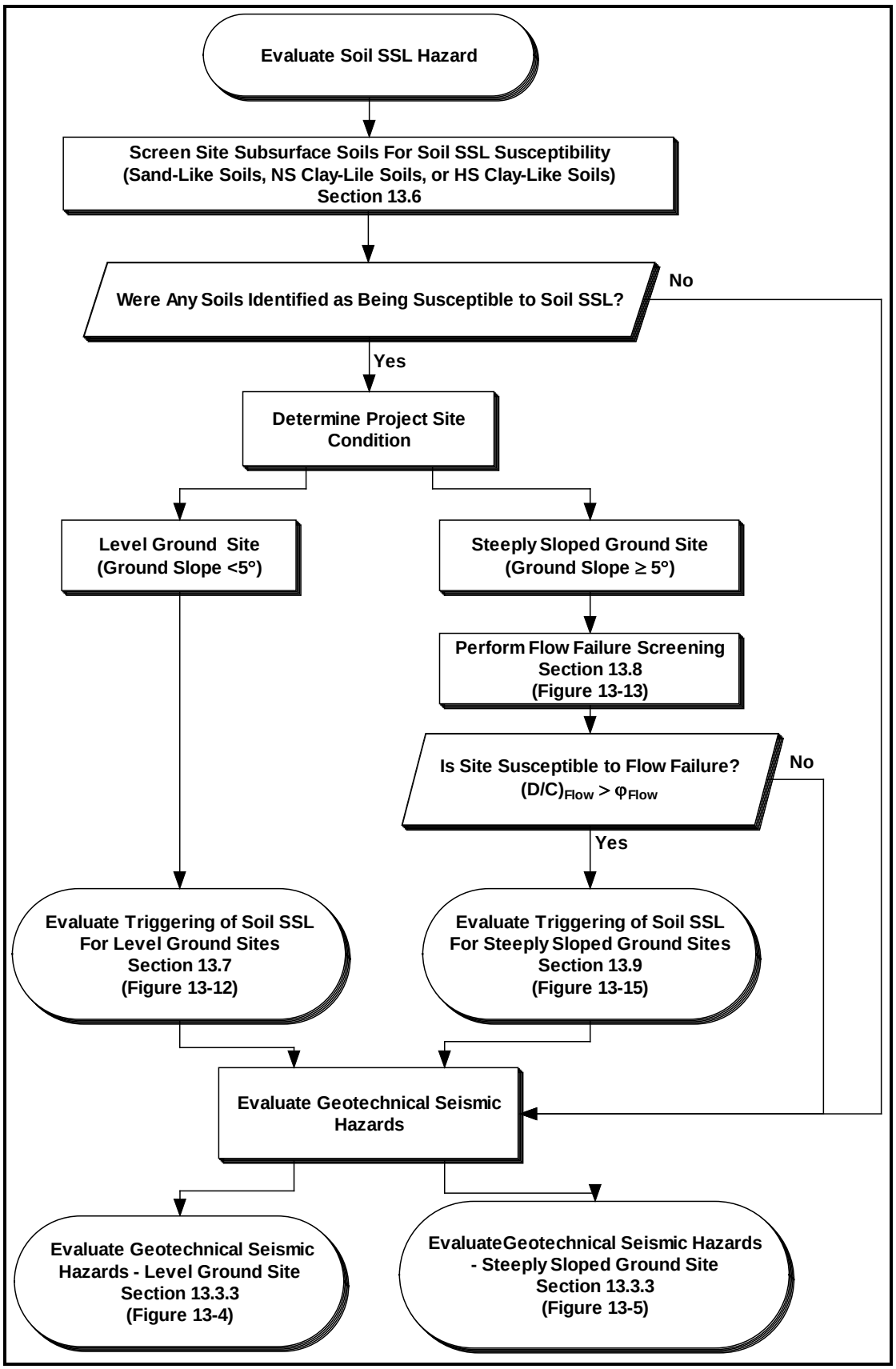

Figure 13-3, Soil SSL Hazard Evaluation Process

13.3.3 Geotechnical Seismic Hazards Evaluation Process

Geotechnical seismic hazards are evaluated after the triggering of soil SSL has occurred. The determination of whether the triggering of soil SSL occurs during the earthquake shaking or after the earthquake shaking is very complex and beyond the scope of the methodology that will be used in the design of standard bridges and typical roadway structures. Therefore, the effects of cyclic liquefaction and cyclic softening shall be assumed to occur during the earthquake shaking and post-earthquake for the evaluation of SSL-induced geotechnical seismic hazards. Cyclic liquefaction of Sand-Like soils shall be assumed to occur instantaneously throughout the full thickness of the Sand-Like soil layer. These fundamental assumptions must be used when selecting soil shear strengths in accordance with Section 13.12.

The overall geotechnical seismic hazard evaluation process for level project sites and steeply sloped project sites is presented in Figures 13-4 and 13-5, respectively.

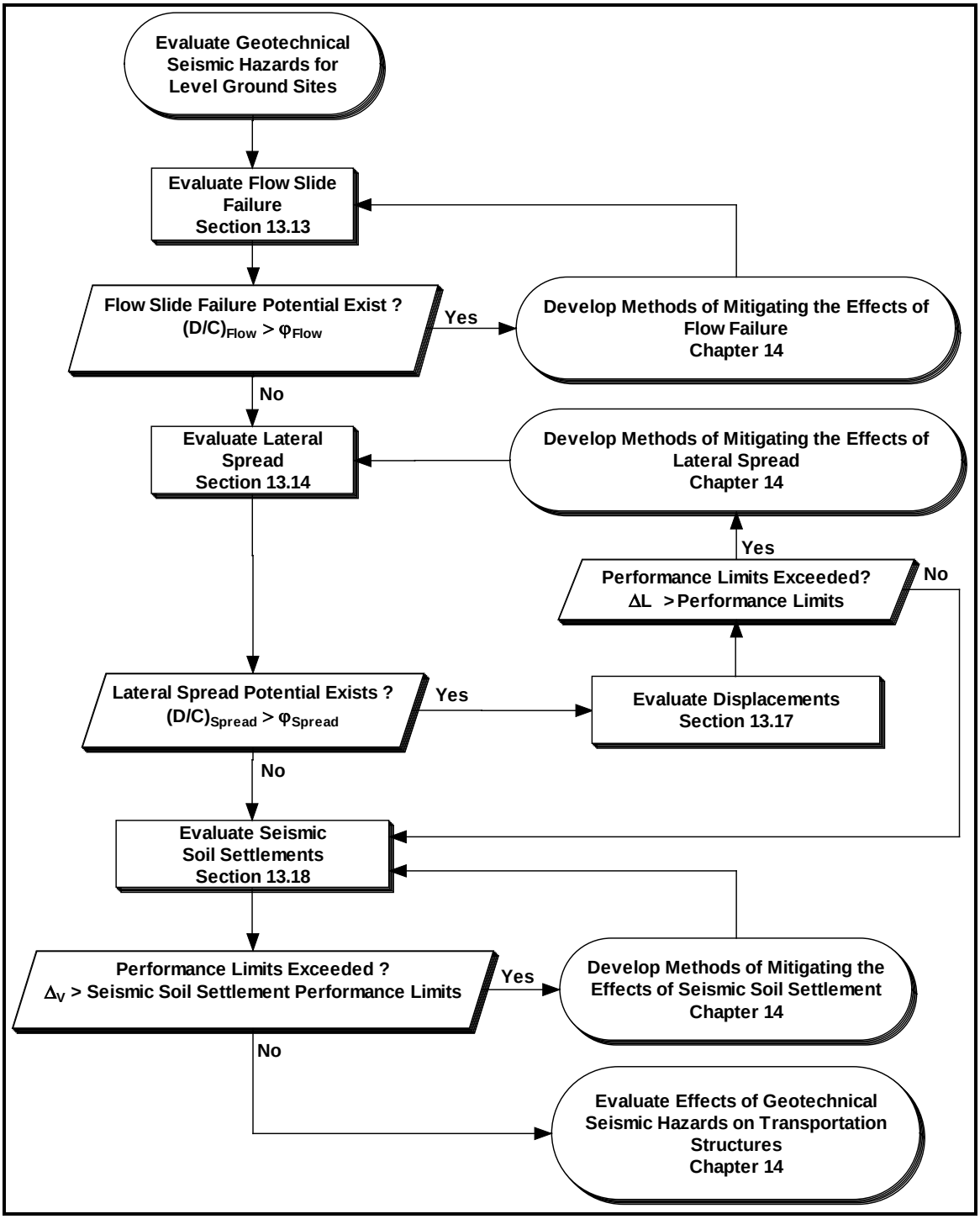

Figure 13-4, Geotechnical Seismic Hazards - Level Ground Sites

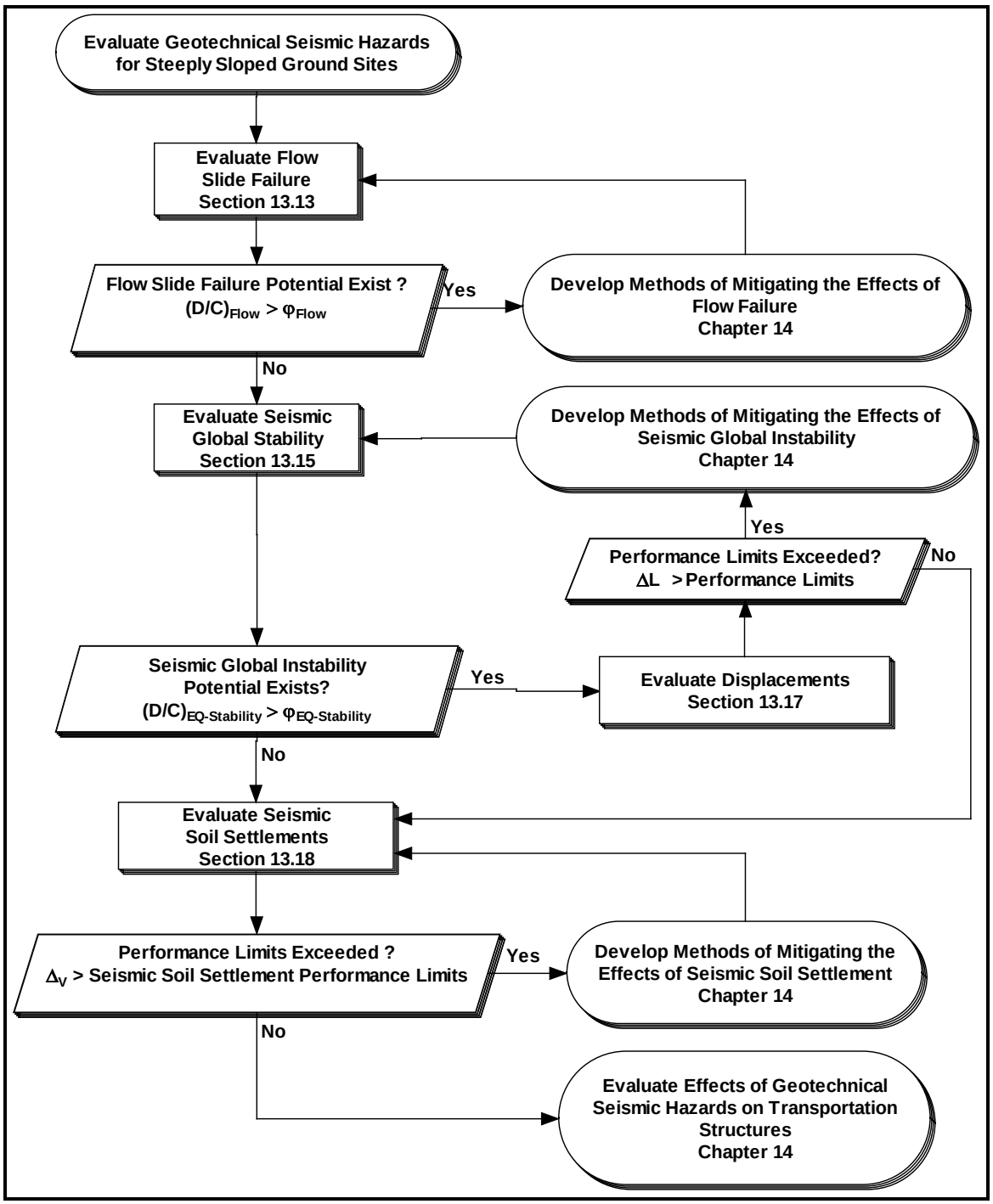

Figure 13-5, Geotechnical Seismic Hazard – Steeply Sloped Ground Sites

13.4 GEOTECHNICAL SEISMIC HAZARD ANALYTICAL METHODOLOGIES

The methodologies presented in this Chapter for evaluating and assessing the impact of the geotechnical seismic hazards on transportation structures are based primarily on limit-equilibrium methods of analyses and empirical/semi-empirical analytical methods that are easily performed and are currently within the state-of-practice of geotechnical earthquake engineering. References have been provided for the design methodologies used in this Manual to allow the designer to become thoroughly familiar with the methodology, its applicability, and its limitations. Within the scope of this Manual, it is not possible to provide sufficient detail and caveats to preclude any misuse of the methods. When necessary, several methods of analyzing the geotechnical seismic hazard have been provided in order to allow for variance in analytical methodologies and to identify trends in results or performance. Several of the methods presented are empirical/semi-empirical based and their applicability to the project site is dependent on the limits of the database used to develop the analytical basis of the method. This Chapter will not address numerical analyses (e.g., finite element, finite difference, etc.), because these methods are typically not performed in the design of standard bridges or typical transportation structures. If numerical analyses are required for a project, the PCS/GDS will provide guidance and/or analytical requirements.

13.5 SOIL SHEAR STRENGTH LOSS MECHANISMS

The mechanism of soil SSL is very complex and has been the subject of much confusion in literature. This is particularly due to the lack of standardization of terminology and the fact that research efforts are still ongoing. Additional confusion has occurred when the method of SSL triggering (static stresses, cyclic loads, etc.) has been used as a means of categorizing the soil SSL mechanism. Current understanding of soil SSL failure mechanisms is based on the study of case histories and laboratory experimentation. One of the problems in the evaluation of field case histories is that more than one geotechnical seismic hazard is typically responsible for the observed failures. This problem can occur when lateral spread movements trigger flow failures and the resulting final deformations observed reflect the influence of all geotechnical seismic hazard failure modes (lateral spread, flow failure, and seismic settlement). Laboratory testing has provided much insight into the mechanisms that trigger soil SSL under a controlled laboratory environment. Laboratory experimentation has limitations in that sample disturbance of the soil structure (i.e. cementation, layering, etc.) can significantly affect the initial and residual soil shear strength results. Another limitation is that laboratory testing can be very complex and is typically not within the standard-of-practice for design of most typical bridge structures. A more detailed explanation of the mechanisms of soil SSL based on field and laboratory observations can be obtained from Robertson and Wride (1997), Kramer and Elgamal (2001), and Idriss and Boulanger (2008). Although the term liquefaction has been used widely in literature (Kramer, 1996 and Robertson and Wride, 1997) to describe several mechanisms of soil SSL, the term liquefaction in this Manual will only be applicable when discussing soil SSL of cohesionless soils that result from cyclic liquefaction.

The predominant soil SSL behavior is used in this Manual to evaluate the soil's susceptibility (Section 13.6) and to determine the most appropriate soil SSL trigger evaluation method for use in geotechnical seismic design (Sections 13.7 for level ground sites and 13.9 for steeply sloped ground sites). Field case histories and laboratory testing have demonstrated that the

predominant soil SSL behavior of the majority of the soils can be grouped into either Sand-Like soils that are subject to cyclic liquefaction failure mechanism or Clay-Like soils that are subject cyclic softening failure mechanism. A description of these soil SSL failure mechanisms is provided in the following Sections.

13.5.1 Cyclic Liquefaction of Sand-Like Soils

Cyclic liquefaction of Sand-Like soils is typically responsible for the most damaging geotechnical seismic hazards that affect transportation infrastructure. Potential damage to transportation facilities due to cyclic liquefaction includes loss of bearing capacity, lateral spread, flow failure, excessive settlements, embankment/slope instability, and reduced lateral and vertical carrying capacity of deep foundations. Even though liquefaction can be triggered by non-seismic loadings such as low amplitude vibrations produced by train traffic/construction equipment or by static loads, such as those that might be caused by rapid drawdown, this Manual will focus on liquefaction triggered by seismic earthquake shaking. Cyclic liquefaction typically occurs in Sand-Like soils that are nonplastic, saturated, and have been deposited during the Quaternary Period (past 1.6 million years ago) in a loose state and are subject to strain softening. Typically, the more recent soil deposits have the greatest susceptibility for cyclic liquefaction. Cyclic liquefaction typically begins during an earthquake when the in-situ soil pore water pressure (u_o) increases ($+\Delta u$). As the increased pore water pressure ($u = u_o + \Delta u$) approaches the total overburden stress (σ_{vo}) the effective overburden stress ($\sigma'_{vo} = \sigma_{vo} - u$) will decrease causing a reduction in grain-to-grain contact that brings about a significant decrease in soil shear strength. The reduction in grain-to-grain contact causes a redistribution of soil particles resulting in densification.

Significant lateral soil deformation may occur as a result of reduced soil shear strength of the liquefied soil zone combined with the seismic inertial forces and/or initial static driving forces that are typically the driving force for soil instability. Other surface manifestations of cyclic liquefaction are often associated with the upward flowing of pore water that generates sand boils at the ground surface. Evidence of sand boils occurring at the ground surface have been found throughout the South Carolina Coastal Plains as indicated in Section 13.5.3. The absence of sand boils is not an indication that cyclic liquefaction has not occurred. Sand boils will not occur if cyclic liquefaction occurs and the drainage paths are restricted due to overlying less permeable layers, i.e., the sand immediately beneath a less permeable soil which can loosen due to pore water redistribution, resulting in subsequent flow failure at this interface. Seismic settlement at the ground surface may occur from cyclic liquefaction induced volumetric strain that develops as seismically induced pore water pressures dissipate.

The determination of the onset of cyclic liquefaction either during or post-earthquake shaking is a very complex analytical problem and beyond the scope of typical SCDOT projects. Several case histories have documented that liquefaction can occur during shaking or post-earthquake (Seed, 1986; Kramer and Elgamal, 2001). The onset and manifestation of cyclic liquefaction is primarily dependent on the magnitude, duration, and proximity of the seismic event, the depth of the liquefied soil zone, stratification and relative permeability of the soil layers above and below the liquefied soil zone, and the susceptibility of the soils to liquefy. Consequently, liquefaction will conservatively be assumed to occur during the earthquake shaking.

13.5.2 Cyclic Softening of Clay-Like Soils

Cyclic softening refers to the soil SSL and deformations in Clay-Like soils. Clay-Like soils are typically moist and plastic clays. Cyclic softening occurs when the earthquake-induced cyclic shear stresses exceed the soil's cyclic shear resistance, causing an accumulation of deformations that result in soil SSL in cohesive soils that exhibit strain softening. Cyclic softening of Clay-Like soils typically results in soil SSL that is dependent on the soil's sensitivity (Chapter 7). Soil deformations may occur as a result of reduced soil shear strength of Clay-Like soils combined with the inertial forces and/or initial static driving forces that are typically the driving force for soil instability. The limited case histories in South Carolina have not documented cyclic softening of Clay-Like soils. Cyclic softening of Clay-Like soils is difficult to document because it does not manifest itself as sand boils at the ground surface as has been documented for cyclic liquefaction of Sand-Like soils.

13.5.3 SC Historical Cyclic Liquefaction

There is significant evidence that soil cyclic liquefaction has historically occurred in the CEUS. Soil liquefaction has been found to have occurred as a result of earthquakes in New Madrid, Missouri 1811 – 1812 and in Charleston, South Carolina 1886. The 1886 Charleston earthquake caused the manifestation of large sand boils as a result of cyclic liquefaction. Sand boils were created as the soil pore water, carrying soil particles, was expelled from the soil causing collapse that resulted in a crater at the ground surface. Figure 13-6 shows a sand boil crater that appeared during the 1886 Charleston earthquake.

Figure 13-6, Sand Boil Crater - 1886 Charleston, SC Earthquake (McGee, et al., 1986)

Hayati and Andrus (2008) developed a liquefaction potential map of Charleston, South Carolina based on the 1886 earthquake. The geologic map of the Charleston Peninsula and Drum Island originally developed by Weems et al. (1997) was used by Hayati and Andrus (2008) to indicate locations of liquefaction and ground deformations as shown in Figure 13-7. For a description of the near surface geologic units and a description of the Cases (indicated on the map as 1 – 27) of cyclic liquefaction evidence and permanent ground deformation see Hayati and Andrus (2008).

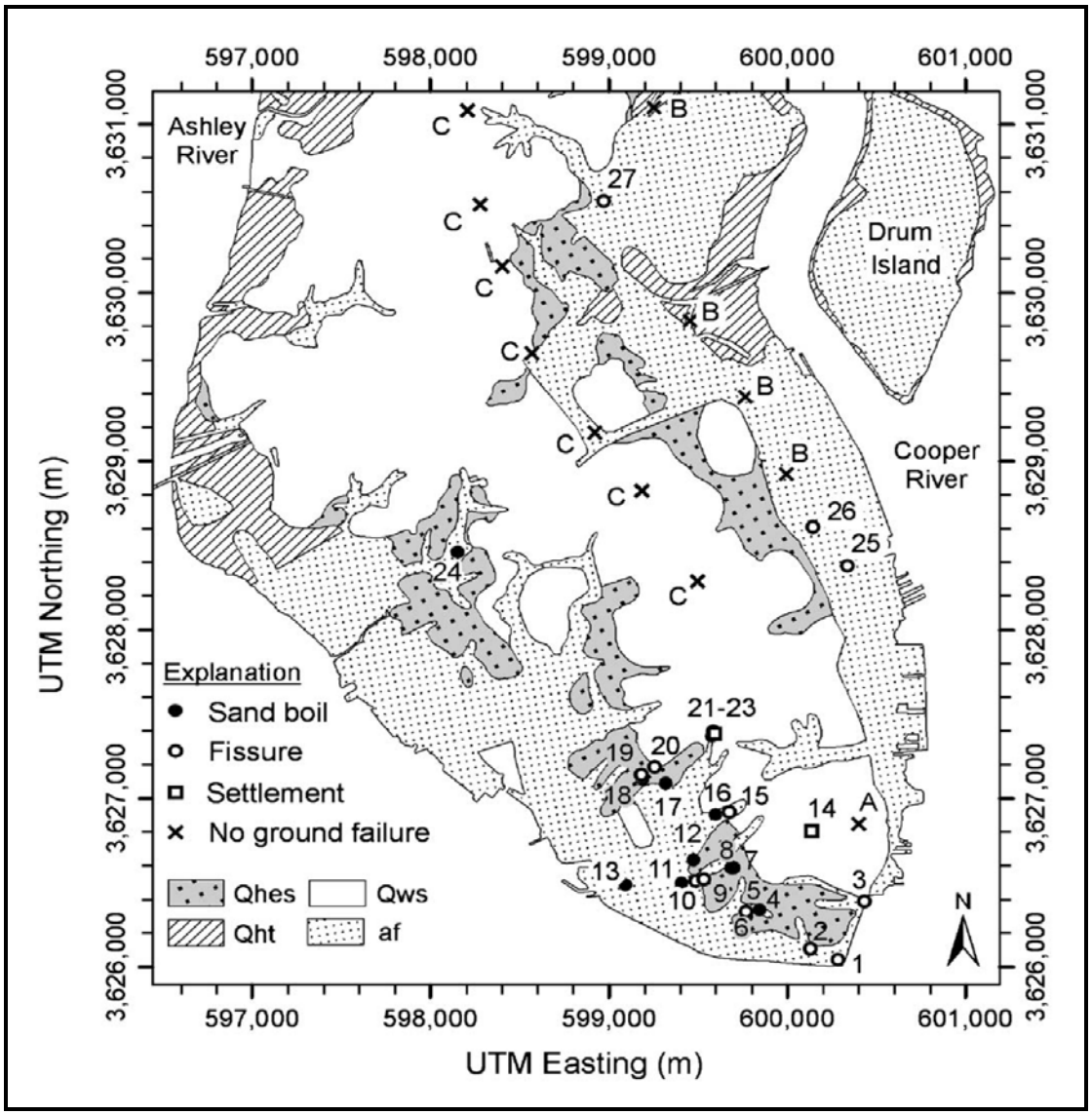

Figure 13-7, 1886 Liquefaction and Ground Deformations Sites (Weems et al., 1997, Hayati and Andrus, 2008 with permission from ASCE)

Paleoliquefaction studies in South Carolina conducted since the mid-1980s have indicated that at least seven episodes of paleoliquefaction have occurred in the past 6,000 years. The earthquakes in the Charleston, SC area appear to have magnitudes greater than 7 and the earthquake cycle suggest a recurrence time of 500-600 years (Talwani and Schaffer, 2001). Paleoliquefaction study site locations in the South Carolina Coastal Plain are shown in Figure 13-8.

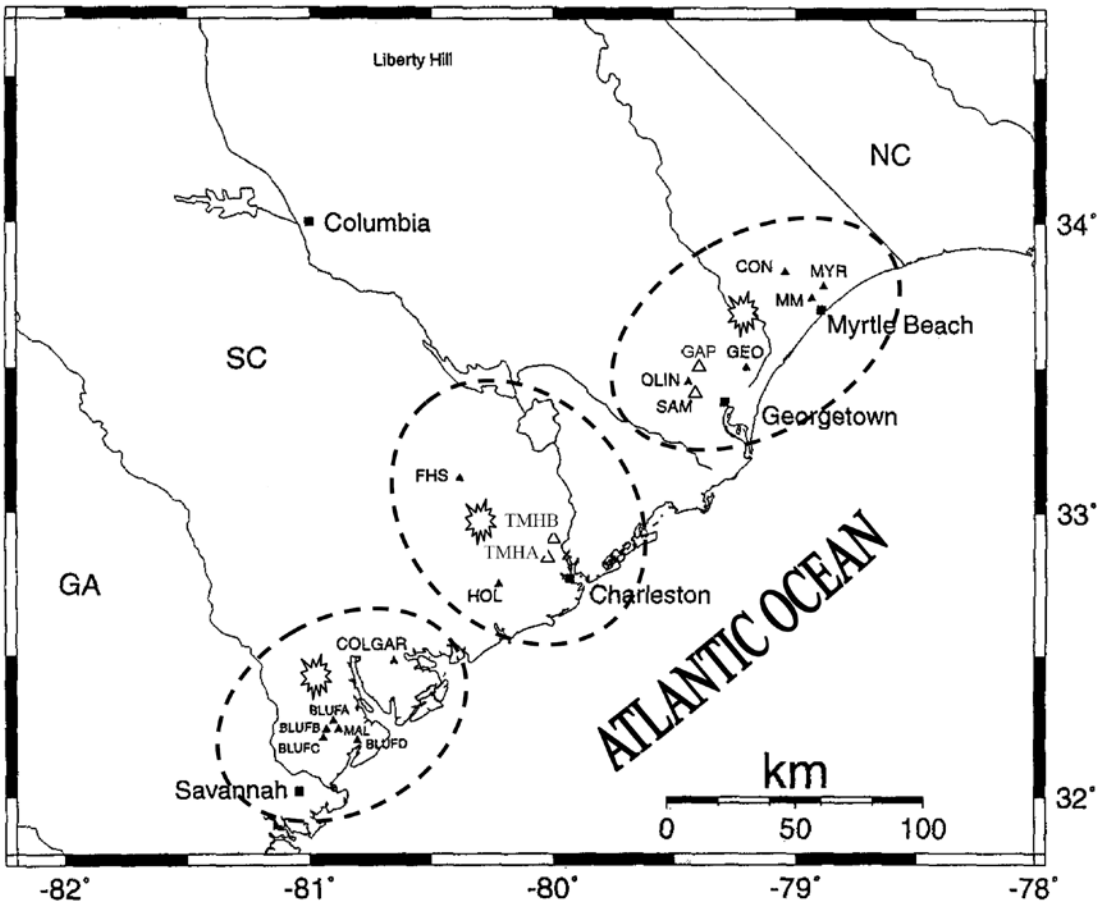

Legend:

- Dashed lines enclose three zones of paleoliquefaction along the South Carolina Coastal Plain. The explosion symbols represent three possible inferred epicentral locations.
- Triangles show the locations of sandblows in South Carolina Coastal Plain. Reports of liquefaction features extend to Columbia and Georgetown and to Sand Hills near Liberty Hill.
- Open triangles indicate the locations of in-situ engineering tests for this study.
- Abbreviations are as follows: Bluffton, BLUF; Colony Gardens, COLGAR; Conway, CON; Four Hole Swamp, FHS; Gapway, GAP; Georgetown, GEO; Hollywood, HOL; Malpherous, MAL; Martin Marietta, MM; Myrtle Beach, MYR; Sampit, SAM; and Ten Mile Hill, TMH

Figure 13-8, Coastal Plain Paleoliquefaction Study Sites (adapted from Talwani and Schaffer, 2001).

The USGS maintains a database of published reports of Quaternary faults, liquefaction features, and tectonic features in the CEUS. The USGS database for South Carolina contains the following three sites with liquefaction features: 2657, Charleston, SC; 2658, Bluffton, SC; and 2659, Georgetown, SC. Liquefaction feature 2657 has geologic evidence of the 1886 Charleston earthquake. Liquefaction features 2658 and 2659 have geologic evidence of prehistoric liquefaction that occurred during the late Quaternary Period (Holocene, <10,000 years ago). Figure 13-9 shows a map, prepared by the USGS, of the liquefaction features in South Carolina. The shaded area on the map indicates areas of potential Quaternary and historic liquefaction.

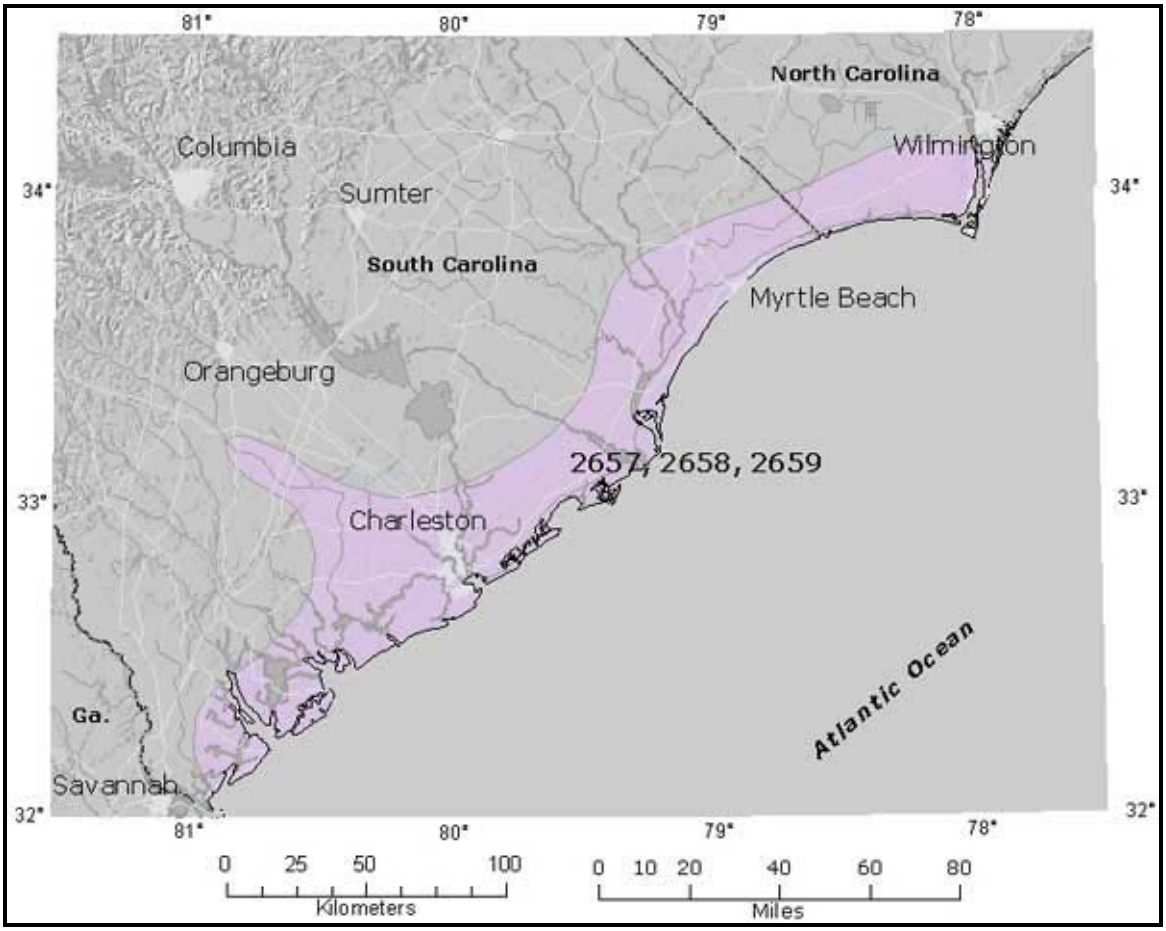

Figure 13-9, SC Quaternary Liquefaction Areas (USGS Website)

A database of extensive liquefaction studies at sites in China, Japan, California, and Alaska has been collected. Even though liquefaction has occurred in the CEUS, none of the liquefaction case histories have been evaluated, since most seismic events with earthquake magnitudes, M_w, greater than 6.5 occurred more than 100 years ago. Liquefaction evaluation in the CEUS and consequently in South Carolina, is relatively more complex than in other areas where liquefaction studies have been made because of the deep vertical soil column (up to 4,000 feet) encountered in the Atlantic Coastal plain, lack of recorded large seismic events, and uncertainty of the mechanisms and subsequent motions resulting from intraplate earthquakes (Schneider and Mayne, 1999). Never the less, historical soil liquefaction studies in the CEUS (Schneider and Mayne, 1999) indicate that current methods to evaluate cyclic liquefaction are in general agreement with predictions of cyclic liquefaction.

13.6 SOIL SHEAR STRENGTH LOSS SUSCEPTIBILITY SCREENING CRITERIA

Screening criteria is based on laboratory testing observations and on site parameters that have been observed to be present when soil SSL occurred in seismic hazard case histories. It has been observed that cyclic liquefaction potential decreases as soils increase in fines content (FC), increase in plasticity index (PI), and decrease in moisture content below the liquid limit (LL).

Screening for earthquake-induced soil SSL have traditionally been focused on cyclic liquefaction of cohesionless soils. Recent studies (Seed et. al, 2003, Boulanger and Idriss, 2004a, 2007; Bray and Sancio, 2006; Idriss and Boulanger, 2008) have stressed the need to evaluate loss in soil shear strength and stiffness due to cyclic liquefaction (low plasticity silts and clays) and cyclic softening (clays and plastic silts).

Seed et. al (2003) proposed the liquefaction susceptibility chart for fine grained soils shown in Figure 13-10 that is based on soil plasticity. The chart is divided into three zones of varying soil SSL susceptibility. Zone A has the highest potential for loss in shear strength resulting from cyclic liquefaction. Zone B was considered a transition area where soils could be subject to soil SSL and would require laboratory cyclic load testing for confirmation of soil shear strength susceptibility. Soils located in Zone C (Zone not covered by Zones A or B) were not susceptible to cyclic liquefaction induced soil SSL but were to be screened for soil SSL due to cyclic softening of sensitive cohesive soils.

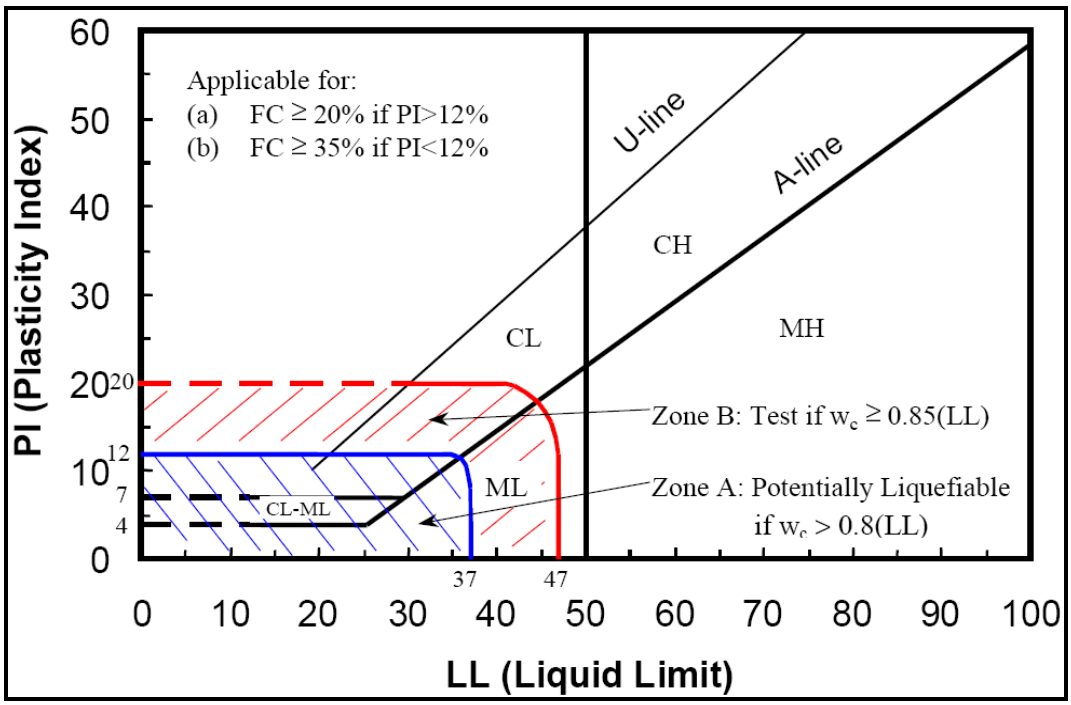

Figure 13-10, Liquefaction Susceptibility Based on Soil Plasticity (Seed, et al. 2003)

The liquefaction guidelines described by Seed et al. (2003) are best considered as envelopes of fine-grained soils that have been observed to experience significant strains or strength loss during earthquakes (Boulanger and Idriss, 2004a, 2006, 2007). Boulanger and Idriss (2004a, 2006, 2007) recommend that the fine-grained cyclic soil behavior would be best described as either Sand-Like or Clay-Like based on the Plasticity Index (PI). Boulanger and Idriss (2004a, 2006, 2007) suggested that there is a narrow soil SSL behavior transition zone between Sand-Like and Clay-Like that ranges from about a PI of 3 to 8 as indicated in Figure 13-11.

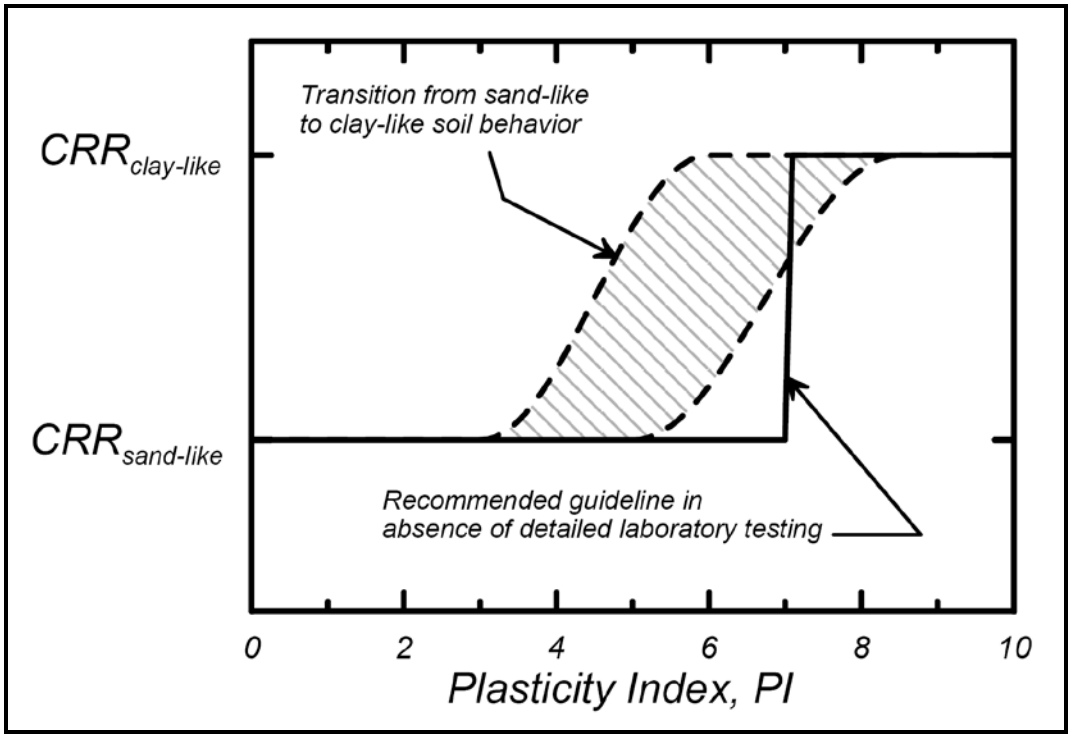

Figure 13-11, Transition from Sand-Like to Clay-Like behavior (Boulanger and Idriss, 2004a, 2006, 2007; Idriss and Boulanger, 2008) (With Permission from ASCE)

The soil SSL susceptibility screening criteria presented by Idriss and Boulanger (2008) for determining if the underlying subsurface soils at a project site are susceptible to soil SSL due to cyclic liquefaction or cyclic softening will be used. The soil SSL behavior screening adopted by SCDOT in the following Sections is consistent with Idriss and Boulanger (2008) and has been expanded to distinguish between normally and highly sensitive clays as indicated below. The soil SSL susceptibility criteria shall be based on the following three categories: (1) Sand-Like Soils (2) Normally Sensitive (NS) Clay-Like Soils, and (3) Highly Sensitive (HS) Clay-Like Soils.

Laboratory cyclic load testing of Sand-Like or Clay-Like soils is typically not required for typical bridges or typical transportation structures but may be required by the PCS/GDS on a project specific basis depending on the risk associated with the geotechnical seismic hazards under evaluation.

13.6.1 Sand-Like Soil

Soil SSL in Sand-Like soils is caused by cyclic liquefaction as described in Section 13.5.1. Sand-Like soils will be screened to a minimum depth of 80 feet below the existing ground surface or 20 feet beyond the lowest deep foundation element; whichever extent of screening is deeper.

Sand-Like soils that are susceptible to cyclic liquefaction are characterized by the following site and soil parameters:

1. Sand-Like soils susceptible to cyclic liquefaction must be below the water table. The water table selection for this evaluation must take into account the seasonal fluctuation of the ground water and the historic and/or possible future rise of the ground water level with respect to the soils being analyzed for liquefaction susceptibility. To determine the location of soils that are adequately saturated for liquefaction to occur, seasonally averaged groundwater elevations should be used. The Natural Resources Conservation Service (NRCS) website (http://websoilsurvey.nrcs.usda.gov/app/) may be consulted for determining the seasonal fluctuation of groundwater. Groundwater fluctuations caused by tidal action or seasonal variations will cause the soil to be saturated only during a limited period of time, significantly reducing the risk that liquefaction could occur within the zone of liquefaction.

2. Low plasticity fine grained soils that classify as CL-ML in the Unified Soil Classification System (USCS) with a Plasticity Index, PI $<$ 5 (measured on soil portion passing the No. 40 sieve) and for all other fine grained soils with a Plasticity Index, PI $<$ 7.

3. Corrected Standard Penetration Test (SPT) blow counts, $N^{*}_{1,60,CS}$ < 30 blows/foot or normalized corrected Cone Penetration Test (CPT) tip resistance, $q_{C,1,N,CS}$ < 170.

13.6.2 Normally Sensitive (NS) Clay-Like Soil

Soil SSL in NS Clay-Like soils is caused by cyclic softening as described in Section 13.5.2. Clay-Like soils will be screened to a minimum depth of 80 feet below the existing ground surface or 20 feet beyond the lowest deep foundation element; whichever extent of screening is deeper.

NS Clay-Like soils that are susceptible to cyclic softening are characterized by the following site soil parameters:

1. Fine grained soils that classify as CL-ML in the USCS with a Plasticity Index, PI $\geq$ 5 (measured on soil portion passing the No. 40 sieve) and for all other fine grained soils with a Plasticity Index, PI $\geq$ 7.

2. Soil sensitivity, S_t $<$ 5 (Chapter 7)

13.6.3 Highly Sensitive (HS) Clay-Like Soil

Soil SSL in HS Clay-Like soils is caused by cyclic softening as described in Section 13.5.2. Clay-Like soils will be screened to a minimum depth of 80 feet below the existing ground surface or 20 feet beyond the lowest deep foundation element; whichever extent of screening is deeper.

HS Clay-Like soils that are susceptible to cyclic softening are characterized by the following site and soil parameters:

1. Fine grained soils that classify as CL-ML in the USCS the Plasticity Index, PI $\geq$ 5 (measured on soil portion passing the No. 40 sieve) and for all other fine grained soils the Plasticity Index, PI $\geq$ 7.
2. Soil sensitivity, $S_t \geq 5$ (Chapter 7)

13.7 SOIL SHEAR STRENGTH LOSS TRIGGERING FOR LEVEL GROUND SITES

The liquefaction triggering analyses for level ground sites will include an evaluation of Sand-Like and Clay-Like soils that were identified to be susceptible to cyclic liquefaction or cyclic softening during the screening process described in Section 13.6. A level ground site condition is defined as either level ground or gently sloping ground (slope angle < 5 degrees), or level/gently sloping ground with a nearby (≤ 150 feet) steep slope or free-face slope that is less than 16 feet in height. This site condition is typically encountered in the South Carolina Coastal Plain under roadways, at grade bridge crossings over non-navigable rivers or small creeks, floodplain crossings, etc. These level ground site conditions typically have very little, if any, initial static shear stresses in the underlying soils and therefore the effects of static shear stresses are typically not taken into account during liquefaction triggering analyses for level ground sites.

The *Simplified Procedures* for determining liquefaction triggering of Sand-Like soils shall be based on SPT in-situ testing or on CPT in-situ testing using the methods described in the Earthquake Engineering Research Institute (EERI) Monograph MNO-12, Soil Liquefaction During Earthquakes (Idriss and Boulanger, 2008).

Alternate methods of evaluating liquefaction triggering of Sand-Like soils such as those described in the 1996 NCEER and 1998 NCEER/NSF workshop (Youd, et al. 2001) may be required on a project specific basis.

The *Simplified Procedure* for determination of cyclic liquefaction triggering is an empirical method based on field investigations of sites that have or have not experienced liquefaction of Sand-Like soils. The *Simplified Procedure* for Sand-Like soils cannot differentiate between the types of liquefaction (flow liquefaction or cyclic softening). The *Simplified Procedure* for determining the onset/triggering of cyclic softening of Clay-Like soils during earthquake events is based on laboratory investigations. The PCS/GDS may require on a project specific basis, more rigorous analytical methods such as non-linear effective stress site response methods and advanced laboratory testing not included in this Manual.

The *Simplified Procedure* compares the earthquake-induced stresses (Demand, D), expressed in terms of an equivalent uniform cyclic stress ratio (CSR^*_{eq}) that has been magnitude-weighted ($CSR^*_{eq} = CSR_{M=7.5}$), with the capacity of the soil's resistance to soil SSL (Capacity, C), expressed in terms of corrected cyclic resistance ratio (CRR^*_{eq}) that also has been magnitude-weighted and normalized to an effective overburden stress of 1 tsf ($CRR^*_{eq} = CRR_{M=7.5,1\ tsf}$). The ratio of the earthquake-induced stresses (Demand, D) divided by the soils resistance to soil SSL (Capacity, C) defines the strength loss ratio $(D/C)_{SL}$. The LRFD equation that is to be used to evaluate the onset of strength loss (SL) at level ground site conditions is provided below:

$$\left(\frac{D}{C}\right)_{SL} = \frac{CSR^{*}_{eq}}{CRR^{*}_{eq}} \leq \varphi_{SL} \qquad \text{Equation 13-1}$$

The onset of cyclic liquefaction (Sand-Like soils) or cyclic softening (Clay-Like soils) occurs when the strength loss ratio $(D/C)_{SL}$ is greater than the strength loss resistance factor (φ_{SL}) provided in Chapter 9 - Geotechnical Resistance Factors.

Since the *Simplified Procedure* is a deterministic procedure, a load factor, γ, of unity (1.0) is used and the resistance factor, φ, accounts for the site variability and the level of acceptable risk to triggering soil SSL. As research advances and soil SSL analytical models are calibrated for LRFD design methodology, adjustments will be made in the implementation of the LRFD design methodology.

The overall process for conducting a soil SSL triggering analysis using the *Simplified Procedure* for level project site conditions is presented in a flow chart in Figure 13-12. The analytical procedures for computing cyclic stress ratio (CSR) and cyclic resistance ratio (CRR) of Sand-Like soils and Clay-like soils are provided in Section 13.10 and Section 13.11, respectively.

Soils that are susceptible to cyclic liquefaction or cyclic softening will require additional analyses to evaluate the effects of the soil shear strength degradation as discussed in Section 13.12. Project sites that have subsurface soils with the potential for soil SSL will require the evaluation for soil SSL-induced geotechnical seismic hazards such as flow slide failure, lateral spread, and soil settlements. The analytical procedures to determine the magnitude and extent of these soil SSL-induced hazards are provided in this Chapter.

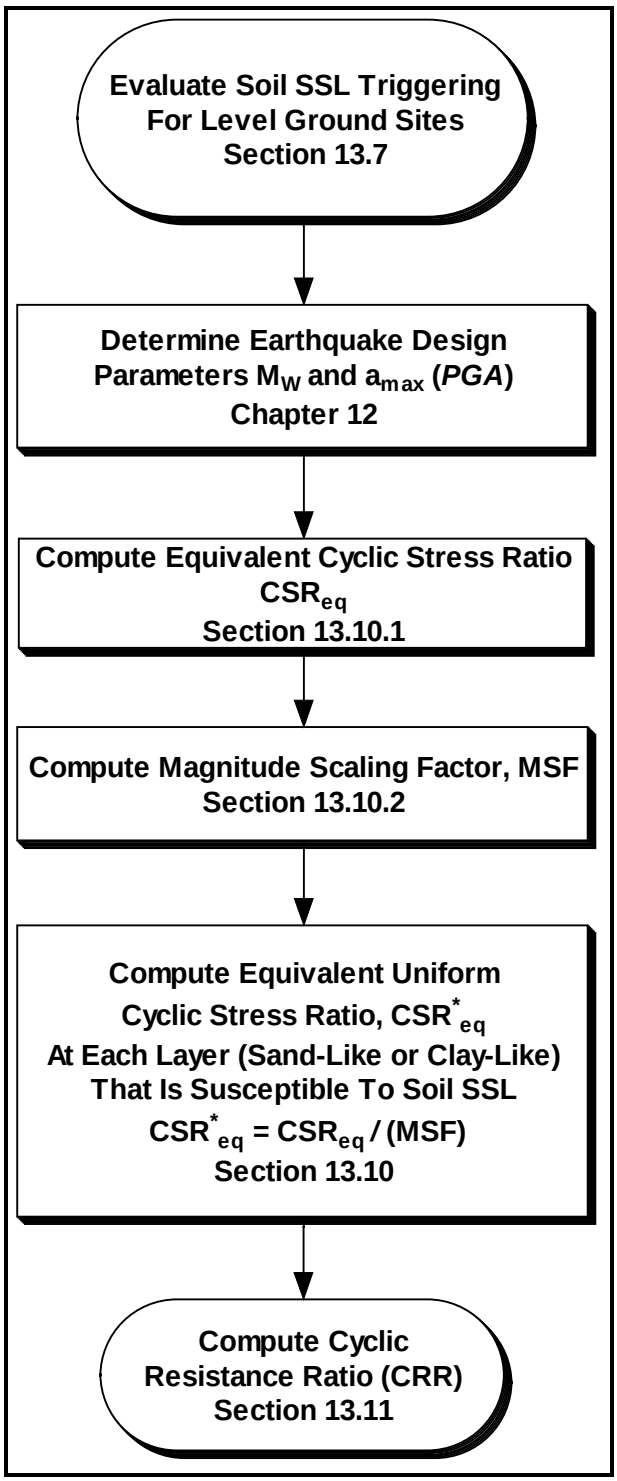

Figure 13-12, Soil SSL Triggering Analysis for Level Ground Sites

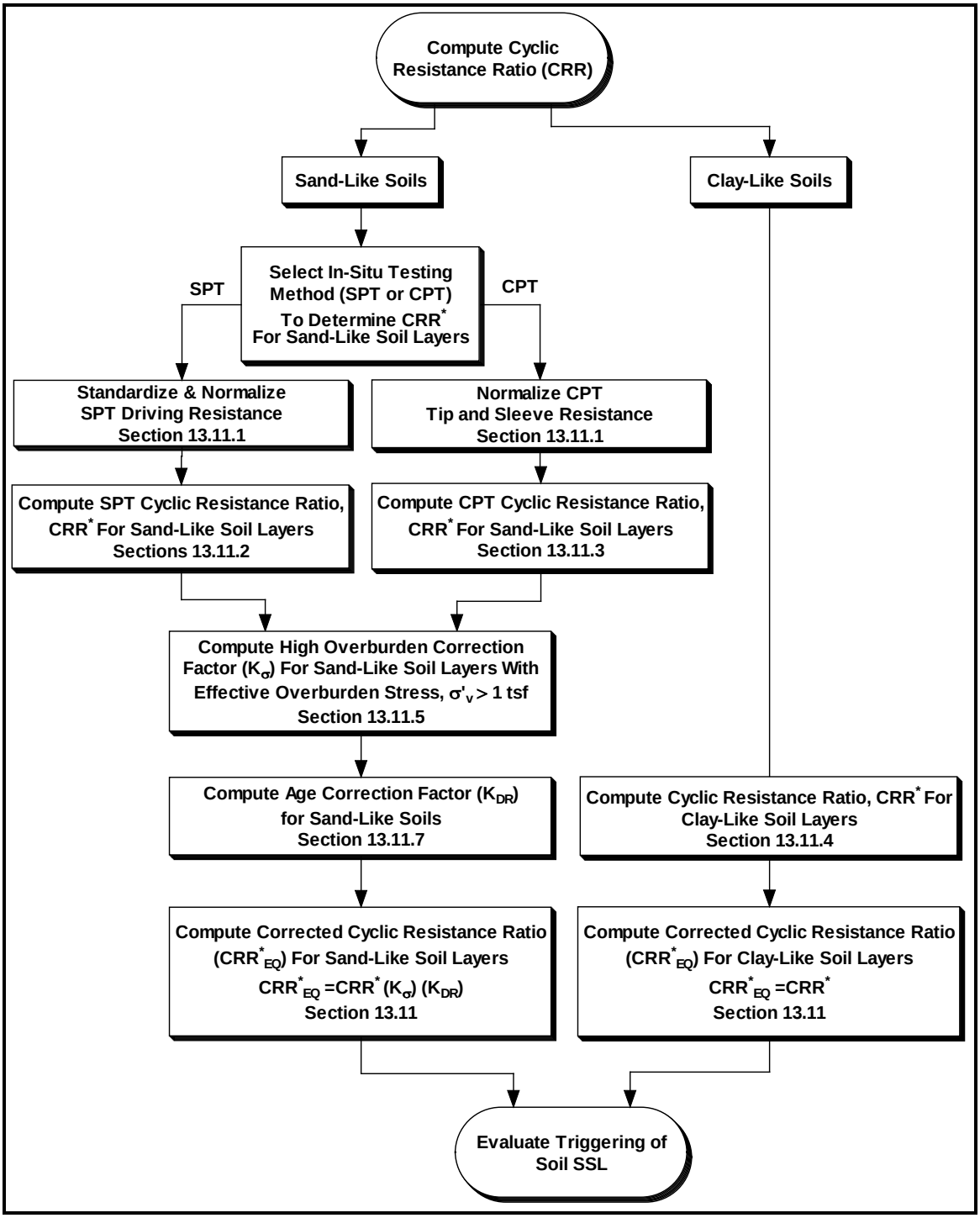

Figure 13-12 (Continued), Soil SSL Triggering Analysis for Level Ground Sites

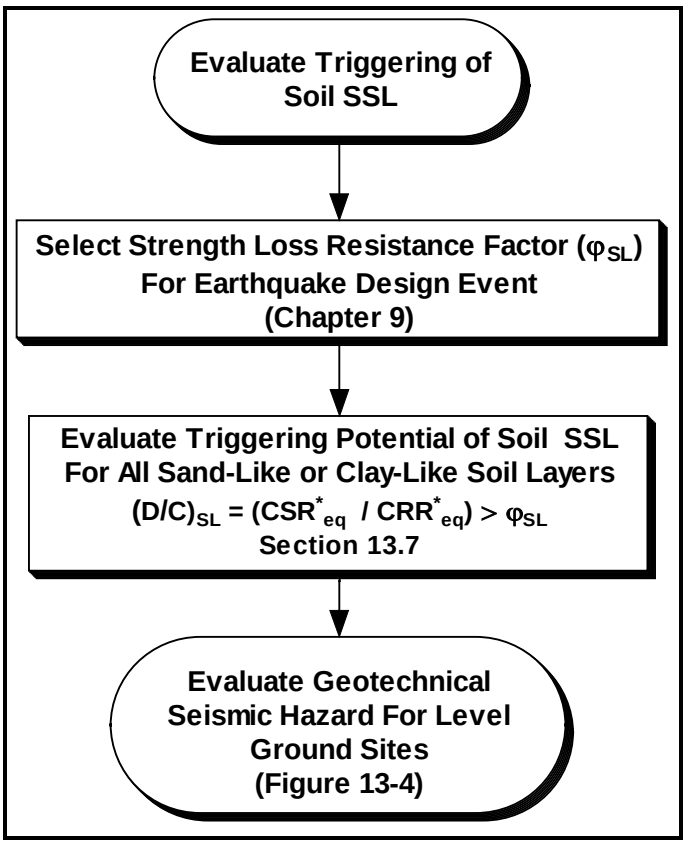

Figure 13-12 (Continued), Soil SSL Triggering Analysis for Level Ground Sites

13.8 FLOW FAILURE SCREENING FOR STEEPLY SLOPED GROUND SITES

Steeply sloped ground sites with soils susceptible to SSl (Section 13.6) will require a screening to determine if there is a high potential for flow failure resulting from soil SSL in Sand-Like and/or Clay-Like soils. Flow failure screening is evaluated by performing a post-seismic-strength-loss (PSSL) slope stability analysis.

In a PSSL slope stability analysis, Sand-Like soils are initially assumed to have cyclic liquefaction residual shear strength (τ_{rl}), NS Clay-Like soils are assumed to have cyclic softening residual shear strength (τ_{rs}), and HS Clay-Like soils are assumed to have remolded shear strength ($\tau_{remolded}$). The PSSL slope stability analysis shall be performed using Spencer's Slope Stability method in accordance with Chapter 17.

The PSSL slope stability is an evaluation of flow failure that is based on the evaluation of the ratio of driving forces (Demand, D) divided by resisting forces (Capacity, C) resulting in a flow failure ratio $(D/C)_{Flow}$. The LRFD equation that is used to evaluate the onset of flow failure is defined by the following equation.

$$\left(\frac{D}{C}\right)_{Flow} \leq \varphi_{Flow} \qquad \text{Equation 13-2}$$

The onset of flow failure occurs when the flow failure ratio $(D/C)_{Flow}$ is greater than the flow failure resistance factor (φ_{Flow}) provided in Chapter 9 - Geotechnical Resistance Factors.

Since slope instability analyses is a deterministic procedure, a load factor, γ, of unity (1.0) is used and the resistance factor, φ, accounts for the site variability and the level of acceptable risk to trigger flow failure. As research advances and flow failure analytical models are calibrated for LRFD design methodology, adjustments will be made in the implementation of the LRFD design methodology.

If the results of the PSSL slope instability analyses indicate the potential for flow failure; then Sand-Like soils and Clay-Like soils must be evaluated for triggering of soil SSL at steeply sloped ground sites. If the potential for flow failure does not exist; then it can be inferred that soil SSL will not occur and an evaluation of geotechnical seismic hazard for steeply sloped ground sites can proceed. The overall evaluation process for screening for flow failure due to PSSL in steeply sloped ground sites is shown in Figure 13-13.

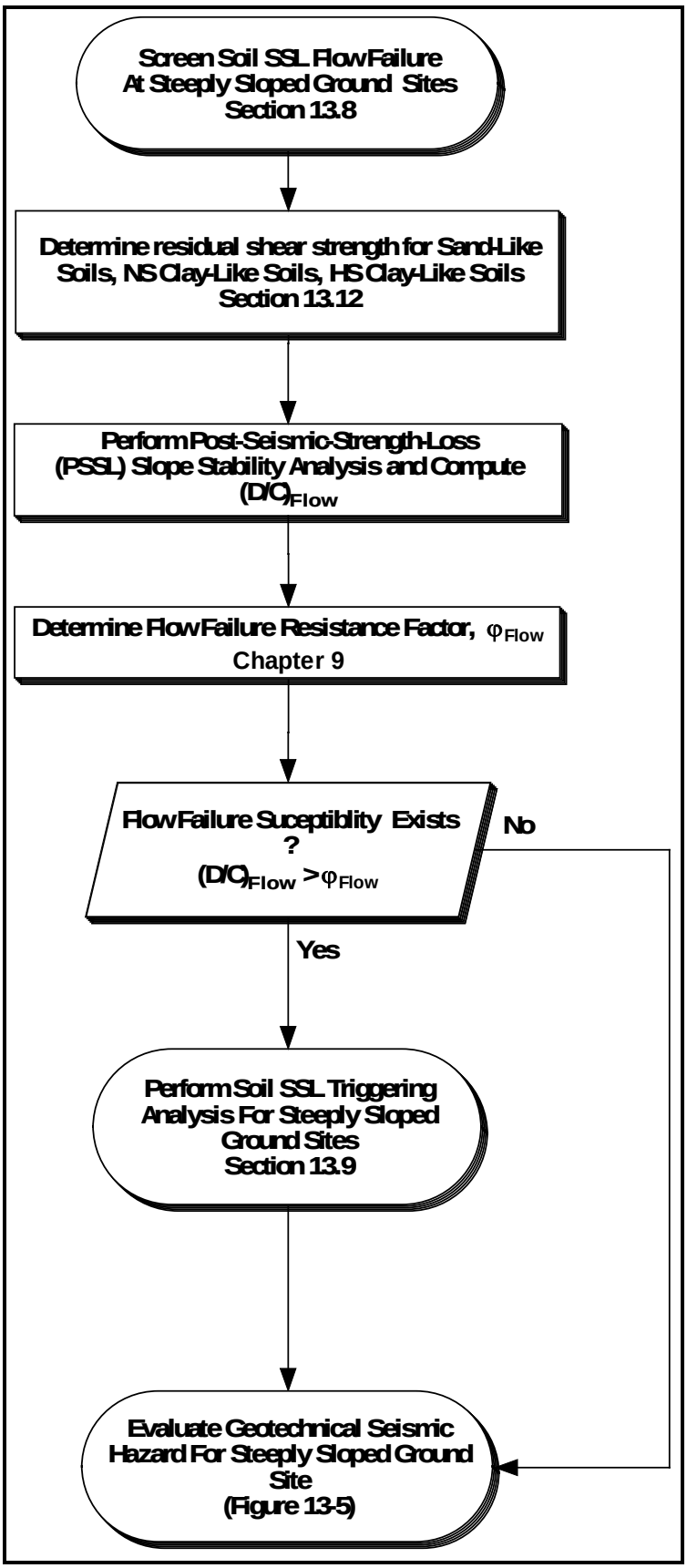

Figure 13-13, Flow Failure Screening - Steeply Sloped Sites

13.9 SOIL SHEAR STRENGTH LOSS TRIGGERING FOR STEEPLY SLOPED GROUND SITES

This Section describes the soil SSL triggering analysis for steeply sloped ground sites. A steeply sloped ground site is defined as a project site with a ground slope angle ≥ 5 degrees or a level ground site with a nearby (≤ 150 feet) steep slope or free-face slope that is ≥ 16 feet in height. This site condition is typically encountered at roadway embankments, cut hillsides, and sites where ERSs are constructed. The sloping ground conditions and any surcharges or surface loads will induce static shear stresses in the underlying soils that must be accounted for when evaluating liquefaction triggering for both Sand-Like and Clay-Like soils. The earthquake-induced stresses plus the static shear stresses (Demand, D) could potentially exceed the soil's resistance to soil SSL (Capacity, C) which would result in a reduction in soil shear strength.

The effects of static shear stress must be included in the evaluation of soils SSL triggering for steeply sloped site conditions by the methods indicated below:

1. **Static Shear Stress Ratio Correction Factor, K_α, Method:** The static shear stress ratio (SSSR) correction factor (K_α) method (Section 13.11.7) is presented by Idriss and Boulanger (2008) to account for static shear stresses in the *Simplified Procedure* method of evaluating soil SSL triggering for steeply sloped ground sites. The SSSR correction factor, K_α, method is further explained in Section 13.9.1.

2. **Shear Strength Ratio Method:** The shear strength ratio (SSR) triggering method computes the ratio of shear stress demand on the soil layer susceptible to soil SSL with the soil's yield strength. This method, developed by Olson and Stark (2003), uses the yield shear strength ratio and soil SSL ratio to evaluate the triggering of soil SSL for steeply sloped ground sites. The SSR method is further explained in Section 13.9.2.

Both methods presented above should be used to evaluate soil SSL triggering evaluation for steeply sloped ground sites, when the initial static stress ratio (α) is less than or equal to 0.35, and the results of each should be compared. When the maximum initial static stress ratio (α) is greater than 0.35, or when complex geometries and loadings need to be evaluated, the shear strength ratio (SSR) method presented in Section 13.9.2 should be used. Soils that are susceptible to cyclic liquefaction or cyclic softening will require additional analyses to evaluate the soil shear strength degradation (Section 13.12). Project sites that have subsurface soils with the potential for soil SSL will require the evaluation of soil SSL-induced geotechnical seismic hazards such as flow slide failure, seismic instability, and seismic soil settlement. The analytical procedures to determine the magnitude and extent of these soil SSL-induced hazards are provided in this Chapter.

13.9.1 Static Shear Stress Ratio Correction Factor, K_α, Method

The static shear stress ratio (SSSR) correction factor (K_α) can be used with the *Simplified Procedure* to evaluate the effects of initial static shear stresses for steeply sloped ground sites.

This is accomplished by multiplying the SSSR correction factor (K_α) by the soil's cyclic resistance ratio (CRR^*) as indicated in Section 13.11. The SSSR correction factor (K_α) proposed by Idriss and Boulanger (2008) is computed as indicated in Section 13.11.7. The SSSR correction factor (K_α) method is limited to a maximum initial static stress ratio α less than or equal to 0.35. The soil SSL triggering process for steeply sloped ground sites is shown in Figure 13-14.

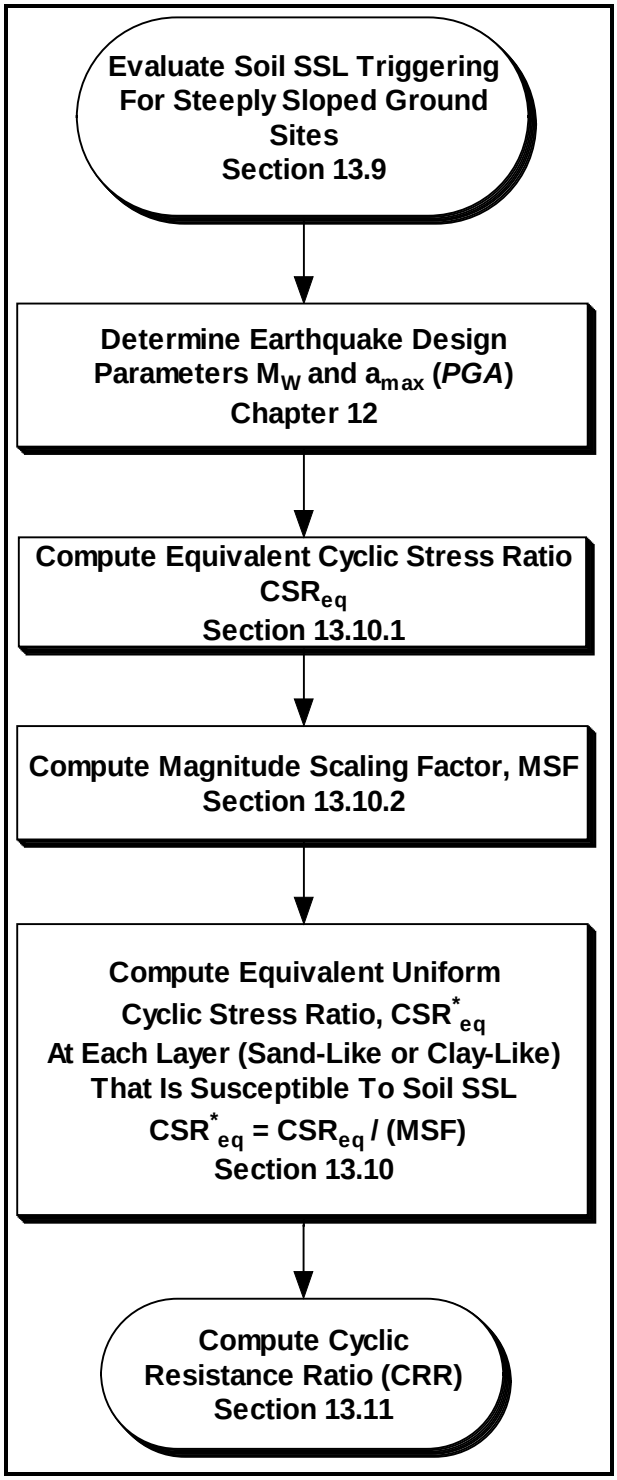

Figure 13-14, Simplified Procedure - Soil SSL At Steeply Sloped Ground Sites

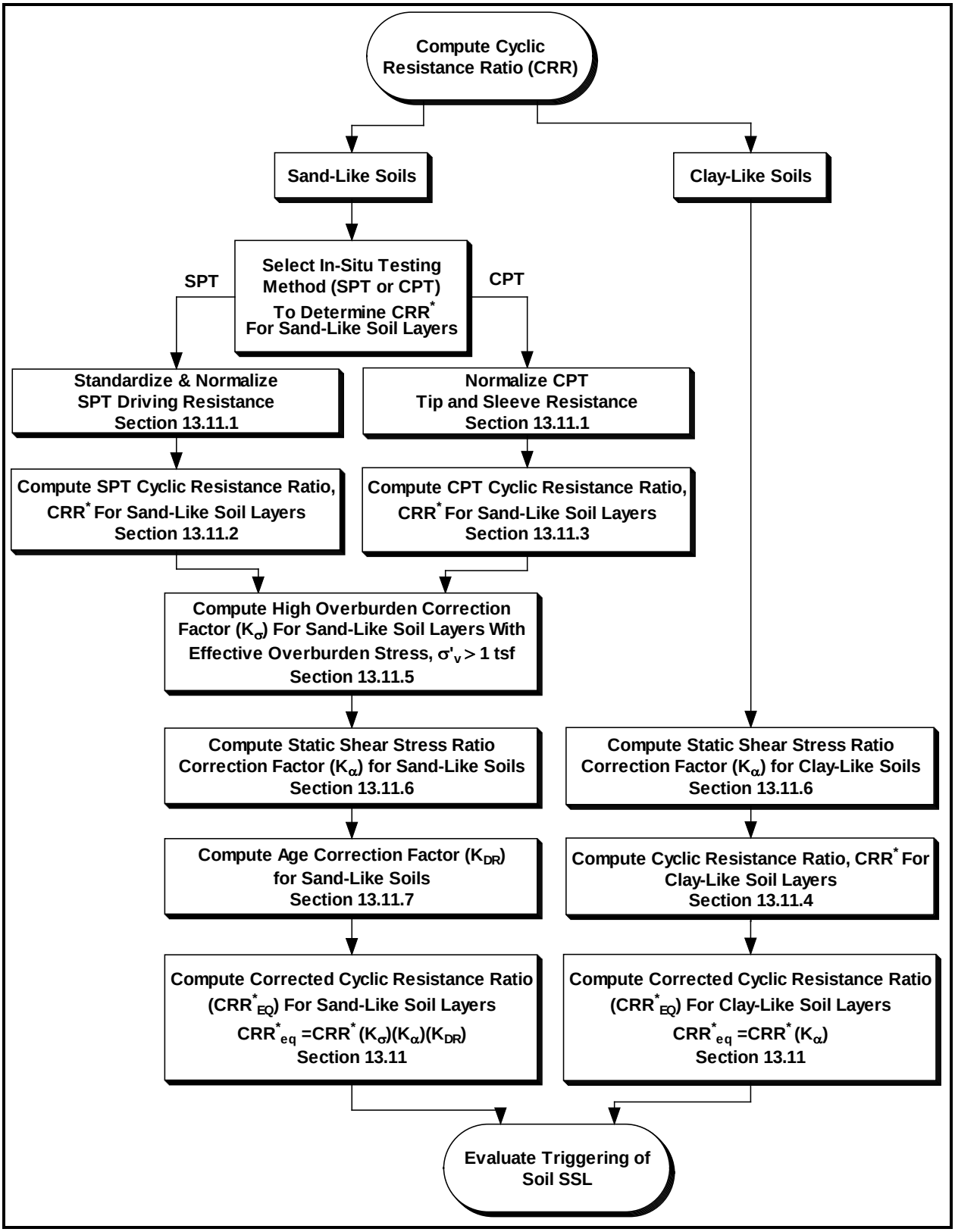

Figure 13-14 (Continued), Simplified Procedure - Soil SSL At Steeply Sloped Ground Sites

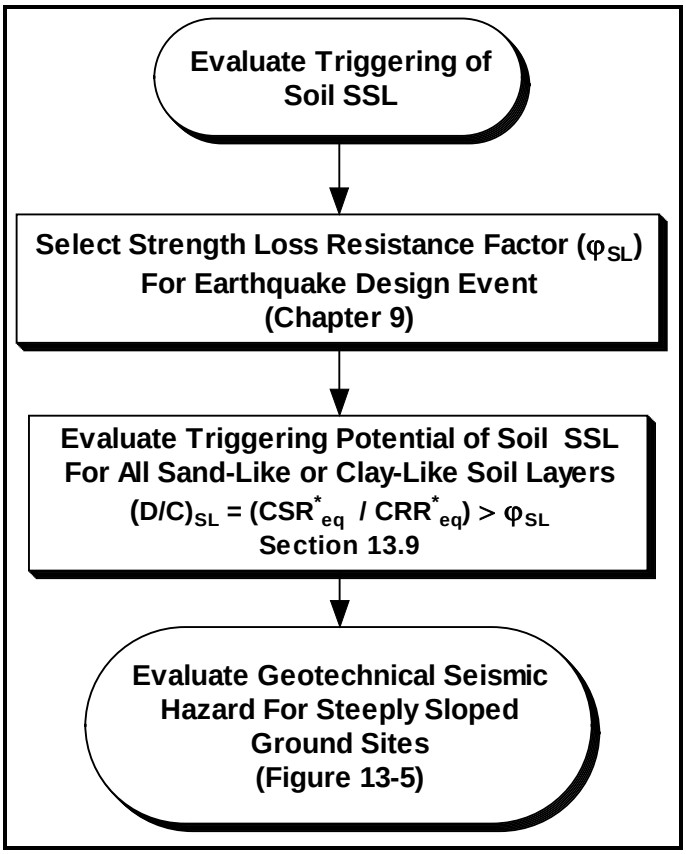

Figure 13-14 (Continued), Simplified Procedure - Soil SSL At Steeply Sloped Ground Sites

13.9.2 Shear Strength Ratio Triggering Method

The Shear Strength Ratio (SSR) method proposed by Olson and Stark (2003) has been adapted to evaluate cyclic liquefaction triggering for Sand-Like soils and cyclic softening of Clay-Like soils at steeply sloped sites subject to static shear stresses. This soil SSL triggering method consists of the following two parts:

1. Screen Sand-Like soils for Contractive behavior based on Contractive/Dilative correlations with in-situ testing (SPT and CPT) for Sand-Like soils (Section 13.9.2.1).

2. Evaluate soil SSL triggering of Sand-Like and Clay-Like soils by dividing the static (Section 13.9.2.3), seismic, and other shear stresses that the soil is exposed to (Demand, D) by the undrained shear strength of the soil (Capacity, C) to obtain the SSL ratio $(D/C)_{SL}$ and determine if the soil SSL triggering potential exists. The overall procedure is presented in Section 13.9.2.2.

13.9.2.1 Screening of Sand-Like Soils For Contractive Behavior

In addition to the soil SSL susceptibility screening criteria indicated in Section 13.6, this method requires the screening of Sand-Like soils for contractive behavior. Sand-Like soils must have contractive behavior in order to be subject to flow failure. The screening for contractive

behavior is accomplished by plotting either SPT ($N^*_{1,60}$) or CPT ($q_{c,1}$) values on the horizontal axis as a function of the pre-failure vertical effective stress (σ'_{vo}) as indicated in Figure 13-15. After the in-situ testing values have been plotted, the Fear and Robertson (1995) soil boundary behavior relationship is plotted on the graph as indicated to determine which Sand-Like soil layers (Section 13.6) meet the contractive soil requirement of the SSR method. The Fear and Robertson (1995) soil boundary for contractive/dilative behavior relationship equations are provided below for CPT and SPT in-situ testing.

$$\left(\sigma'_{vo}\right)_{SPT-Boundary} = 9.58 \times 10^{-4} \left(N^*_{1,60}\right)^{4.79} \qquad \text{Equation 13-3}$$

$$\left(\sigma'_{vo}\right)_{CPT-Boundary} = 1.10 \times 10^{-2} \left(q_{c,1}\right)^{4.79} \qquad \text{Equation 13-4}$$

Where,

- σ'_{vo} = Effective overburden stress (or σ'_v), units of kPa.
- $N^*_{1,60}$ = Normalized SPT-N values (Blows/foot) See Chapter Section 13.11.1 for SPT corrections.
- $q_{c,1}$ = CPT corrected tip resistance, units of MPA. See Section 13.11.1 for CPT corrections.

SPT or CPT values of Sand-Like soils that plot on the *Contractive* side of the boundary (left of boundary) are confirmed to be susceptible to flow failure as indicated by the liquefaction case histories evaluated by Olson and Stark (2003) plotted in Figure 13-15.

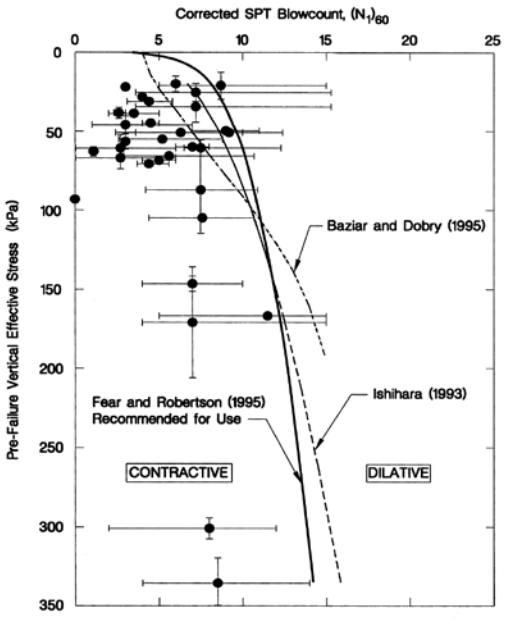

SPT ($N_{1,60}$) Contractive Behavior Evaluation

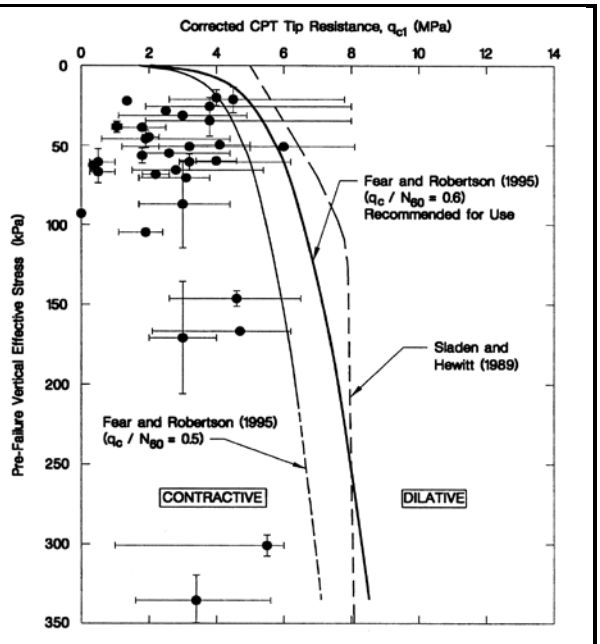

CPT ($q_{c,1}$) Contractive Behavior Evaluation

Figure 13-15, Contractive Soil Behavior Evaluation (Olson and Stark, 2003 with permission from ASCE)

13.9.2.2 Evaluate Soil SSL SSR Triggering Method

Soil SSL triggering of Sand-Like and Clay-Like soils is determined by dividing the static, seismic, and other shear stresses that the soil is subjected to (Demand, D) by the undrained shear strength of the soil (Capacity, C) to obtain the strength loss ratio $(D/C)_{SL}$. The LRFD equation that is used to evaluate the onset of strength loss (SL) at steeply sloped ground site conditions is provided below:

$$\left(\frac{D}{C}\right)_{SL} \leq \varphi_{SL} \qquad \text{Equation 13-5}$$

The Demand (D) is computed by adding the static driving shear stress (τ_{Static}), average seismic shear stress ($\tau_{Seismic}$), and other shear stresses (τ_{Other}) as indicated by the following equation.

$$D = \gamma\left(\tau_{Static} + \tau_{Seismic} + \tau_{Other}\right) \qquad \text{Equation 13-6}$$

The Capacity (C) of the soil is the undrained peak shear strength (τ_{Peak}) as determined for either Sand-Like Soils (Cohesionless) or Clay-Like Soils (Cohesive) as determined from Chapter 7. The peak undrained shear strength for cohesionless soils should be estimated based on the yield shear strength ($\tau_{Yield} = S_u(yield)$) and the peak undrained shear strength ($\tau = \tau_{Yield}$) for cohesive soils should be estimated from either laboratory testing or in-situ testing.

The triggering of soil SSL for steeply sloped ground sites occurs when the strength loss ratio $(D/C)_{SL}$ is greater than the strength loss resistance factor (φ_{SL}) provided in Chapter 9.

$$\left(\frac{D}{C}\right)_{SL} = \frac{\left(\tau_{Static} + \tau_{Seismic} + \tau_{Other}\right)}{\tau_{Peak}} > \varphi_{SL} \qquad \text{Equation 13-7}$$

Since the SSR method for evaluating soil SSL triggering at steeply sloped project site conditions is a deterministic procedure, a load factor, γ, of unity (1.0) is used and the resistance factor, φ_{SL}, accounts for the site variability and the level of acceptable risk of soil SSL. As research advances and soil SSL analytical models are calibrated for LRFD design methodology, adjustments will be made in the implementation of the LRFD design methodology.

The process to evaluate triggering of soil SSL for steeply sloped ground is as follows:

1. The triggering of soil SSL begins by conducting a slope stability of the pre-failure geometry. The slope stability search should evaluate both circular and sliding wedge potential failure surfaces in accordance with Chapter 17. Spencer's Slope Stability method is required.

2. The critical failure surface is then divided into *n* slices (typically 10 to 15 slices) of length, L_i.

3. Compute the static shear stress (τ_{Static}) for each slope stability slice (length, L_i) susceptible to soil SSL at the onset of flow failure, in accordance with Section 13.9.2.3.

4. Compute the average, magnitude weighted, seismic induced stress ($\tau_{Seismic}$) for each slice (length, L_i) susceptible to soil SSL in accordance with the following equation.

$$\tau_{Seismic} = \frac{0.65 \times \tau_{max}}{MSF} \qquad \text{Equation 13-8}$$

Where,

τ_{max} = Maximum earthquake induced shear stress. τ_{max} is computed by the *Simplified Procedure* in accordance with the Section 13.10.1.1 or by performing a site-specific response analysis in accordance with Section 13.10.1.2.

MSF = Magnitude Scaling Factor computed in accordance with Section 13.10.2.

5. Compute any other shear stresses (τ_{Other}) that may be applicable such as those induced by surcharges, foundation loadings, etc.

6. Determine the value of the peak undrained shear strength ratio ($\tau_{Peak}/\sigma'_{vo} = \tau_{Yield}/\sigma'_{vo}$) for Sand-Like soils (cohesionless soils) or the undrained shear strength ratio ($\tau_{Peak}/\sigma'_{vo} = S_u/\sigma'_{vo}$) for Clay-Like soils (cohesive soils) in accordance with Chapter 7. Compute the undrained shear strength for Sand-Like soils ($\tau = \tau_{Yield} = S_u(yield)$) or Clay-Like soils ($\tau = S_u$) for each slice of the critical failure surface by multiplying the peak undrained shear strength ratio (τ/σ'_{vo}) by the effective overburden stress (σ'_{vi}) for each slice.

7. Compute the soil SSL resistance ratio $(D/C)_{SL}$ as indicated by the following equation for each slice.

$$\left(\frac{D}{C}\right)_{SL} = \frac{\left(\tau_{Static} + \tau_{Seismic} + \tau_{Other}\right)}{\tau} \qquad \text{Equation 13-9}$$

8. The onset of cyclic liquefaction in Sand-Like soils or cyclic softening in Clay-Like soils, occurs when the strength loss ratio $(D/C)_{SL-i}$ for each slice (length, L_i) susceptible to soil SSL is greater than the LRFD resistance factor (φ_{SL}) presented in Chapter 9 as indicated by the following equation.

$$\left(\frac{D}{C}\right)_{SL-i} > \varphi_{SL} \qquad \text{Equation 13-10}$$

The overall process for conducting a soil SSL triggering analysis using the SSR method for steeply sloped project site conditions is presented in a flow chart in Figure 13-16.

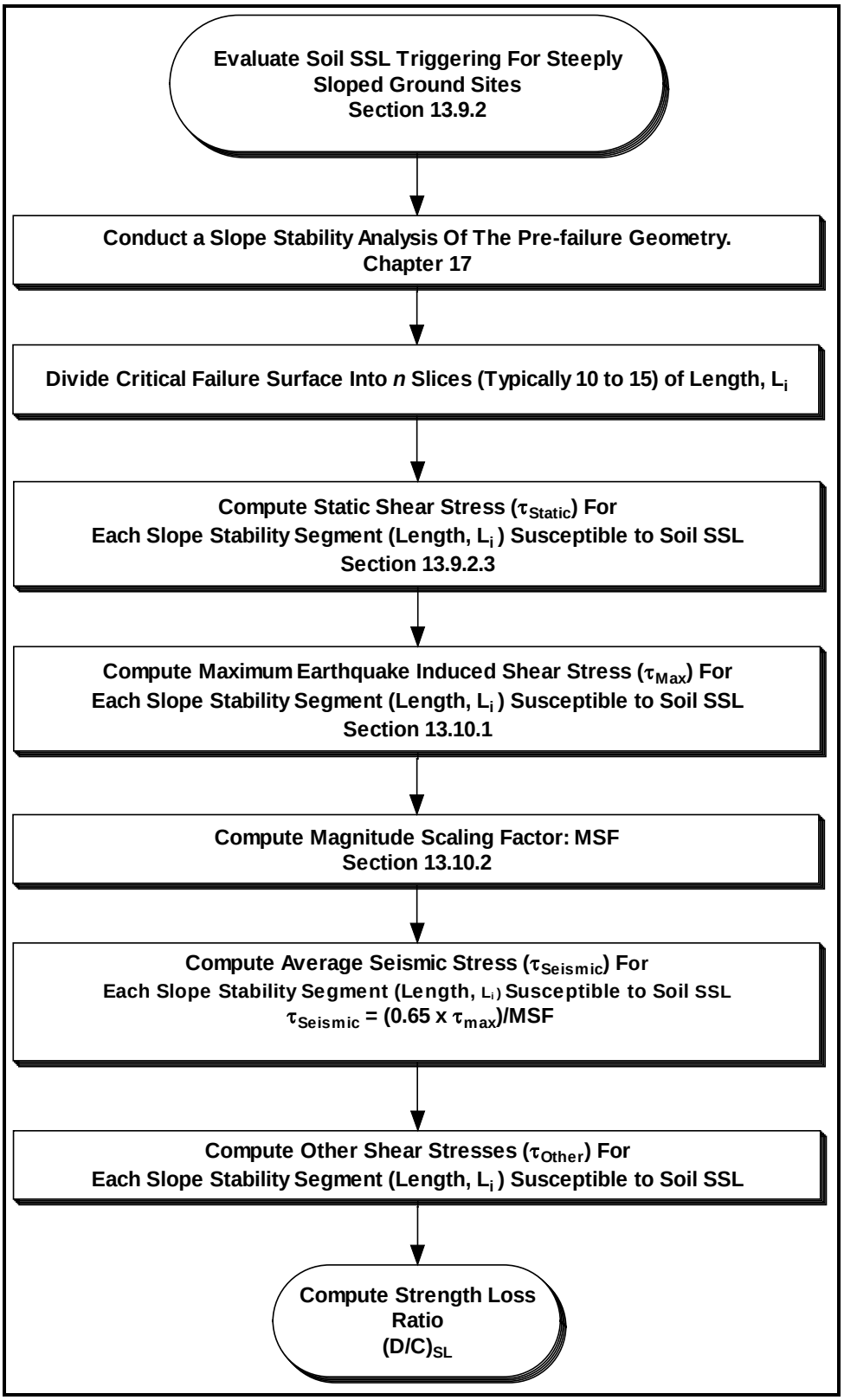

Figure 13-16, SSRA Soil SSL Triggering At Steeply Sloped Ground Sites

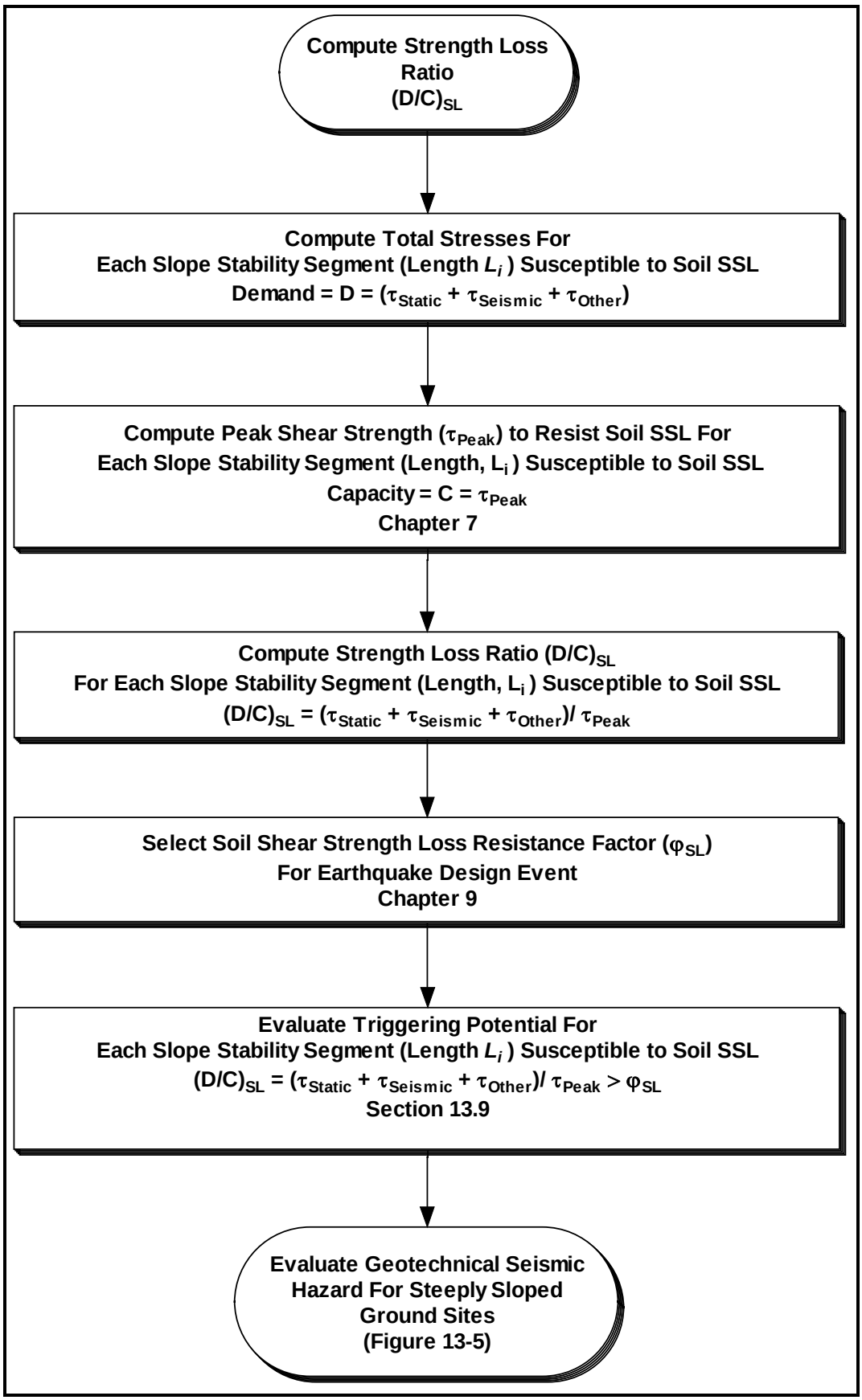

Figure 13-16 (Continued), SSRA Soil SSL Triggering At Steeply Sloped Ground Sites

13.9.2.3 Static Shear Stress (τ_{Static}) of Soils Susceptible to Soil SSL

The static shear stress (τ_{Static}) at the onset of flow failure ($(D/C)_{Stability}$ = 1) for each soil layer susceptible to soil SSL (Sand-Like soils and Clay-Like soils) can be computed by performing a slope stability back analysis of the pre-failure geometry. The slope stability search should evaluate both circular and sliding wedge potential failure surfaces in accordance with Chapter 17 with Spencer's Slope Stability method being required as well. Slope stability back analysis of the static shear stress (τ_{Static}) for a single soil layer susceptible to soil SSL is relatively straight forward when compared to slope failure surfaces that have multiple soil layers that are susceptible to soil SSL as indicated by the following procedure.

1. **Single Layer of Soil SSL:** The soil layers that intersect the failure surface that are not susceptible to SSL are assigned fully mobilized drained or undrained shear strengths. The soil layers susceptible to soil SSL that intersect the failure surface are initially assigned a "trial" soil shear strength (τ). The "trial" soil shear strength (τ) should range from the residual shear stress due to soil SSL (τ_{rl}, τ_{rs}, or $\tau_{remolded}$) to the fully mobilized undrained or drained shear strengths (τ or τ'). The soil shear strength (τ) for the layer susceptible to soil SSL is varied iteratively until the slope stability ratio, $(D/C)_{Stability}$ = 1 that is equivalent to the static driving stress (τ_{Static}) prior to flow failure of the slope. Alternatively, some slope stability software allow the input of the static shear strength ratio directly ($\alpha = \tau_{Static}/\sigma'_{vo}$) for soil layers susceptible to soil SSL. For this software option, the static shear strength ratio (α) is varied iteratively until the slope stability ratio, $(D/C)_{Stability}$ = 1 that is equivalent to the static shear strength ratio ($\alpha = \tau_{Static}/\sigma'_{vo}$) prior to failure of the slope.

2. **Multiple Layers of Soil SSL:** A comprehensive methodology for multiple layers of soils susceptible to soil SSL within the failure surface has not been fully developed as of this time. The following procedure can conservatively evaluate soil SSL triggering when multiple soil layers are susceptible to soil SSL.

   A. Determine the static shear stress (τ_{Static}) for each soil layer susceptible to soil SSL by assuming that each layer behaves independently of the other layers using the method described above in Item 1 for "Single Layer of Soil SSL." This assumption does not take into account any redistribution of static shear stresses between soil layers that are susceptible to soil SSL.

   B. Continue with the soil SSL triggering analysis.

   C. Each layer that has a shear loss ratio $(D/C)_{SL} > \varphi_{SL}$ shall be conservatively assumed to have the potential for soil SSL triggering.

D. Each layer that has a shear loss ratio $(D/C)_{SL} \leq \varphi_{SL}$, indicates that soil SSL triggering would not occur if it were a single layer of soil. Since there are multiple layers of soil SSL susceptibility this soil layer may still be subject to soil SSL as a result of static shear stress redistribution when soil SSL occurs in other layers within the failure surface. Another slope stability back analysis of the layer being evaluated to determine the static shear stress (τ_{Static}) for this layer is required using the method described above for "Single Layer of Soil SSL" and the following soil shear strength parameters. Soils not susceptible to soil SSL are assigned fully mobilized drained or undrained shear strengths. Soils that have been identified as having the potential for soil SSL are assigned residual shear stress due to soil SSL (τ_{rl}, τ_{rs}, or $\tau_{remolded}$) in accordance with Section 13.12. Continue with the soil SSL triggering analysis. If the soil layer being re-analyzed has a shear loss ratio $(D/C)_{SL} > \varphi_{SL}$, the layer shall be conservatively assumed to have the potential for soil SSL triggering. If the shear loss ratio $(D/C)_{SL} \leq \varphi_{SL}$, the layer shall be assumed not to be subject to soil SSL triggering.

An alternative to this procedure that is complex and requires significant experience would be to perform a numerical analysis of the slope stability to evaluate the static shear stresses (τ_{Static}) for the soil layers susceptible to soil SSL. Numerical modeling of the slope stability to obtain static stresses will require approval from the PCS/GDS. If numerical modeling is permitted, only the static driving shear stresses (τ_{Static}) or static shear strength ratio ($\alpha = \tau_{Static}/\sigma'_{vo}$) computed will be used for the evaluation of soil SSL triggering potential. The numerical modeling shall be compared to the method provided above.

3. If the static shear strength ratio is computed directly ($\alpha = \tau_{Static}/\sigma'_{vo}$) for soil layers susceptible to soil SSL, the static shear stress (τ_{Static}) for this layer can be computed by multiplying the static shear strength ratio (α) by the effective overburden stress, σ'_{vi}, for that segment represented along the soil failure surface.

4. If the soil shear strength (τ) that has been computed corresponds to the static driving stress (τ_{Static}) prior to failure of the slope, then divide the complete critical failure surface into n slices (typically 10 to 15 slices) of length, L_i.

5. Determine the weighted average effective vertical overburden stress (σ'_{vo}) as indicated by the following equation:

$$\bar{\sigma}'_{vo} = \frac{\sum_{i=1}^{n} \sigma'_{vi} L_i}{\sum_{i=1}^{n} L_i} \qquad \text{Equation 13-11}$$

Where σ'_{vi} = effective vertical overburden stress at each failure slice along the soil failure surface.

6. Calculate the average static shear stress ratio ($\tau_{Static} / \bar{\sigma}'_{vo}$) for all soil layers susceptible to soil SSL.σ

7. Compute the static driving shear stress(τ_{Static}) for each slice of the critical failure surface (length, L_i) by multiplying the average static shear stress ratio ($\tau_{Static} / \bar{\sigma}'_{vo}$) for that soil layer by the effective overburden stress for the slice, σ'_{vi}, along the soil failure surface.

8. The static shear strength ratio ($\alpha = \tau_{Static} / \sigma'_{vo}$) for soil layers can be computed by dividing static driving shear stress (τ_{Static}) by the effective overburden stress for the slice, σ'_{vi}, along the soil failure surface.

13.10 CYCLIC STRESS RATIO (CSR)

The earthquake-induced cyclic stresses in the soil (Demand, D) are quantified by the cyclic stress ratio (CSR). The equivalent uniform cyclic stress ratio, CSR^*_{eq}, is the equivalent uniform earthquake-induced stress that has been magnitude-weighted (M_w = 7.5) as shown in the following equation:

$$CSR^*_{eq} = CSR_{eq,7.5} = \frac{CSR_{eq}}{(MSF)} \qquad \text{Equation 13-12}$$

Where,

CSR_{eq} = is the equivalent earthquake-induced stress (Section 13.10.1)
MSF = is the Magnitude Scaling Factor (Section 13.10.2)

13.10.1 Equivalent Earthquake-Induced Stress (CSR_{eq})

The equivalent earthquake-induced stress, CSR_{eq}, sometimes referred to as the average earthquake-induced stress, is defined as shown in the following equation:

$$CSR_{eq} = 0.65\, CSR_{Peak} \qquad \text{Equation 13-13}$$

Where CSR_{Peak} is the maximum earthquake-induced cyclic stress ratio. Note that a factor of 0.65 is included in Equation 13-13 to obtain an "average" or equivalent CSR_{eq} value. The method of computing the maximum earthquake-induced stress ratio, CSR_{Peak}, depends on the method of performing the site response analysis discussed in Chapter 12.

13.10.1.1 Simplified Procedure Determination of CSR_{Peak}

The *Simplified Procedure* for determination of the CSR_{Peak} should typically be used for evaluation of soil SSL. The *Simplified Procedure* for computing CSR_{Peak} is shown in the following equation:

$$CSR_{Peak} = \frac{\tau_{Max}}{\sigma'_{vo}} = \left(\frac{a_{max}}{g}\right)\left(\frac{\sigma_v}{\sigma'_{vo}}\right) r_d \qquad \text{Equation 13-14}$$

Where,

a_{max} = Peak horizontal ground acceleration is in units of acceleration due to gravity (g) . The peak horizontal ground acceleration is determined from the three-point design response spectrum method in Chapter 12.

σ_v = Total overburden stress

σ'_{vo} = Effective overburden stress

r_d = Shear stress reduction coefficient (dimensionless)

τ_{max} = Maximum earthquake induced stress with depth. In the Simplified Procedure the maximum earthquake induced stress (τ_{max}) is approximated by the following equation.

$$\tau_{Max} = \left(\frac{a_{max}}{g}\right)\sigma_v \, r_d \qquad \text{Equation 13-15}$$

The shear stress reduction coefficient, r_d, is a parameter that describes the ratio of cyclic stresses for a flexible column to the cyclic stresses of a rigid column ($r_d = \tau_{soil\ column}/\tau_{rigid}$). For an r_d = 1, the flexibility of the soil column would correspond to rigid body behavior. One-dimensional dynamic site response studies (Seed and Idriss, 1971: Golesorkhi, 1989; Idriss, 1999; and Cetin et al., 2004) have shown that the shear stress reduction factor is dependent on the ground motion characteristics (i.e. intensity and frequency content), shear wave velocity profile of the site (i.e. site stiffness), and nonlinear dynamic soil properties. Idriss (1999) performed several hundred parametric site response analyses and developed a shear stress reduction coefficient, r_d that was expressed as a function of depth and earthquake moment magnitude (M_W) as indicated in Figure 13-17.

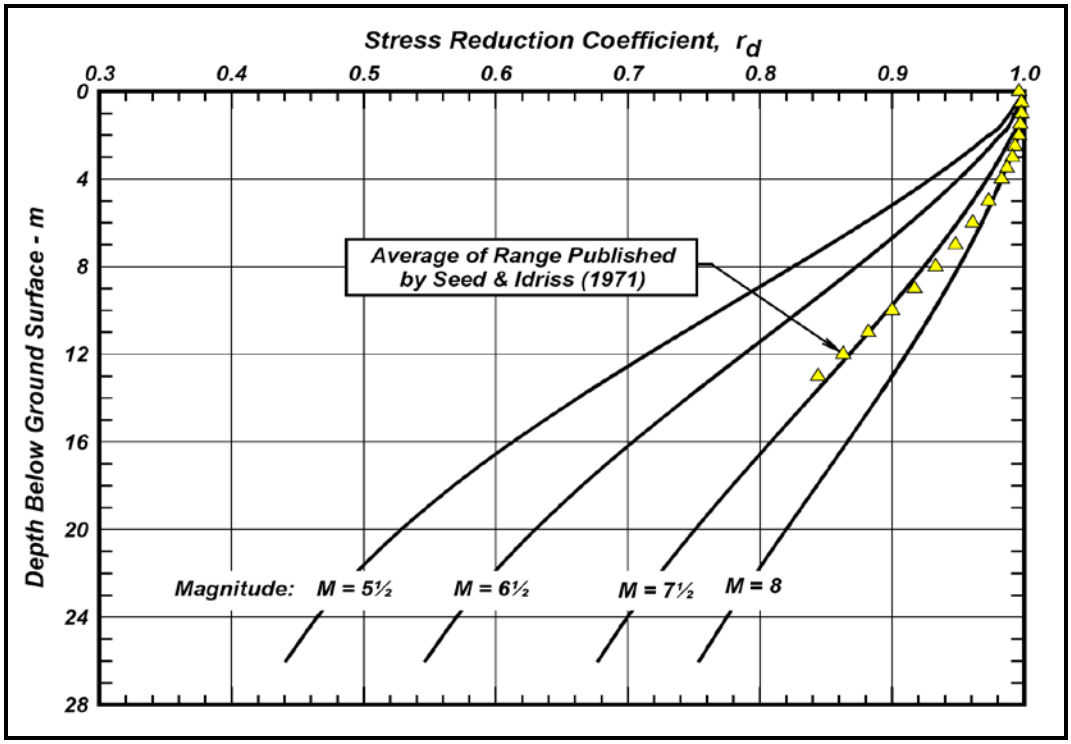

Figure 13-17, Variations of Shear Stress Reduction Coefficient, r_d (Idriss, 1999)

Shear stress reduction coefficient (r_d) equations for US customary units were modified from SI equations proposed by Idriss (1999) as indicated below.

$$r_d = \exp\left(\alpha + \left(\beta \cdot M_w\right)\right) \qquad \text{Equation 13-16}$$

$$\alpha = -1.012 - 1.126 \sin\left(\left(\frac{\left(\frac{z}{3.28}\right)}{11.73}\right) + 5.133\right) \qquad \text{Equation 13-17}$$

$$\beta = 0.106 + 0.118 \sin\left(\left(\frac{\left(\frac{z}{3.28}\right)}{11.28}\right) + 5.142\right) \qquad \text{Equation 13-18}$$

Where,

z = Depth below ground surface (feet)
M_W = Earthquake moment magnitude

Note that the arguments inside the "**sin**" terms above are in radians. For the purposes of evaluating soil SSL, the CSR_{Peak} should not be evaluated using this method for depths greater than 80 feet (24 m). The uncertainty increases for shear stress reduction coefficients (r_d) at depths greater than *z* > 65 feet (20 m). When the maximum earthquake-induced stress ratio,

CSR_{Peak}, is required for depths greater than 80 feet, a site-specific response analysis (Section 13.10.1.2) may be warranted with approval of the PCS/GDS.

13.10.1.2 Site Specific Response Determination of CSR_{Peak}

When approved by the PCS/GDS, the maximum earthquake-induced stress ratio, CSR_{Peak}, can be computed for depths greater than 80 feet (24 m) by using the results of a site-specific seismic response analysis (Chapter 12) as indicated by the following equation.

$$CSR_{Peak} = \frac{\tau_{max}}{\sigma'_{vo}} \qquad \text{Equation 13-19}$$

Where τ_{max} is the maximum earthquake-induced cyclic shear stress that is obtained from the site-specific response analysis of the ground motions and σ'_{vo} is the effective overburden stress at the depth being evaluated. Site-specific seismic response analyses referenced in Chapter 12 are typically one-dimensional equivalent linear analyses. Because the one-dimensional equivalent linear analyses have a reduced reliability as ground shaking levels (PGA) increase above 0.40g in softer soils or where the maximum shearing strain amplitudes exceed 1 to 2 percent, a comparison with the *Simplified Procedure* should be performed for depths greater than 80 feet (24 m) and the more conservative values should be used. In lieu of using the more conservative analytical results, the PCS/GDS should be consulted to determine if a nonlinear effective stress site response method should be used to determine the maximum earthquake-induced shear stress, τ_{max}.

13.10.2 Magnitude Scaling Factor (MSF)

The Magnitude Scaling Factor, MSF, is used to scale the equivalent uniform earthquake-induced stresses, CSR_{eq}, to the duration that is typical of an average earthquake event of magnitude, $M_w = 7.5$. A large amount of scatter in the magnitude scaling factor, MSF, is observed from various studies presented in Youd et al. (2001), particularly at the lower range of earthquake moment magnitudes ($5.5 < M_w < 6.5$). Boulanger and Idriss (2007) have recommended MSF for Sand-Like soils (MSF_{Sand}) and for Clay-Like soils (MSF_{Clay}) as indicated in Figure 13-18. Because the predominant earthquake in South Carolina had an approximate earthquake magnitude of 7.3 and the target scaling earthquake is a 7.5, the variability observed in the magnitude scaling factor studies should have minimal impact on the liquefaction analyses.

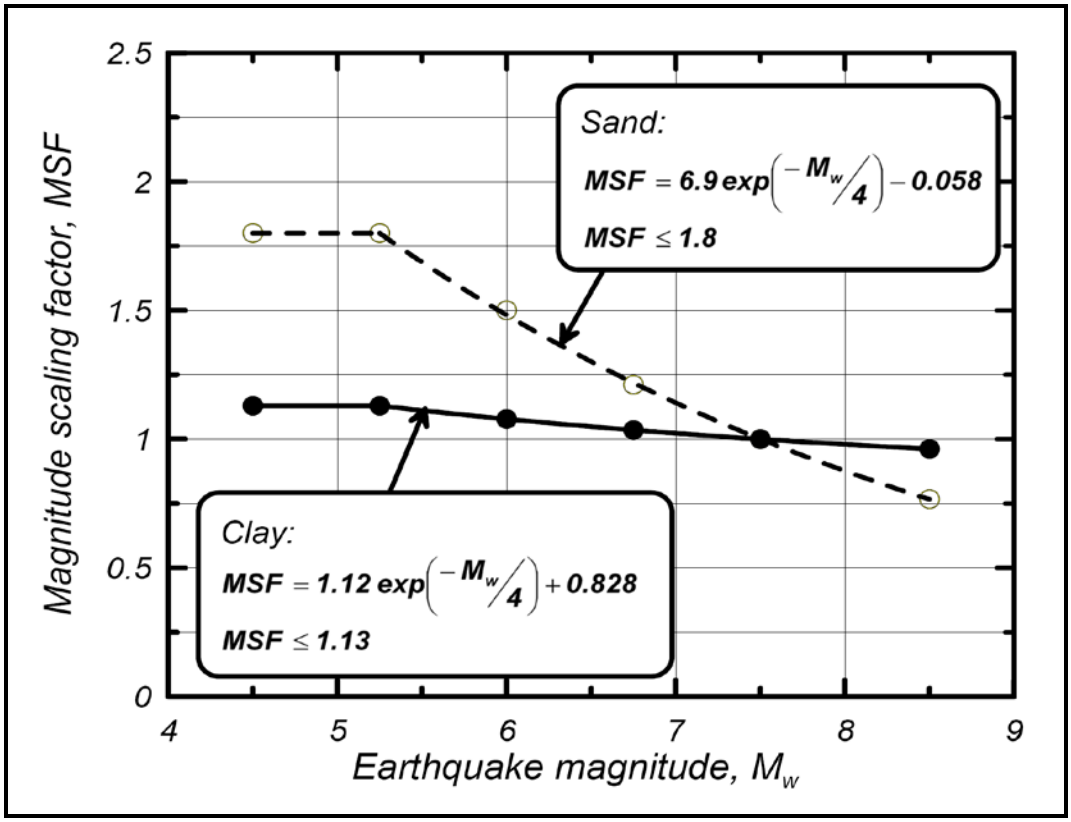

Figure 13-18, Magnitude Scaling Factor (MSF)
(Boulanger and Idriss, 2007 with permission from ASCE)

In lieu of using Figure 13-18, the following equations may be used to compute the MSF_{Sand} and MSF_{Clay}.

$$MSF_{Sand} = 6.9 \cdot \exp\left(-0.25M_W\right) - 0.058 \le 1.80 \qquad \text{Equation 13-20}$$

$$MSF_{Clay} = 1.12 \cdot \exp\left(-0.25M_W\right) + 0.828 \le 1.13 \qquad \text{Equation 13-21}$$

Where, M_w is the moment magnitude of the design earthquake being evaluated for soil SSL triggering.

13.11 CYCLIC RESISTANCE RATIO (CRR)

The soil's resistance to soil SSL (Capacity, C) is quantified by the cyclic resistance ratio (CRR). The cyclic resistance ratio (CRR) for Sand-Like soils is typically characterized as a curvilinear boundary that indicates the relationship between cyclic stress ratio (CSR) and in-situ testing results from SPT or CPT. The cyclic resistance ratio (CRR) for Clay-Like soils is typically characterized as a linear reduction of the undrained shear strength that indicates the relationship between cyclic stress ratio (CSR) and in-situ testing results from SPT or CPT. A typical cyclic resistance ratio (CRR) curve for Sand-Like soils is shown in Figure 13-19(A) and for Clay-Like soils is shown in Figure 13-19(B).

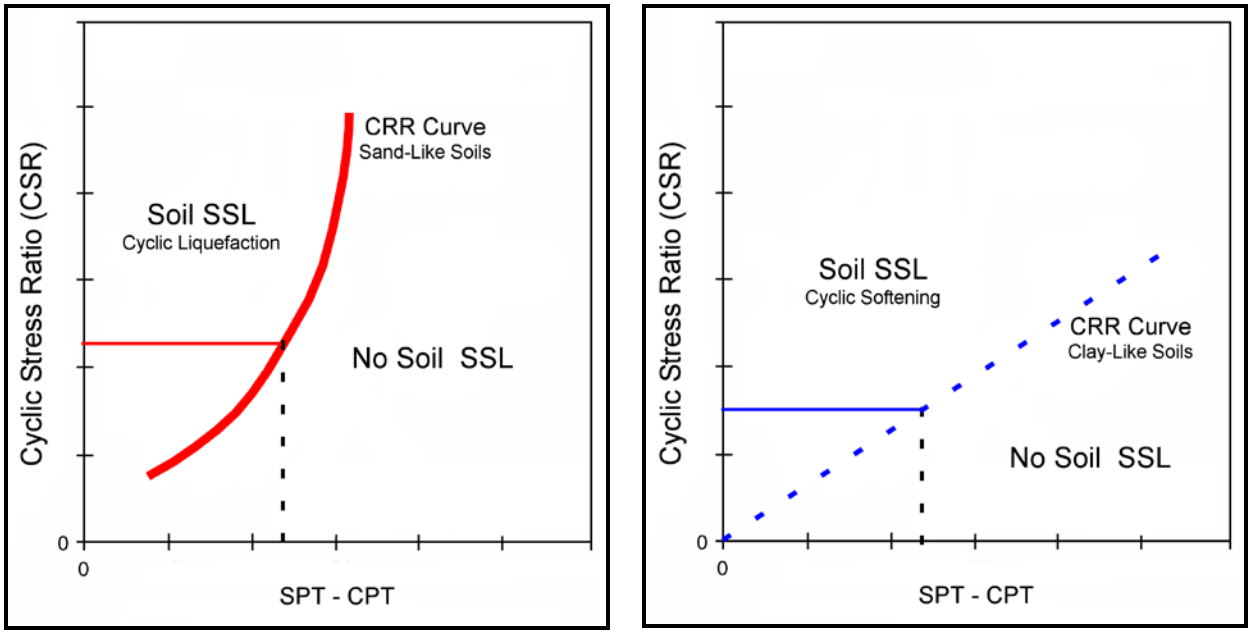

(A) CRR Curve Sand-Like Soils **(B) CRR Curve Clay-Like Soils**

Figure 13-19, Typical CRR Curve

For a specific earthquake-induced CSR value, the value located on the CRR boundary establishes a threshold in-situ testing value whereas in-situ testing results greater than the threshold value will not be susceptible to soil SSL and values less than the threshold value are subject to soil SSL.

Several empirical procedures have been developed to determine the cyclic resistance ratio (CRR) of Holocene (< 10,000 years) Sand-Like soils based on in-situ testing. In-situ testing that is acceptable to be used on SCDOT projects are Standard Penetration Testing (SPT) and Cone Penetrometer Testing (CPT). A comparison of advantages and disadvantages of these in-situ tests for determination of CRR are presented in Table 13-2. SPT and CPT measured results must be adjusted in accordance with Section 13.11.1.

Table 13-2, CRR Determination Based on Types of In-situ Testing (Modified after Youd and Idriss, 1997)

Feature	Type of In-situ Testing	
	SPT	**CPT**
Number of test measurements at liquefaction sites	Substantial	Many
Type of stress-strain behavior influencing test	Partially Drained, Large strain	Drained, Large Strain
Quality control and repeatability	Poor to Good	Very Good
Detection of variability of soil deposits	Good	Very Good
Soil types in which test is recommended	Non-Gravel	Non-Gravel
Test provides sample of soil	Yes	No
Test measures index or engineering property	Index	Index

The normalized cyclic resistance ratio curves (CRR^{*} = $CRR_{M=7.5,1\ tsf}$) for Sand-Like soils presented in Sections 13.11.2 and 13.11.3 are magnitude weighted (M_W=7.5) and normalized to a reference effective overburden stress of σ'_V = 1 tsf. These correlations were derived based on

the relative state parameter index (ξ_R) by Idriss and Boulanger (2004). The corresponding CRR-ξ_R relationships derived from these two liquefaction correlations are shown in Figure 13-20 to illustrate the consistency between the SPT and CPT methods to predict field cyclic resistance ratio.

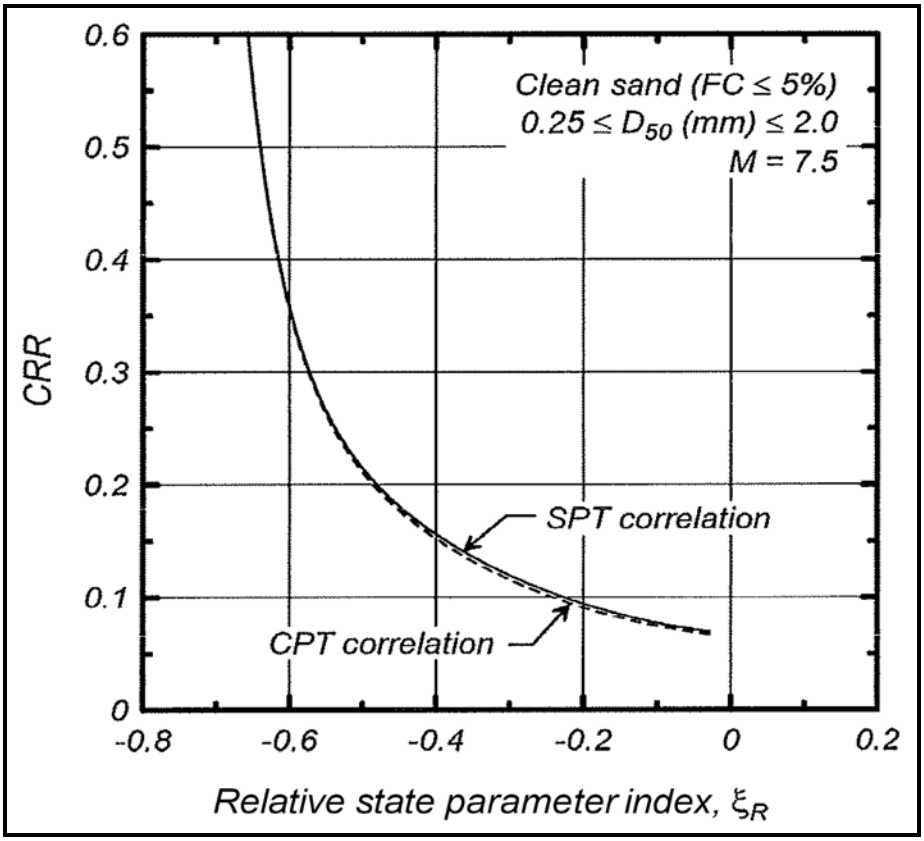

Figure 13-20, Field CRR-ξ_R Correlations Based on SPT and CPT (Idriss and Boulanger, 2004)

The normalized cyclic resistance ratio ($CRR^* = CRR_{M=7.5}$) for Clay-Like soil presented in Section 13.11.4 is magnitude weighted ($M_W = 7.5$).

Shear wave velocities (V_s) and the Becker Penetration Tests (BPT) methods for determination of the soil's resistance for liquefaction shall not be used for routine SCDOT soil SSL evaluations unless approved by the PCS/GDS.

The normalized cyclic resistance ratio (CRR^*) correlations must be further corrected to account for the effects of high overburden stress on Sand-Like soils (K_σ), effects of soil aging in Sand-Like soils (K_{DR}), and effects of initial static shear stress on Sand-Like Soils and Clay-Like Soils (K_α). The corrected and normalized cyclic resistance ratio curves (CRR^*_{eq}) are computed as indicated in the following general equation:

$$\boldsymbol{CRR^*_{eq} = CRR^* (K_\sigma)(K_{DR})(K_\alpha)} \qquad \text{Equation 13-22}$$

Where,

CRR* = $CRR_{M=7.5,1\ tsf}$ = normalized cyclic resistance ratio magnitude weighted (M_W=7.5) and normalized to a reference effective overburden stress of σ'_V = 1 tsf. (Sand-Like Soil: Sections 13.11.2 & 13.11.3; Clay-Like Soil: Section 13.11.4)

K_σ = High overburden stress correction factor for Sand-Like Soils (Section 13.11.5)

K_{DR} = Age correction factor for Sand-Like Soils (Section 13.11.6)

K_α = Static shear stress ratio correction factor for Sand-Like and Clay-Like soils (Section 13.11.7)

13.11.1 In-Situ Testing Corrections For Evaluating Soil SSL

13.11.1.1 Correlations For Relative Density From SPT and CPT

Correlations to compute relative density (D_r) from SPT and CPT testing may be required for soil SSL analyses. The correlations proposed by Boulanger (2003b) to relate SPT N-values ($N^*_{1,60}$) and CPT tip resistance ($q_{c,1,N}$) to relative density (D_r) are provided below.

$$D_R = \left(\frac{N^*_{1,60}}{46}\right)^{0.5} \qquad \text{Equation 13-23}$$

$$D_R = 0.478\left(q_{c,1N}\right)^{0.264} - 1.063 \qquad \text{Equation 13-24}$$

Where,

$N^*_{1,60}$ = Corrected SPT N-value (Section 13.11.1.3) in blows per foot

$q_{c,1,N}$ = Normalized CPT tip resistance (Section 13.11.1.4) (unitless)

The relative density correlations (Equations 13-23 and 13-24) for SPT and CPT results can be combined to develop an SPT equivalent correlation for normalized CPT tip resistance as indicated by the following Equation.

$$N^*_{1,60} = 46\left[0.478\left(q_{c,1N}\right)^{0.264} - 1.063\right]^2 \qquad \text{Equation 13-25}$$

13.11.1.2 Overburden Reference Correction Factors For Sand-Like Soils For SPT And CPT

In order to obtain consistencies between SPT and CPT, these corrections shall only apply to Chapter 13. Normalized overburden reference (σ'_V = 1 tsf) correction factors developed by Boulanger (2003b) should be used when evaluating soil SSL as indicated by the following equation:

$$C_N = \left(\frac{P_a}{\sigma'_{vo}}\right)^m \qquad \text{Equation 13-26}$$

Where,

P_a = Atmospheric Pressure (1 atm = 1 tsf)

σ'_{vo} = Effective overburden stress (Use same units as used for P_a)

m = Exponent that was developed for sands at different relative densities (D_R) from calibration chamber data for SPT and CPT in-situ testing. Boulanger (2003b) recommended that exponent m to be computed as indicated below:

$$\boldsymbol{m} = 0.784 - \left(0.521 \cdot \boldsymbol{D_R}\right) \qquad \text{Equation 13-27}$$

Relative density (D_R) correlations for SPT and CPT in Section 13.11.1.1 can be used to compute exponent m proposed by Boulanger (2003b) based on Equation 13-27.

The normalized effective overburden factor (C_N) can be determined for SPT values of $N^*_{1,60} \leq$ 46 blows/foot by using the following equation.

$$\boldsymbol{C_N} = \left(\frac{\boldsymbol{P_a}}{\boldsymbol{\sigma'_{vo}}}\right)^{0.784 - 0.0768\sqrt{\boldsymbol{N^*_{1,60}}}} \leq 1.7 \qquad \text{Equation 13-28}$$

The normalized effective overburden factor (C_N) can be determined for normalized CPT tip resistance values of $21 \leq q_{c,1,N} \leq 254$ (unitless) by using the following equation.

$$\boldsymbol{C_N} = \left(\frac{\boldsymbol{P_a}}{\boldsymbol{\sigma'_{vc}}}\right)^{1.338 - 0.249\left(\boldsymbol{q_{c,1,N}}\right)^{0.264}} \leq 1.7 \qquad \text{Equation 13-29}$$

Where,

$N^*_{1,60}$ = Corrected SPT N-value computed (Section 13.11.1.3) in blows per foot

$q_{c,1,N}$ = Normalized CPT tip resistance ($q_{c,1}$) (Section 13.11.1.4) (unitless)

The computation of the normalized effective overburden factor (C_N) indicated in Equations 13-28 and 13-29 for SPT and CPT, respectively, requires the iteration until there is convergence because C_N for SPT depends on $N^*_{1,60}$ and C_N for CPT depends on $q_{c,1,N}$. The normalized effective overburden factor (C_N) for SPT and CPT results are plotted in Figure 13-21.

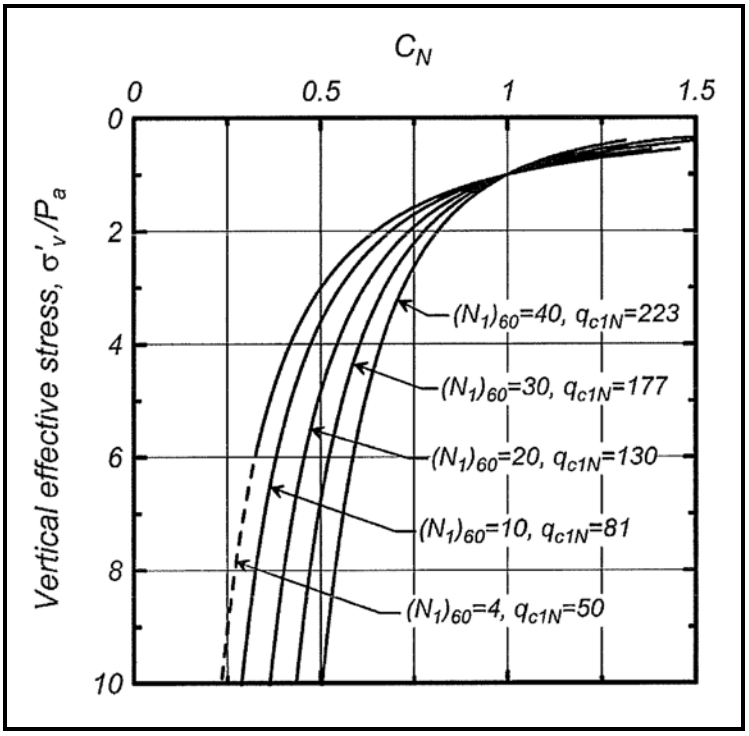

Figure 13-21, Overburden Correction Factor C_N
(Boulanger, 2003b with permission from ASCE)

13.11.1.3 SPT Blow Count Corrections for Soil SSL Evaluations

The measured Standard Penetration Test blow count, N_{meas}, must be standardized and adjusted for overburden prior to being used in soil SSL triggering analyses. Standardized SPT driving resistance, N^*_{60}, accounts for the effects of using non-standard SPT testing by applying corrections to account for hammer energy, SPT equipment, and procedural effects. The standardized SPT driving resistance, N^*_{60}, is adjusted to an effective reference overburden of σ'_V = 1 tsf. The corrected SPT blow count, $N^*_{1,60}$, is computed as indicated by the following equation.

$$N^*_{1,60} = N_{meas}\left(C_R C_S C_B C_E C_N\right) \qquad \text{Equation 13-30}$$

Where,

- N_{meas} = Measured SPT driving resistance. Units of blows per foot of penetration
- C_R = Rod length correction factor
- C_S = Nonstandard sampler correction factor
- C_B = Borehole diameter correction factor
- C_E = Hammer energy correction factor
- C_N = Normalized effective overburden reference of σ'_V = 1 tsf correction factor

The correction factors C_R, C_S, C_B, and C_E are provided in Chapter 7. The normalized effective overburden reference (σ'_V = 1 tsf) correction factor, C_N, is provided in Section 13.11.1.2.

13.11.1.4 CPT Corrections for Soil SSL Evaluations

The measured CPT tip resistance (q_c) and sleeve resistance (f_s) are influenced by the effective overburden stress. This effect is accounted for by adjusting the measured resistances to a reference effective overburden stress of σ'_V = 1 tsf by using correction factor C_N developed for CPT in Section 13.11.1.2. The CPT tip resistance (q_c) measurements obtained in thin stiff layers is corrected by a thin layer correction factor (C_{thin}) as indicated in Chapter 7. The corrected CPT tip resistance ($q_{c,1}$) is computed by adjusting the measured CPT tip resistance (q_c) to a reference effective overburden stress of σ'_V = 1 tsf and correcting for thin layers as indicated by the following equation.

$$q_{c,1} = C_N C_{thin} q_c \qquad \text{Equation 13-31}$$

The normalized corrected CPT tip resistance ($q_{c,1,N}$) is computed by dividing the corrected CPT resistance ($q_{c,1}$) by the atmospheric pressure (P_a = 1 atm = 1 tsf) to eliminate units as indicated by the following equation.

$$q_{c,1,N} = \frac{q_{c,1}}{P_a} \qquad \text{Equation 13-32}$$

The corrected CPT sleeve resistance (f_s) is adjusted to a reference effective overburden stress of σ'_V = 1 tsf as indicated in the following equation.

$$f_{s,1} = C_N f_s \qquad \text{Equation 13-33}$$

The C_N correction factor used for tip resistance (q_c) and sleeve resistance (f_s) are the same value.

13.11.2 Sand-Like Soil - SPT Based CRR* Curves

The Cyclic Resistance Ratio (CRR) correlations for SPT in-situ testing presented by Idriss and Boulanger (2008) shall be used to evaluate Sand-Like soils. Deterministic cyclic resistance ratio curves ($CRR^* = CRR_{Mw=7.5,1\ tsf}$) are moment magnitude weighted, adjusted to a reference effective overburden stress of σ'_V = 1 tsf, and adjusted for fines content. Similarly to the cyclic stress ratio, CSR, a reference earthquake of moment magnitude, M_w, of 7.5 is used. The corrected SPT blow count ($N^*_{1,60}$) is adjusted to an equivalent clean sand (CS) blow count based on the fines content (FC) as indicated by the following equation.

$$N^*_{1,60,CS} = N^*_{1,60} + \Delta N^*_{1,60} \qquad \text{Equation 13-34}$$

Where,

$N^*_{1,60}$ = SPT blow count normalized to a reference effective overburden stress of σ'_V = 1 tsf, corrected for energy (60% - see Section 13.11.1.3). Units of blows/foot

$\Delta N^*_{1,60}$ = Fines content correction for 5% < FC < 35%. The variation in $\Delta N^*_{1,60}$ with fines content is shown in Figure 13-22.

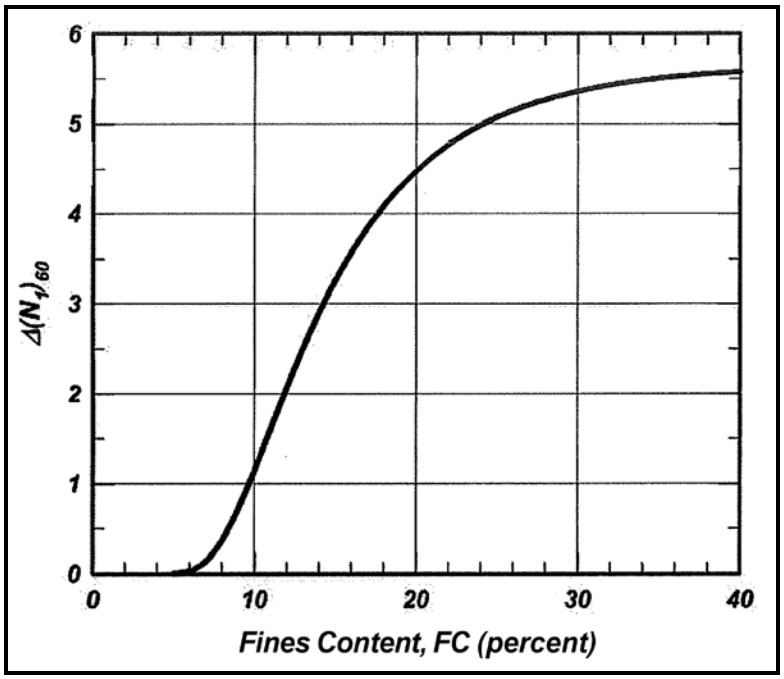

Figure 13-22, Variation in $\Delta N^*_{1,60}$ With Fines Content (Idriss and Boulanger, 2008)

In lieu of using Figure 13-22 the following equation may be used.

$$\Delta N^*_{1,60} = \exp\left(1.63 + \left(\frac{9.7}{FC + 0.01}\right) - \left(\frac{15.7}{FC + 0.01}\right)^2\right) \leq 5.5 \qquad \text{Equation 13-35}$$

Where Fines content (FC) is in percent. Fines content (FC) is based on the soil fraction passing the No. 4 sieve.

Figure 13-23 shows the Idriss and Boulanger (2004) recommended deterministic CRR^* curves for SPT in-situ testing based on an earthquake moment magnitude, $M_w = 7.5$, effective overburden reference stress, $\sigma'_v = 1.0$ tsf, and fines content FC < 5%.

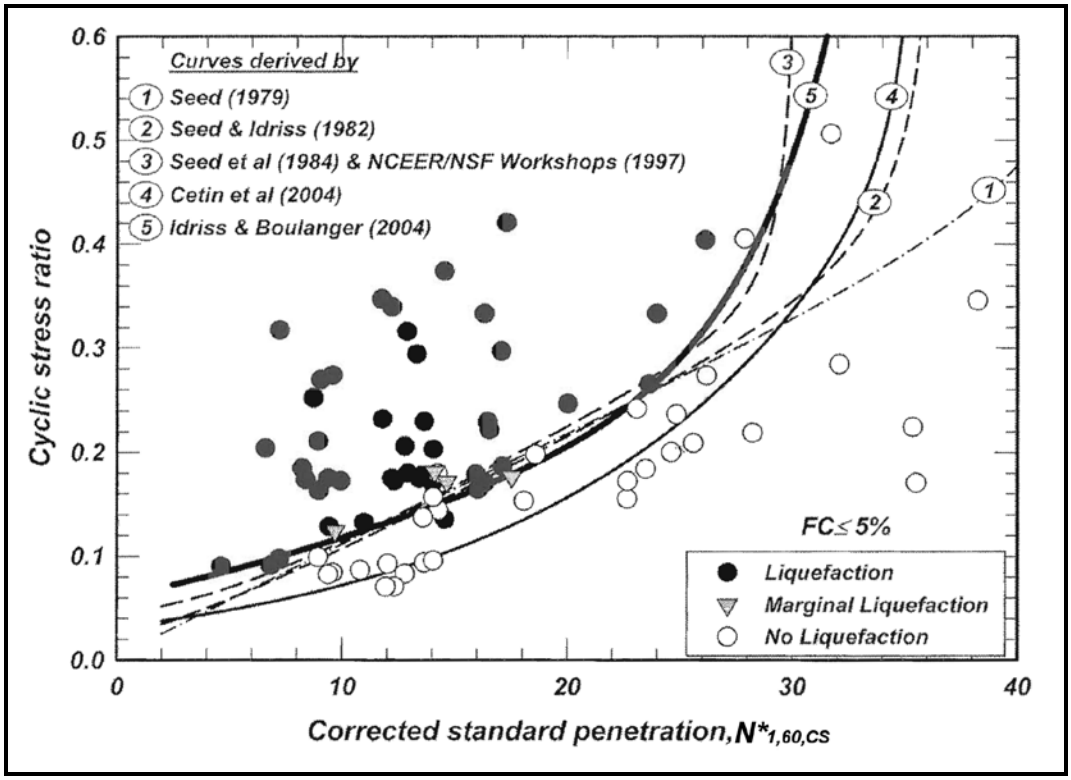

Figure 13-23, SPT Liquefaction Triggering Correlation (CRR^*)
M_w = 7.5; σ'_{vo} = 1.0 tsf; FC ≤ 5%
(Idriss and Boulanger, 2004)

In lieu of using Figure 13-23 the following equation may be used.

$$CRR^* = CRR_{M_w=7.5,1tsf} = \exp\left[\left(\frac{N^*_{1,60,cs}}{14.1}\right) + \left(\frac{N^*_{1,60,cs}}{126}\right)^2 - \left(\frac{N^*_{1,60,cs}}{23.6}\right)^3 + \left(\frac{N^*_{1,60,cs}}{25.4}\right)^4 - 2.8\right] \quad \text{Equation 13-36}$$

13.11.3 Sand-Like Soil - CPT Based CRR^* Curves

The cyclic resistance ratio (CRR) correlations for CPT in-situ testing presented by Idriss and Boulanger (2008) shall be used to evaluate Sand-Like soils. Deterministic cyclic resistance ratio curves ($CRR^* = CRR_{Mw=7.5,1\ tsf}$) are moment magnitude weighted, adjusted to a reference effective overburden stress of σ'_V = 1 tsf, and adjusted for fines content. Similarly to the cyclic stress ratio, CSR, a reference earthquake of moment magnitude, M_w, of 7.5 is used. The normalized corrected CPT tip resistance ($q_{c,1,N}$) is adjusted to an equivalent clean sand (CS) tip resistance based on the fines content (FC) as indicated by the following equation.

$$q_{c,1,N,CS} = q_{c,1,N} + \Delta q_{c,1,N} \quad \text{Equation 13-37}$$

Where,

$q_{c,1,N}$ = Normalized corrected CPT tip resistance (Section 13.11.1.4) (unitless)

$\Delta q_{c,1,N}$ = Fines content correction for FC > 5%

The variation in $\Delta q_{c,1,N}$ with fines content (FC) based on Idriss and Boulanger, 2008 can be obtained from Figure 13-24 for FC > 5%.

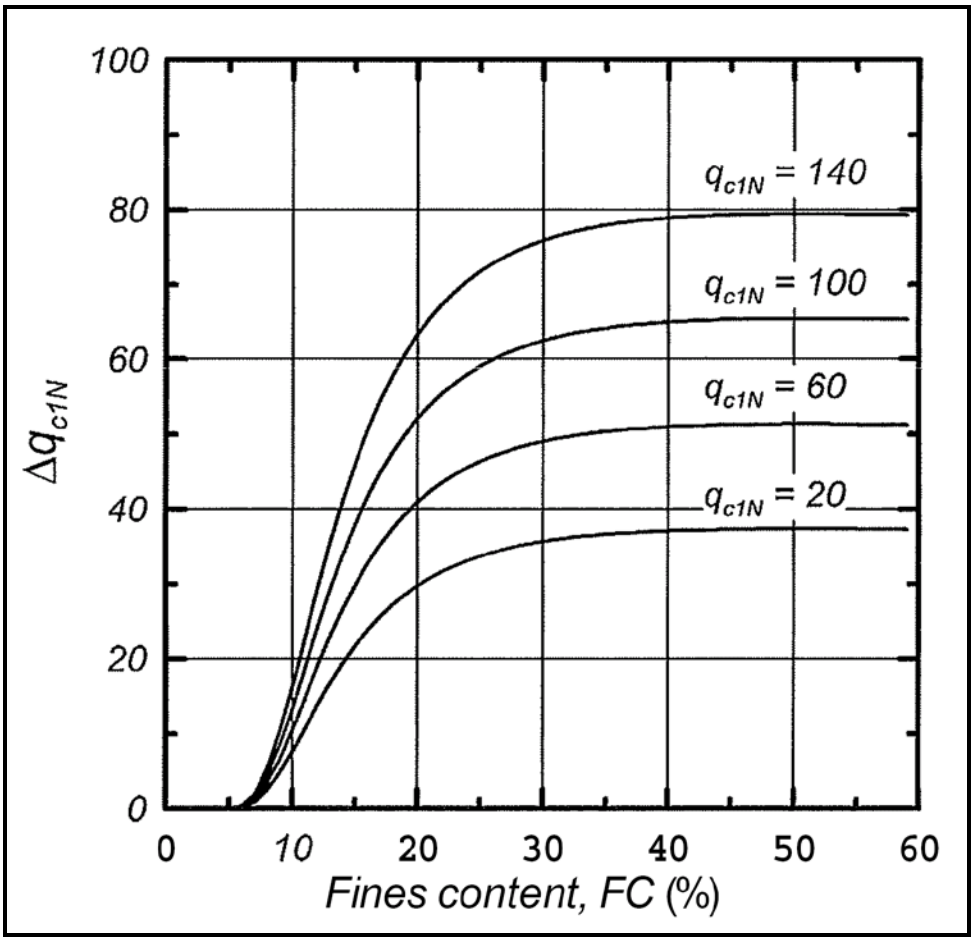

Figure 13-24, Variation in $\Delta q_{c,1,N}$ With Fines Content (Idriss and Boulanger, 2008)

In lieu of using Figure 13-24 the following equation may be used.

$$\Delta q_{c,1,N} = \left(5.4 + \left(\frac{q_{c,1,N}}{16}\right)\right) \cdot \exp\left(1.63 + \left(\frac{9.7}{FC + 0.01}\right) - \left(\frac{15.7}{FC + 0.01}\right)^2\right) \quad \text{Equation 13-38}$$

Where Fines content (FC) is in percent. Fines content (FC) is based on the soil fraction passing the No. 4 sieve.

Figure 13-25 shows the Idriss and Boulanger (2004) recommended deterministic CRR^* curves for CPT in-situ testing based on an earthquake moment magnitude, $M_w = 7.5$, effective overburden reference stress, σ'_v=1.0 tsf, and fines content FC < 5%.

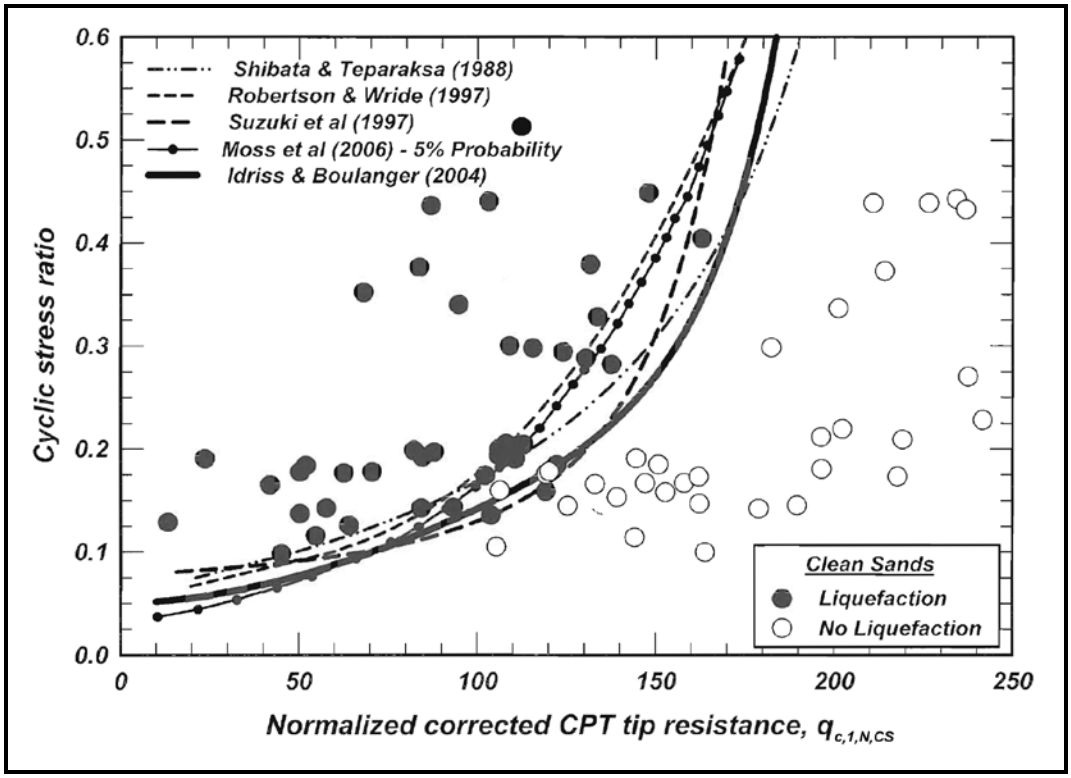

Figure 13-25, CPT Liquefaction Triggering Correlation (CRR*)
M_w = 7.5; σ'$_{vo}$ = 1.0 tsf; *FC* ≤ 5%
(Idriss and Boulanger, 2004)

In lieu of using Figure 13-25 the following equation may be used.

$$CRR^{*} = CRR_{M_W=7.5,\sigma'_{vo}} = \exp\left[\left(\frac{q_{c,1,N,CS}}{540}\right)+\left(\frac{q_{c,1,N,CS}}{67}\right)^{2}-\left(\frac{q_{c,1,N,CS}}{80}\right)^{3}+\left(\frac{q_{c,1,N,CS}}{114}\right)^{4}-3.0\right] \quad \text{Equation 13-39}$$

13.11.4 Clay-Like Soil CRR* Curves

The cyclic resistance ratio (CRR) correlations presented by Idriss and Boulanger, (2008) shall be used to evaluate Clay-Like soils. Deterministic cyclic resistance ratio curves (CRR* = $CRR_{M=7.5}$) are magnitude weighted. Similarly to the cyclic stress ratio, CSR, a reference earthquake moment magnitude, M_w, of 7.5 is used. The CRR of Clay-Like soils will typically be determined by using empirical correlations. CRR of Clay-Like soils can also be determined by cyclic laboratory testing with approval from the PCS/GDS. Boulanger and Idriss (2007) developed empirical correlations based on the undrained shear strength profile and the consolidation stress history profile.

The preferred empirical correlation for determining the cyclic resistance ratio curves (CRR* = $CRR_{Mw=7.5}$) for Clay-Like soils is based on the undrained shear strength profile using the relationship shown in Figure 13-26, where undrained shear strengths have been obtained from laboratory testing. If in-situ testing methods (SPT or CPT) are used to obtain undrained shear strengths then CRR* correlations using the consolidation stress history profile presented in Figure 13-26 should be used as a check on the in-situ testing shear strength correlations.

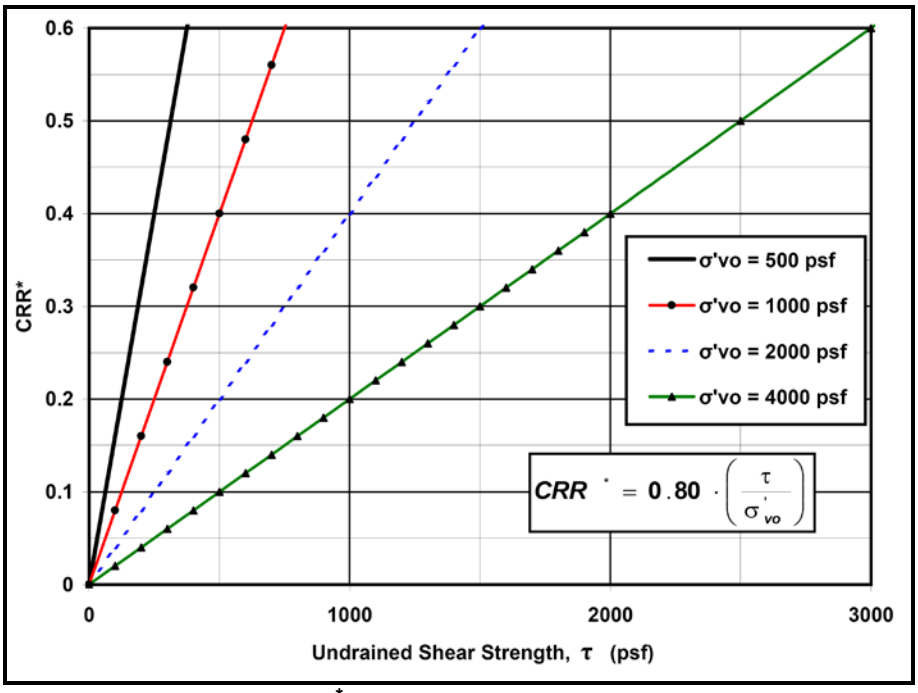

Figure 13-26, CRR* Clay-Like – Shear Strength Correlation
(Modified from Boulanger and Idriss, 2007 with permission from ASCE)

In lieu of using Figure 13-26, the following equation may be used to determine the cyclic resistance ratio curves (CRR* = $CRR_{Mw=7.5}$) for Clay-Like soils.

$$CRR^{*} = CRR_{M_w=7.5} = 0.80\left(\frac{\tau}{\sigma'_{vo}}\right) \qquad \text{Equation 13-40}$$

Where,

τ = Undrained shear strength (S_u). Laboratory and in-situ testing methods for determining S_u are presented in Chapter 7.

σ'_{vo} = effective overburden stress

Boulanger and Idriss (2007) have suggested using the empirical correlations developed from SHANSHEP laboratory testing (Ladd et al., 1977) shown in Figure 13-27. These correlations are based on a relationship between the undrained shear strength ratio and the consolidation stress history. The overconsolidation ratio (OCR) provides a measure of the consolidation stress history. These correlations require a consolidation stress history profile that is sometimes difficult to accurately evaluate without performing consolidation tests at various depths. It has also been observed that the undrained shear strength ratio can vary based on the type of clay formation used as shown Chapter 7 and in Figure 13-27. This method should only be used for preliminary analyses or to evaluate the cyclic resistance ratio (CRR^{*}) determined by the undrained shear strength ratio, particularly if in-situ testing is used to estimate the undrained shear strength of Clay-Like soils.

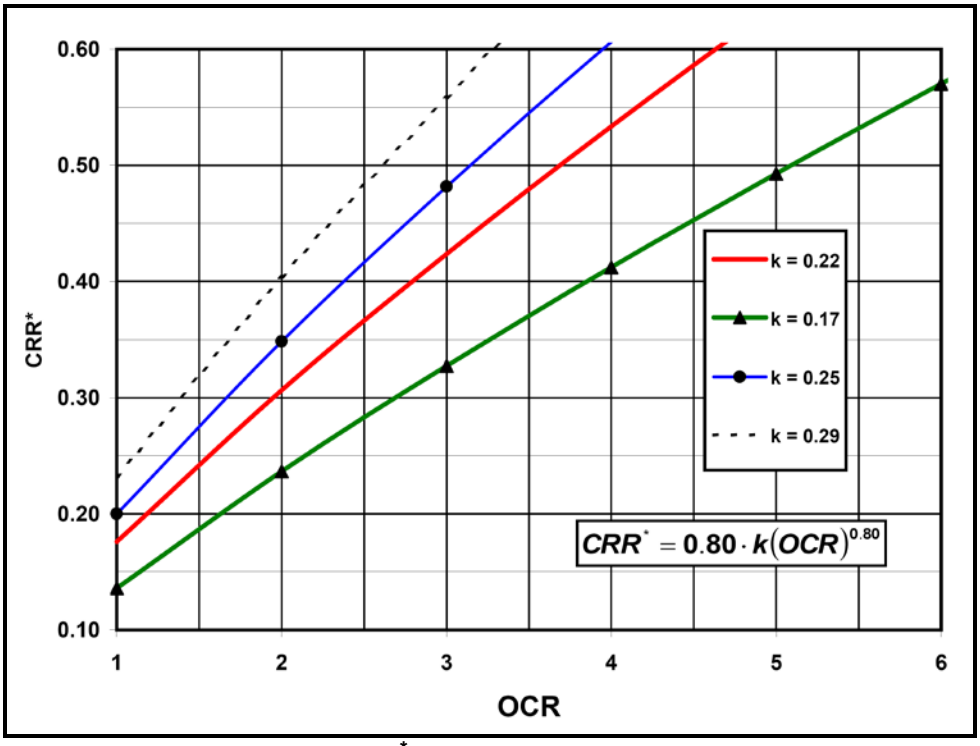

Figure 13-27, CRR^* Clay-Like Soils – OCR Correlation

In lieu of using Figure 13-27, the following equation may be used to compute the cyclic resistance ratio curves ($CRR^* = CRR_{M=7.5,1\ tsf}$) for Clay-Like soils based on OCR.

$$CRR^* = 0.80 \cdot k(OCR)^n \qquad \text{Equation 13-41}$$

Where,

k = Shear strength ratio for normally consolidated soils (OCR=1) typically ranges between 0.17 and 0.29. Use k=0.22 (DSS testing) as recommended by Boulanger and Idriss (2007) unless laboratory testing and local correlations indicate otherwise.

OCR = Overconsolidation ratio (σ'_p / σ'_{vo}) (See Chapter 7)

n = soil constant typically taken as 0.80 for unstructured and uncemented soils.

13.11.5 High Overburden Correction For Sand-Like Soils (K_σ)

The high overburden correction, K_σ, accounts for the increased susceptibility of Sand-Like soils to cyclic liquefaction, at the same CSR, with large increases in effective overburden stress. For Clay-Like soils there is no increase, therefore, a high overburden correction, K_σ, = 1.0 shall be used.

The high overburden correction factors for Sand-Like soils presented by Idriss and Boulanger (2008) shall be used. These high overburden correction factors are based on the relative state parameter index (ξ_R). These correction factors were then correlated with corrected SPT blow counts ($N^*_{1,60}$ – Section 13.11.1.3) and normalized corrected CPT tip resistance ($q_{c,1,N}$ – Section 13.11.1.4). The high overburden corrections, K_σ, for effective overburden $\sigma'_{vo} > 1$ tsf, are plotted for selected values of $N^*_{1,60}$ and $q_{c,1,N}$ in Figure 13-28.

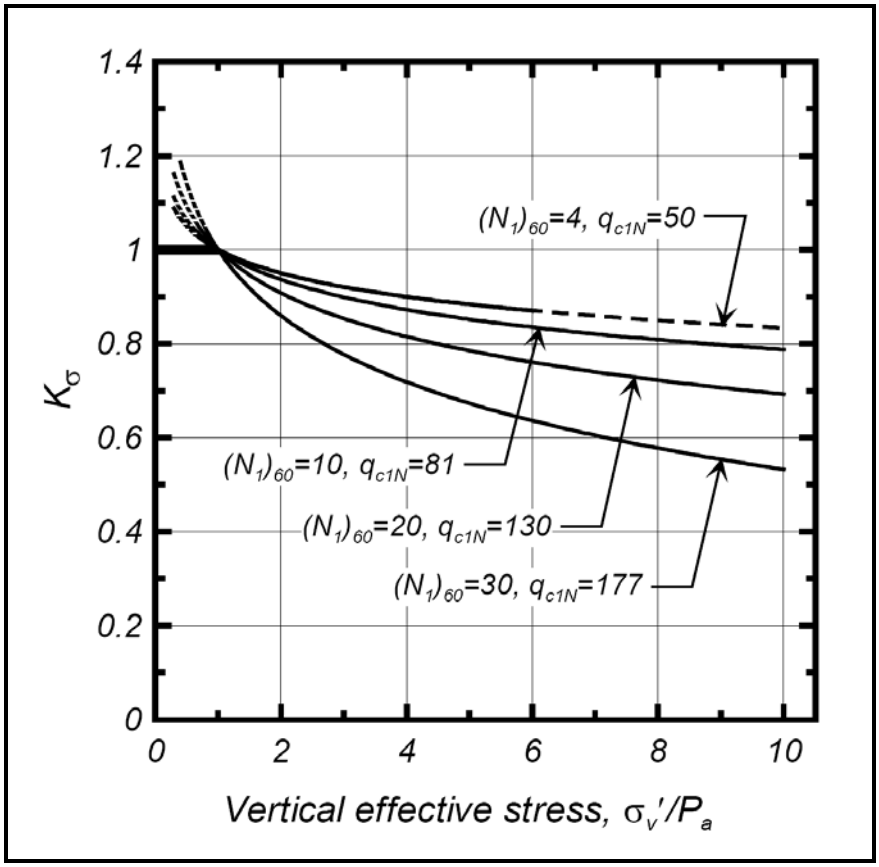

Figure 13-28, High Overburden Correction (K_σ) (σ'_{vo} > 1 tsf) (Boulanger, 2003a with permission from ASCE)

In lieu of using Figure 13-28, the following equation may be used to compute the K_σ of Sand-Like soils. These correlations are based on Q ≈ 10, K_o ≈ 0.45, D_R ≤ 0.9, and $(\sigma'_{vo}/P_a) \leq 10$.

$$K_\sigma = 1 - C_\sigma \ln\left(\frac{\sigma'_{vo}}{P_a}\right) \leq 1.1 \qquad \text{Equation 13-42}$$

Where,

- σ'_{vo} = Effective overburden stress (or σ'_v), units of tsf.
- P_a = Atmospheric pressure, taken as 1 tsf
- C_σ = Coefficient used to correlate D_R, $N^*_{1,60}$, and $q_{c,1,N}$ to K_σ
- D_R = Relative density, where $D_R \leq 0.90$ (90%)
- $N^*_{1,60}$ = Corrected SPT blow count, where $N^*_{1,60} \leq 37$ blows/foot
- $q_{c,1,N}$ = Corrected and normalized CPT tip resistance, where $q_{c,1,N} \leq 211$ unitless

The coefficient C_σ can be expressed in terms of relative density (D_R), corrected SPT blow count ($N^*_{1,60}$), and corrected and normalized CPT tip resistance ($q_{c,1,N}$) based on Boulanger and Idriss (2004a) as indicated by the following equations.

$$C_\sigma = \frac{1}{18.9 - 17.3 D_R} \leq 0.3 \qquad \text{Equation 13-43}$$

$$C_\sigma = \frac{1}{18.9 - 2.55\left(N^*_{1,60}\right)^{0.5}} \leq 0.3 \qquad \text{Equation 13-44}$$

$$C_\sigma = \frac{1}{37.3 - 8.27\left(q_{c,1N}\right)^{0.264}} \leq 0.3 \qquad \text{Equation 13-45}$$

13.11.6 Age Correction Factor For Sand-Like Soils (K_{DR})

The susceptibility of Sand-Like soils to cyclic liquefaction has been found to be a function of geologic age and origin. Soils that were formed during the Quaternary period (past 1.6 million years ago - Mya), include the Holocene and Pleistocene epochs and shall be considered to have a moderate to very high potential for liquefaction. Pre-Pleistocene age (more than 1.6 Mya) deposits shall be considered to have a lower susceptibility to liquefaction. Youd and Perkins (1978) proposed geologic susceptibility chart for cyclic liquefaction of sedimentary cohesionless soil deposits that was based on soil deposition and geologic age as indicated in Table 13-3. The soil resistance to cyclic liquefaction tends to increase with increase in age as observed in Table 13-3.

Soil formations that are Pre-Pleistocene (>1.6 Mya) potentially will have a lower susceptibility to experience cyclic liquefaction unless the soils are found in areas where there is evidence of the soils having experienced cyclic liquefaction. Soils found in Pre-Pleistocene areas that have been subjected to cyclic liquefaction will have the same susceptibility to cyclic liquefaction as soils formed during the Holocene period. Figure 13-8 provides the location of paleoliquefaction sites that have been studied and Figure 13-9 provides a map developed by the USGS that identifies areas in South Carolina that potentially have experienced Quaternary liquefaction.

Simplified liquefaction-triggering methods used to compute the Cyclic Resistance Ratio (CRR) for Sand-Like soils such as those proposed by Youd and Idriss (1997) and Idriss and Boulanger (2008) were developed from case histories of relatively young Holocene (< 10,000 years ago) soils. A study by Leon et al. (2006) has demonstrated that Pleistocene Sand-Like soils in the upper 20 feet of several locations within the South Carolina Coastal Plain may have increased resistance to liquefaction due to aging. The location of paleoliquefaction sites in the Coastal Plain that were used by Leon et al. (2006) are shown in Figure 13-8.

Table 13-3, Liquefaction Susceptibility of Sedimentary Deposits
(Modified after Youd and Perkins, 1978 with permission from ASCE)

Type of Deposit [(1)]	General Distribution of Cohesionless Sediments in Deposits	Likelihood that Cohesionless Sediments, When Saturated, Will be Susceptible to Liquefaction (By Age of Deposit)			
		Modern < 500 yr	**Holocene 500 yr to 10 ka**	**Pleistocene 10ka – 1.6 Mya**	**Pre-Pleistocene > 1.6 Mya**
(a) Continental Deposits					
River Channel	Locally Variable	Very High	High	Low	Very Low
Floodplain	Locally Variable	High	Moderate	Low	Very Low
Alluvial Fan & Plain	Widespread	Moderate	Low	Low	Very Low
Marine Terraces & Plains	Widespread	---	Low	Very Low	Very Low
Delta and Fan-delta	Widespread	High	Moderate	Low	Very Low
Lacustrine and Playa	Variable	High	Moderate	Low	Very Low
Colluvium	Variable	High	Moderate	Low	Very Low
Talus	Widespread	Low	Low	Very Low	Very Low
Dunes	Widespread	High	Moderate	Low	Very Low
Loess	Variable	High	High	High	Unknown
Glacial Till	Variable	Low	Low	Very Low	Very Low
Tuff	Rare	Low	Low	Very Low	Very Low
Tephra	Widespread	High	High	Unknown	Unknown
Residual Soils	Rare	Low	Low	Very Low	Very Low
Sebka	Locally Variable	High	Moderate	Low	Very Low
(b) Coastal Zone					
Delta	Widespread	Very High	High	Low	Very Low
Estuarine	Locally Variable	High	Moderate	Low	Very Low
Beach - High Wave-energy	Widespread	Moderate	Low	Very Low	Very Low
Beach - Low Wave-energy	Widespread	High	Moderate	Low	Very Low
Lagoonal	Locally Variable	High	Moderate	Low	Very Low
Fore Shore	Locally Variable	High	Moderate	Low	Very Low
(c) Artificial					
Uncompacted Fill	Variable	Very High	---	---	---
Compacted Fill	Variable	Low	---	---	---

Definitions:
ka = thousands of years ago
Mya = millions of years ago

[(1)] Notes:
The above types of soil deposits may or may not exist in South Carolina. All of the soil deposits included by the original authors have been kept for completeness.

A study was recently conducted at the Savannah River Site (SRS) by Lewis et al. (2007) to re-evaluate the soil aging effects on the liquefaction resistance of Sand-Like soils that were encountered within shallow subsurface Tertiary soils from the Eocene (53 Mya) and Miocene (23 Mya) epochs. The results of these studies indicate that there is a significant increase in the CRR of sand with time as indicated by Figure 13-29.

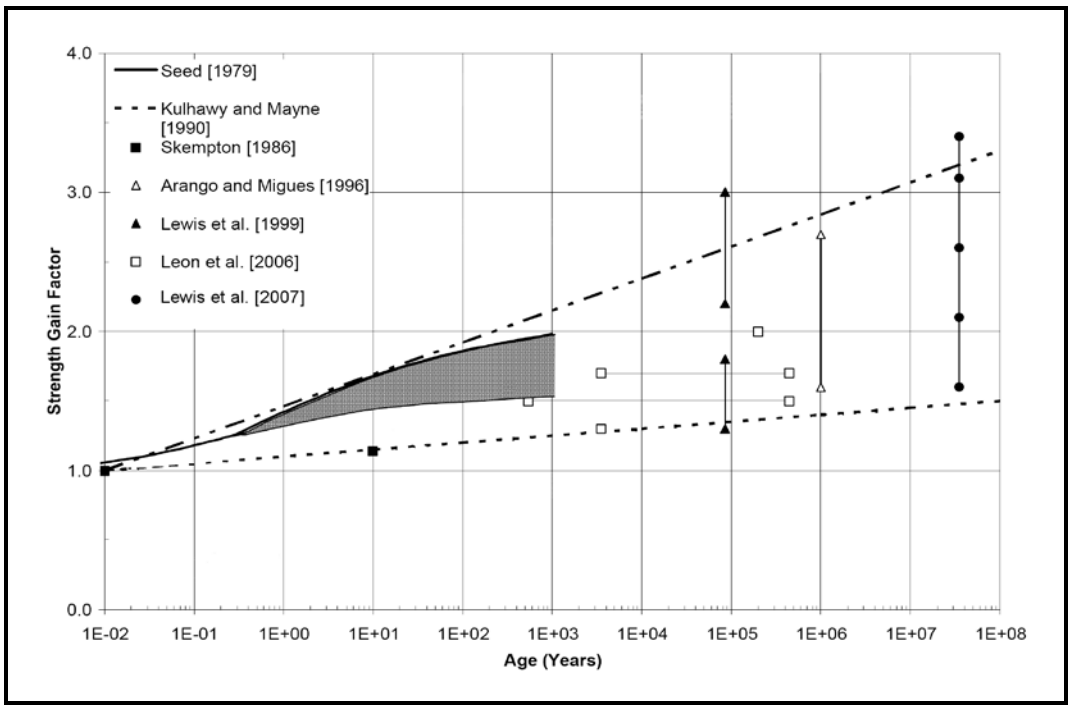

Figure 13-29, Sand-Like Soil Strength Gain With Age (Adapted from Lewis et al., 2007)

Hayati and Andrus (2008) reviewed the results of nine published studies on the effects of aging on liquefaction resistance of soils and developed a regression line (Solid Line) shown in Figure 13-30 that represents the average variation in liquefaction age correction factor (K_{DR}) with time (t). The age correction factor (K_{DR}) is the ratio of resistance-corrected cyclic resistance ratio of the aged soil (CRR_{DR}) to the cyclic resistance ratio of recently deposited soil ($CRR_{Holocene}$) as indicated by the following equation.

$$K_{DR} = \frac{CRR_{DR}}{CRR_{Holocene}} \qquad \text{Equation 13-46}$$

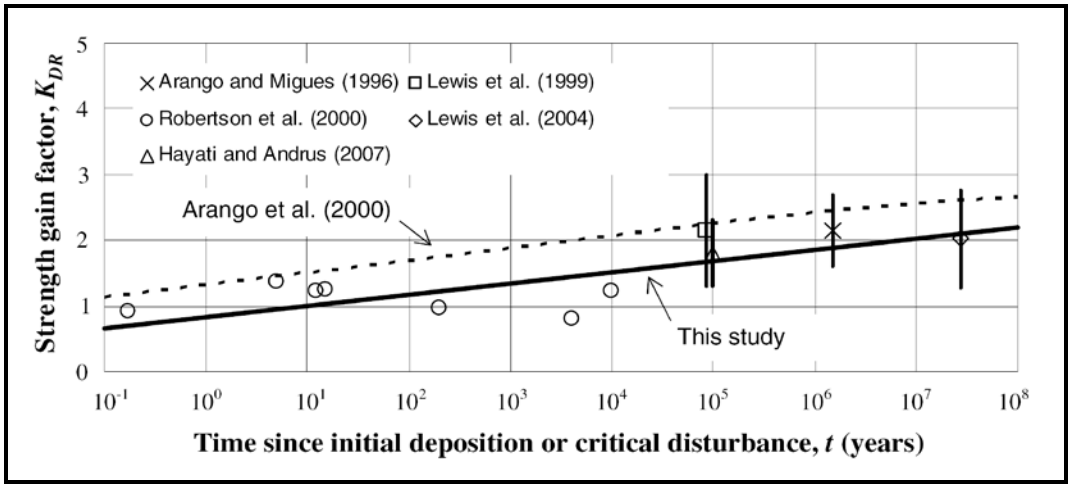

Figure 13-30, Relationship Between Strength Gain Factor and Time (Hayati and Andrus, 2008 with permission from ASCE)

A liquefaction age correction factor of K_{DR} = 1.0 corresponds to a soil deposit with an age of approximately 10 years. The time, t, is the time since initial deposition (K_{DR} = 1.0) or critical disturbance in years. Critical disturbance occurs when the effects of soil aging are removed as a result of grain-to-grain contacts being broken and reformed such as has been observed when Sand-Like soils experience cyclic liquefaction.

The age correction factor (K_{DR}) shown in Figure 13-30 can be computed using the following equation.

$$K_{DR} = 0.17 \log_{10}(t) + 0.83 \qquad \text{Equation 13-47}$$

Because it is difficult to evaluate the age of the soil, Andrus et al. (2009) have developed a concept for evaluating aged sands, MERV, ratio of measured shear wave velocity, $V_{s\text{-}meas}$, to estimated shear wave velocity from SPT or CPT ($V_{S\text{-}SPT}$ or $V_{S\text{-}CPT}$) as indicated by the following equations.

$$MERV = \frac{V_{S-Meas}}{V_{S-SPT}} \qquad \text{Equation 13-48}$$

$$MERV = \frac{V_{S-Meas}}{V_{S-CPT}} \qquad \text{Equation 13-49}$$

Where,

$V_{s\text{-}meas}$ = Measured shear wave velocity by Crosshole (CH), Seismic CPT (SCPT), Suspension Logger (SL), or other approved method.

$V_{S\text{-}SPT}$ = Estimated shear wave velocity using SPT ($N^*_{1,60,CS}$) by using the following equation:

$$V_{S-SPT} = V_{s,1cs-SPT} = 87.8\left(N^*_{1,60,CS}\right)^{0.253} \qquad \text{Equation 13-50}$$

$V_{S\text{-}CPT}$ = Estimated shear wave velocity using CPT ($N^*_{1,60,CS}$) by using the following equation:

$$V_{S-CPT} = V_{s,1cs-CPT} = 62.6\left(q_{c,1N,CS}\right)^{0.231} \qquad \text{Equation 13-51}$$

Andrus et al. (2009) proposed the following relationship between MERV and time (t in years) since initial deposition or critical disturbance.

$$MERV = \left(0.0820 \cdot \log_{10}(t)\right) + 0.935 \qquad \text{Equation 13-52}$$

Andrus et al. (2009) proposed a relationship between the age correction factor, K_{DR}, (Equation 13-47) and MERV (Equation 13-52) as indicated by the following equation.

$$K_{DR} = \left(2.07 \cdot MERV\right) - 1.11 \qquad \text{Equation 13-53}$$

An approximate relationship between South Carolina Coastal Plain Geology, MERV, and K_{DR} is presented in Table 13-4. The use of an age correction factor, $K_{DR} > 1.0$ for Sand-Like soils will require that the MERV for the soil formation be computed and compared with values presented in Table 13-4. Sand-Like soil formations with a MERV $\leq$ 1.3 shall be assumed to be either Holocene age soils or aged soil formations that have been subjected to critical disturbance such as cyclic liquefaction. Values listed in Table 13-4 should not be exceeded without the approval of the PCS/GDS.

Table 13-4, Coastal Plain Sand-Like Soil Age Correction Factor, K_{DR} (MERV)
(adapted from South Carolina Geological Survey – Willoughby et al. , 1999)

Time Scale		Time	SC Coastal Plain Physiographic Province			MERV	K_{DR}
Period	Epoch	(MYA)	Upper	Middle	Lower		
Quaternary	Holocene	0.01	Coastal Sands River Bottoms Alluvium	Coastal Sands River Bottoms Alluvium	Coastal Sands River Bottoms Alluvium Tidal Marsh Estuarine Deposits Fresh Water Stream Swamp Deposits	1.02	1.00
	Pleistocene	1.6		Socastee Formation Wando Formation Penahloway Formation	Silver Bluff Beds Princess Anne Formation Pamlico Formation Socatee Formation Wando Formation Ten Mile Hill Formation Canepatch Formation Ladson Formation Penhaloway Formation Wicomico Formation Waccamaw Formation Daniel Island Beds	1.31	1.60
Tertiary	Pliocene	5.3	Pinehurst Formation	Okefenokee Terrace Duplin Formation Bear Bluff Formation	Lower Beds at Windy Hill Lower Waccamaw Formation Pringletown Beds Raysor Formation Goose Creek Limestone Bear Bluff Formation Givhans Beds Duplin Formation Wabasso Beds	1.45	1.90
	Miocene	23	Altamaha Formation Coharie Formation Citronelle Formation	Coharie Formation	Coosawhatchie Formation Rudd Branch Beds Markhead Formation Parachula Formation Edisto Formation Hawtorne Formaiton	1.50	2.00
	Oligocene	36.6		Suwanee Limestone	Chandler Bridge Formation Ashley Formation Suwanee Limestone Lazaretto Creek Formation	1.55	2.10
	Eocene	53	Tobaco Road Sand Dry Branch Formation Orangeburg District Bed McBean Formation Santee Limestone Warley Hill Formation Huber Formation Congaree Formation Fourmile Branch Formation Tinker Formation Hazelhurst Formation	Ocala Limestone Orangeburg District Bed Santee Limestone Warley Hill Formation Congaree Formation Hazelhurst Formation	Parkers Ferry Formation Harleyville Formation Cross Formation Santee Limestone Fishburne Formation Drayton Limestone Hazelhurst Formation Ocala Limestone		
	Paleocene	65	Snapp Formation Lang Syne Formation Sawdust Landing Fm. Black Mingo Formation Elenton Formation	Lang Syne Formation Williamsburg Formation Sawdust Landing Fm. Black Mingo Formation	Williamsburg Formation Rhems Formation Black Mingo Formation	1.57	2.15
Mesozoic	Upper Cretaceous	99.6	Tar Heel Formation Black Creek Formation Middendorf Formation	Pee Dee Formation Donoho Creek Formation Black Creek Formation Middendorf Formation Bladen Formation Tar Heel Formation	Pee Dee Formation Steel Creek Formation Black Creek Formation Middendorf Formation Donoho Creek Formation Tar Heel Formation Bladen Formation Tuscaloosa Formation	1.59	2.18
	Lower Cretaceous Jurassic Triassic	250.0	**Transitional Material between Coastal Plain Sediment and Piedmont Rocks**			-	-
Paleozoic	Permian Pennsylvanian Mississippian Devonian Silurian Ordovicin Cambrian	570.0	**Piedmont**			-	-

13.11.7 Static Shear Stress Ratio Correction Factor (K_α)

The static shear stress ratio correction factor, K_α, accounts for the effects of initial static shear stresses on cyclic resistance of the soils beneath sloping ground. The static shear stresses are typically expressed as the static shear stress ratio (α) that is defined as the initial static shear stress (τ_s) divided by the effective normal consolidation stress (σ'_{vc}) as indicated by the following equation.

$$\alpha = \frac{\tau_S}{\sigma'_{vc}} = \frac{\tau_S}{\sigma'_{vo}} \qquad \text{Equation 13-54}$$

The initial static shear stress (τ_s) is the static soil shear stress that exists prior to the earthquake shaking occurring and can be computed as indicated in Section 13.11.7.1. The effective normal consolidation stress is typically assumed to be equal to the effective overburden stress (σ'_{vc} = σ'_{vo}) because most design situations assume enough time has elapsed that the soils have been consolidated under the sustained loading. For under consolidated soils, the existing effective consolidation stress (σ'_{vc}) shall be used.

The static shear stress ratio correction factor, K_α, is defined as the ratio of CRR at some value of α divided by the CRR at a value of $\alpha = 0$ as indicated by the following equation.

$$K_\alpha = \frac{(CRR)_\alpha}{(CRR)_{\alpha=0}} \qquad \text{Equation 13-55}$$

The static shear stress ratio correction factor, K_α, for Sand-Like soils and Clay-Like soils can be computed in accordance with Sections 13.11.7.2 and 13.11.7.3, respectively.

13.11.7.1 Initial Static Shear Stress (τ_s) of Soils Susceptible to Soil SSL

The initial static shear stress (τ_s) for each soil layer susceptible to soil SSL (Sand-Like soils and Clay-Like soils) can be computed by performing a slope stability analysis of the pre-failure geometry. The slope stability analysis should be performed in accordance with Chapter 17 with Spencer's method required. The slope stability analysis should be evaluated using both circular and sliding wedge potential failure surfaces. The slope stability analysis should then be performed by using undrained shear strengths for cohesive soil layers and fully mobilized drained shear strengths for cohesionless soils. Determine the slope stability ratio, $(D/C)_{Stability}$ using the following equation.

$$\left(\frac{D}{C}\right)_{Stability} = \frac{1}{FS} = \varphi_{Stability} \qquad \text{Equation 13-56}$$

The initial static shear stress (τ_s) is defined as the soil shear stress along the failure surface that corresponds to slope stability ratio of $(D/C)_{Stability} = 1$. The initial static shear stress (τ_s) along the critical failure surface can be computed by reducing soil shear strengths based on the computed

slope stability ratio, $(D/C)_{Stability}$ for the pre-failure geometry. The reduced undrained shear strengths for cohesive soil layers, c_s, can be computed using the following equation.

$$c_s = c \cdot \left(\frac{D}{C}\right)_{Stability} = \frac{c}{FS} = c \cdot \varphi_{Stability} \qquad \text{Equation 13-57}$$

Where,

c = Undrained shear strengths, $S_u = c$

$\left(\frac{D}{C}\right)_{Stability}$ = Slope stability ratio for the pre-failure geometry

FS = Factor of Safety for the pre-failure geometry

$\varphi_{Stability}$ = Resistance Factor for the pre-failure geometry

The initial static shear stress (τ_s) along the critical failure surface for cohesive soils is computed by the following equation.

$$\tau_s = c_s \qquad \text{Equation 13-58}$$

The reduced drained shear strength for a cohesionless soil layer is computed by reducing the internal friction angle, ϕ_s, and can be computed using the following equation.

$$\phi_s = \arctan\left[\tan\phi \cdot \left(\frac{D}{C}\right)_{Stability}\right] = \arctan\left[\frac{\tan\phi}{FS}\right] = \arctan\left[\tan\phi \cdot \left(\varphi_{Stability}\right)\right] \qquad \text{Equation 13-59}$$

Where,

ϕ = Internal friction angle

$\left(\frac{D}{C}\right)_{Stability}$ = Slope stability ratio for the pre-failure geometry

FS = Factor of Safety for the pre-failure geometry

$\varphi_{Stability}$ = Resistance Factor for the pre-failure geometry

The initial static shear stress (τ_s) along the critical failure surface for cohesionless soils is computed by the following equation.

$$\tau_s = \sigma'_{vo} \cdot \tan\phi_s \qquad \text{Equation 13-60}$$

Alternatively, some slope stability software allows the input of the shear strength ratio directly (τ/σ'_{vo}). The static shear strength ratio (α) for cohesive soils can be computed by the following equation.

$$\alpha = \left(\frac{\tau_s}{\sigma'_{vo}}\right) = \left(\frac{\tau}{\sigma'_{vo}}\right) \cdot \left(\frac{D}{C}\right)_{Stability} = \frac{\tau}{\sigma'_{vo} \cdot FS} = \varphi_{Stability} \cdot \left(\frac{\tau}{\sigma'_{vo}}\right) \qquad \text{Equation 13-61}$$

The static shear strength ratio (α) for cohesionless soils can be computed by the following equation.

$$\alpha = \left(\frac{\tau_{S}}{\sigma'_{vo}} \right) = (\tan\phi) \cdot \left(\frac{D}{C} \right)_{Stability} = \frac{\tan\phi}{FS} = \varphi_{Stability} \cdot \tan\phi \qquad \text{Equation 13-62}$$

The initial static soil shear stress computed should be checked by using the reduced soil shear strengths (τ_S or α) to perform a slope stability analysis and determine if the slope stability ratio, $(D/C)_{Stability}$, for the critical failure surface corresponds to a slope stability ratio of $(D/C)_{Stability} = 1$. If the slope stability ratio of $(D/C)_{Stability} \neq 1$, the soil shear strength should be further adjusted until a slope stability ratio of $(D/C)_{Stability} = 1$ is achieved.

13.11.7.2 K_α For Sand-Like Soils

Harder and Boulanger (1997) observed variations in cyclic shear stresses as a function relative density (D_R) and effective overburden stress (σ'_{vo}) when they summarized available cyclic laboratory test data. It was observed that cyclic resistance of dense sands can increase significantly as the static shear stress ratio (α) increases and that cyclic resistance of loose sands decreases as the static shear stress ratio (α) decreases.

Boulanger (2003b) developed static shear stress ratio correction factor, K_α, for Sand-Like soils based on the relative state parameter index (ξ_R). These correction factors were then correlated for use with normalized SPT N-values ($N^*_{1,60}$ – Section 13.11.1.3) normalized and effective overburden corrected CPT tip resistance ($q_{c,1,N}$ – Section 13.11.1.4). The static shear stress ratio correction factor, K_α, for selected effective overburden stresses of σ'_{vo} = 1 tsf and σ'_{vo} = 4 tsf, and Q=10 (Sand), are provided for SPT values of $N^*_{1,60}$ in Figure 13-31 and CPT values of $q_{c,1,N}$ in Figure 13-32.

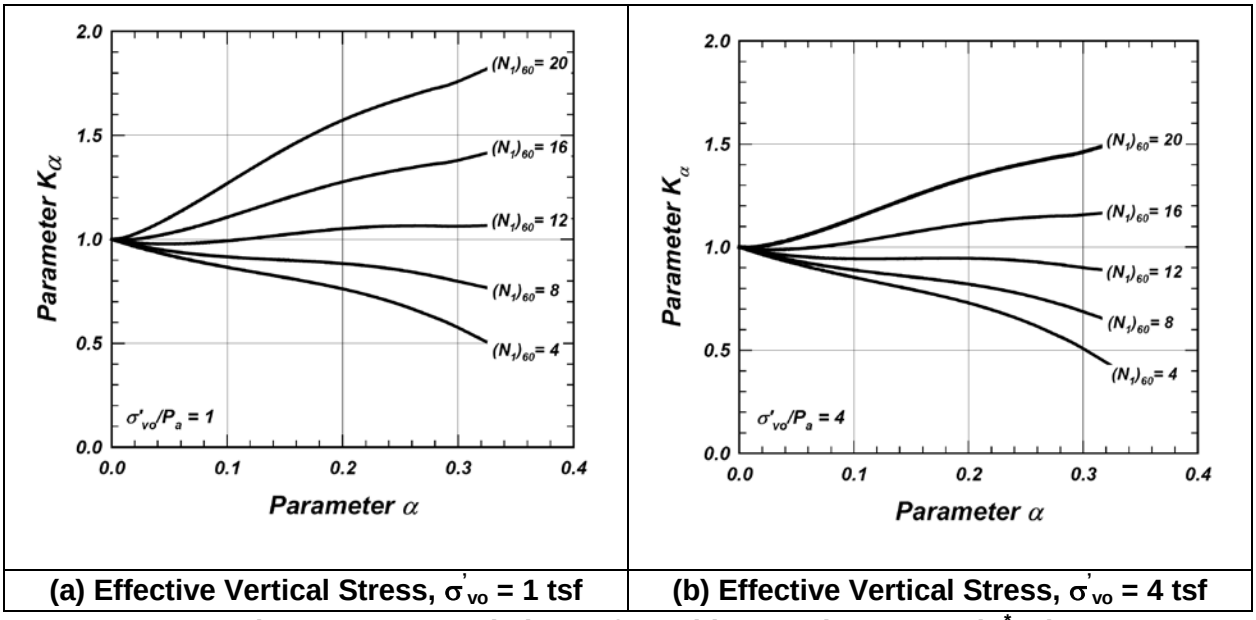

(a) Effective Vertical Stress, σ'_{vo} = 1 tsf | **(b) Effective Vertical Stress, σ'_{vo} = 4 tsf**

Figure 13-31, Variations of K_α with SPT Blow Count ($N^*_{1,60}$) (Boulanger, 2003b)

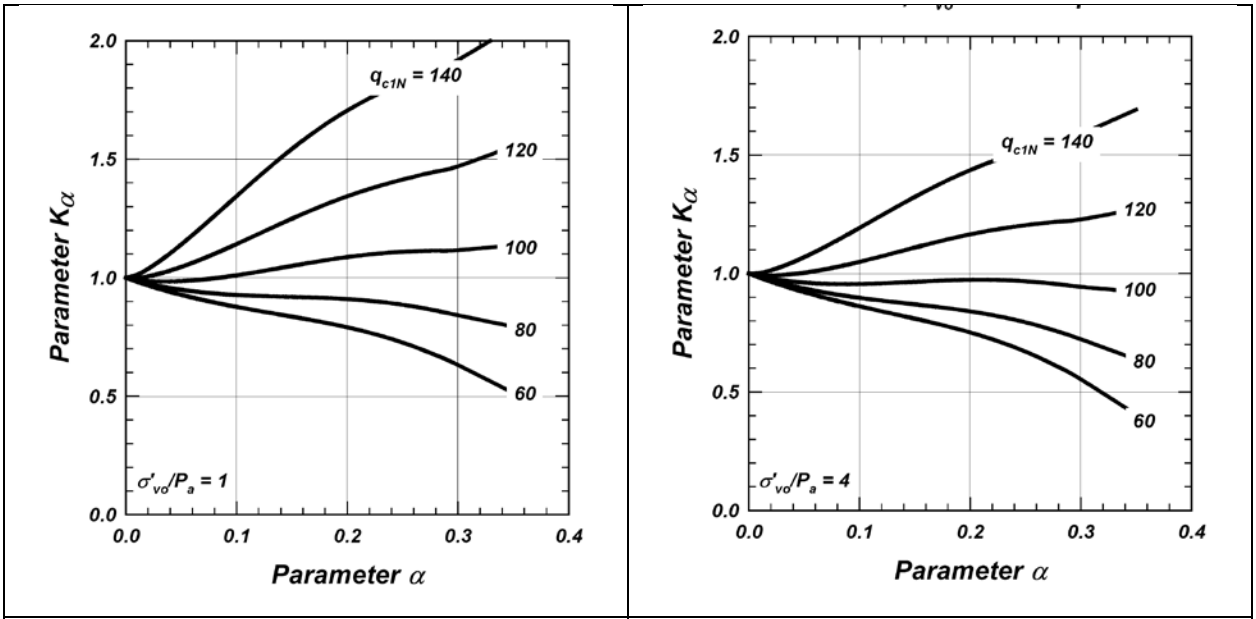

(a) Effective Vertical Stress, σ'_{vo} = 1 tsf | **(b) Effective Vertical Stress, σ'_{vo} = 4 tsf**

Figure 13-32, Variations of K_α with CPT Tip Resistance ($q_{c,1,N}$) (Boulanger, 2003b)

In lieu of using Figures 13-31 and 13-32, the following equation may be used to compute the K_α. The following equations were developed from data that limits the static shear stress ratio to $\alpha \leq 0.35$ and relative state parameter index to $-0.6 \leq \xi_R \leq 0.1$.

$$K_\alpha = a + b \cdot \left[\exp\left(\frac{-\xi_R}{c} \right) \right]$$ Equation 13-63

Where,

a = $1267 + 636\alpha^2 - (634 \cdot \exp(\alpha)) - (632 \cdot \exp(-\alpha))$

b = $\exp(-1.11 + 12.3\alpha^2 + (1.31 \cdot \ln(\alpha + 0.0001)))$

c = $0.138 + 0.126\alpha + 2.52\alpha^3$

α = Static shear stress ratio as per Equation 13-62 and Section 13.11.7.1 (limited to $\alpha \leq 0.35$)

ξ_R = Relative state parameter index (ξ_R) used to correlate D_R, $N^*_{1,60}$, and $q_{c,1,N}$ to K_α (Limited to: $-0.6 \leq \xi_R \leq 0.1$)

$$\xi_R = \frac{1}{Q - \ln\left(\frac{100(1+2K_o)\sigma'_{vo}}{3P_a} \right)} - D_R$$ Equation 13-64

$$\xi_R = \frac{1}{Q - \ln\left(\frac{100(1+2K_o)\sigma'_{vo}}{3P_a} \right)} - \left(\frac{N^*_{1,60}}{46} \right)^{0.5}$$ Equation 13-65

$$\xi_R = \frac{1}{Q - \ln\left(\frac{100(1+2K_o)\sigma'_{vo}}{3P_a} \right)} - \left(0.478 (q_{c,1N})^{0.264} - 1.063 \right)$$ Equation 13-66

Where,

D_R = Relative density, where $D_R \leq 0.90$ (90%)

$N^*_{1,60}$ = Standardized and normalized SPT blow count, where $N^*_{1,60} \leq 37$ blows/foot

$q_{c,1,N}$ = Normalized CPT tip resistance, where $q_{c,1,N} \leq 211$ (unitless)

Q = Empirical Constant: Q=10 for Quartz and feldspar (Sand), Q=8 for limestone, Q=7 for anthracite, and Q=5.5 for chalk.

K_o = At-rest lateral earth pressure coefficient

σ'_{vo} = Effective vertical overburden stress

13.11.7.3 K_α For Clay-Like Soils

Boulanger and Idriss (2007) developed static shear stress ratio correction factor, K_α, for Clay-Like soils based on laboratory testing of Drammen clay (Goulois et al., 1985) that was consolidated under a sustained static shear stress. The relationship developed from these laboratory tests for K_α versus $(\tau_S/S_U)_{\alpha=0}$ for Clay-Like soils are shown in Figure 13-33.

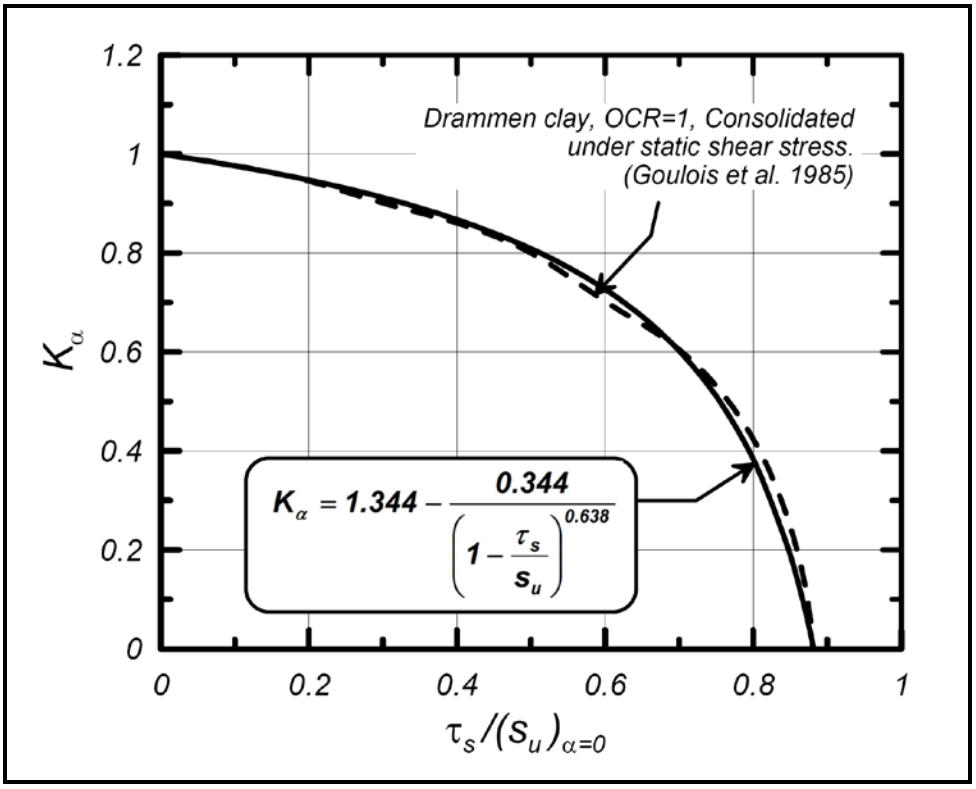

Figure 13-33, K_α versus $(\tau_S/S_U)_{\alpha=0}$ For Clay-Like Soil (NC Drammen Clay) (Boulanger, 2007)

The static shear stress ratio correction factor, K_α, relationship shown in Figures 13-33 is presented in the following equation as a function of (τ_s/S_U) and ($\alpha = \tau_s/\sigma'_{vc}$).

$$K_\alpha = 1.344 + \frac{0.344}{\left(1 - \frac{\tau_s}{S_U}\right)^{0.638}} = \frac{0.344}{\left(1 - \left(\frac{\alpha}{S_U/\sigma'_{vc}}\right)\right)^{0.638}} \qquad \text{Equation 13-67}$$

Where,

τ_s = Initial static shear stress

S_u = Undrained shear strength

σ'_{vc} = Effective vertical consolidating stress

S_u/σ'_{vc} = Undrained shear strength ratio (See Chapter 7)

α = Static shear stress ratio as per Equation 13-61and Section 13.11.7.1 (limited to $\alpha \leq 0.35$)

Boulanger (2003b) recommended using an empirical shear strength ratio relationship (S_u/σ'_{vc}) such as those developed by Ladd and Foot (1974) that take the form of the following equation:

$$\left(\frac{S_u}{\sigma'_{vc}}\right) = k(OCR)^n \qquad \text{Equation 13-68}$$

Where,

k = Shear strength ratio for normally consolidated soils (OCR=1). Typically range between 0.17 and 0.29. Use k=0.22 (DSS testing) as recommended by Boulanger (2007) unless laboratory testing available.

OCR = Overconsolidation ratio (σ'_p / σ'_{vo}) (See Chapter 7)

n = soil constant typically taken as 0.80 for unstructured and uncemented soils.

The static shear stress ratio correction factor, K_α, presented in Equation 13-67 can be combined with the empirical shear strength ratio shown in Equation 13-68 to develop static stress correction factor (K_α) that is a function of the consolidation stress history as shown in Figure 13-34 and Equation 13-69.

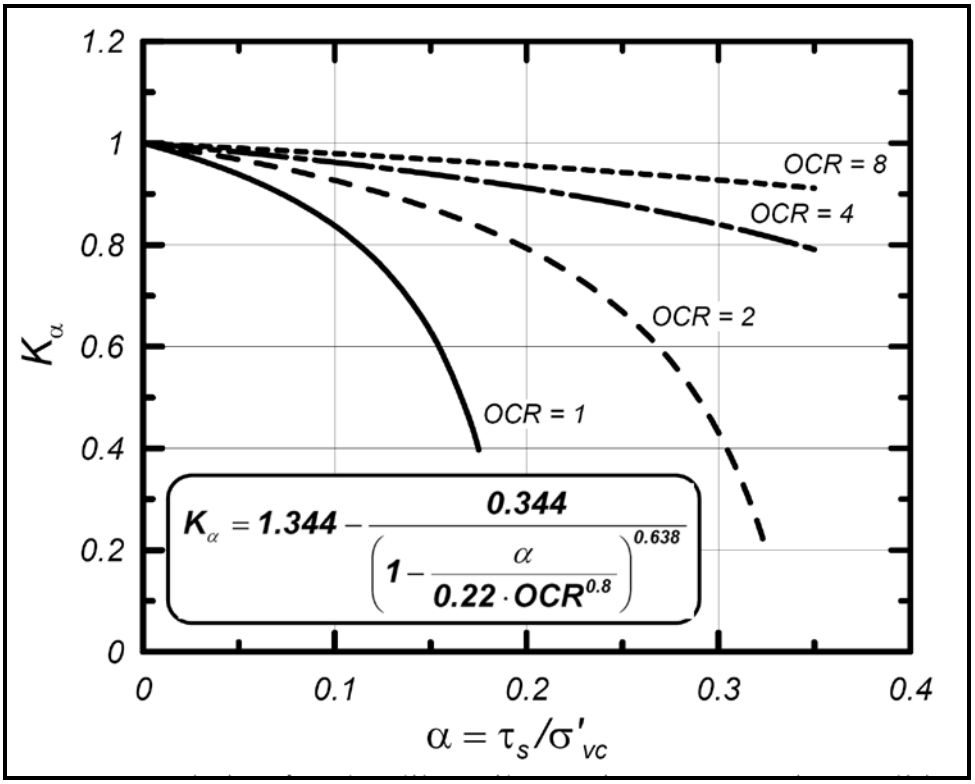

Figure 13-34, K_α versus $(\tau_S/S_U)_{\alpha=0}$ For Clay-Like Soil ($1 \le OCR \le 8$) (Boulanger, 2007)

$$K_\alpha = 1.344 + \frac{0.344}{\left(1 - \left(\frac{\alpha}{k(OCR)^n}\right)\right)^{0.638}} = 1.344 + \frac{0.344}{\left(1 - \left(\frac{\alpha}{0.22(OCR)^{0.8}}\right)\right)^{0.638}} \qquad \text{Equation 13-69}$$

13.12 SOIL SHEAR STRENGTH FOR SEISMIC ANALYSES

When performing seismic analyses, for soils that are not subject to losses in shear strength, the appropriate undrained shear (τ) or drained shear (τ') strengths should be used, in accordance with Chapter 7. Soils that are subject to cyclic strain-softening should use residual soil shear strengths. Undrained/drained soil shear strengths can be evaluated in accordance with the field and laboratory testing procedures specified in Chapter 5.

During strong earthquake shaking, cyclic liquefaction of Sand-Like soils or cyclic softening of Clay-Like soils may result in a sudden loss of strength and stiffness. Laboratory testing to determine residual shear strength of soils that have been subject to cyclic liquefaction or cyclic softening is difficult and not typically performed. The standard-of-practice is to use correlated residual undrained shear strengths of cohesionless soils as indicated in Sections 13.12.1 and 13.12.2 and to use correlated cyclic shear strength of cohesive soils as indicated in Sections 13.12.3 and 13.12.4. Guidance in selection of soil shear strengths for seismic analyses is presented in Section 13.12.5.

13.12.1 Sand-Like Soil Cyclic Shear Strength Triggering

The shear strength of Sand-Like soils that should be used in seismic analyses is dependent on the results of the liquefaction triggering and on pore pressure generation. The liquefaction triggering resistance ratio $(D/C)_{SL}$ for level site conditions and steeply sloped site conditions are presented in Sections 13.7 and 13.9, respectively. Figure 13-31 shows a relationship between liquefaction triggering resistance ratio $(D/C)_{SL}$ and the excess pore pressure ratio, R_u, that was proposed by Marcuson et al. (1990) for level sites.

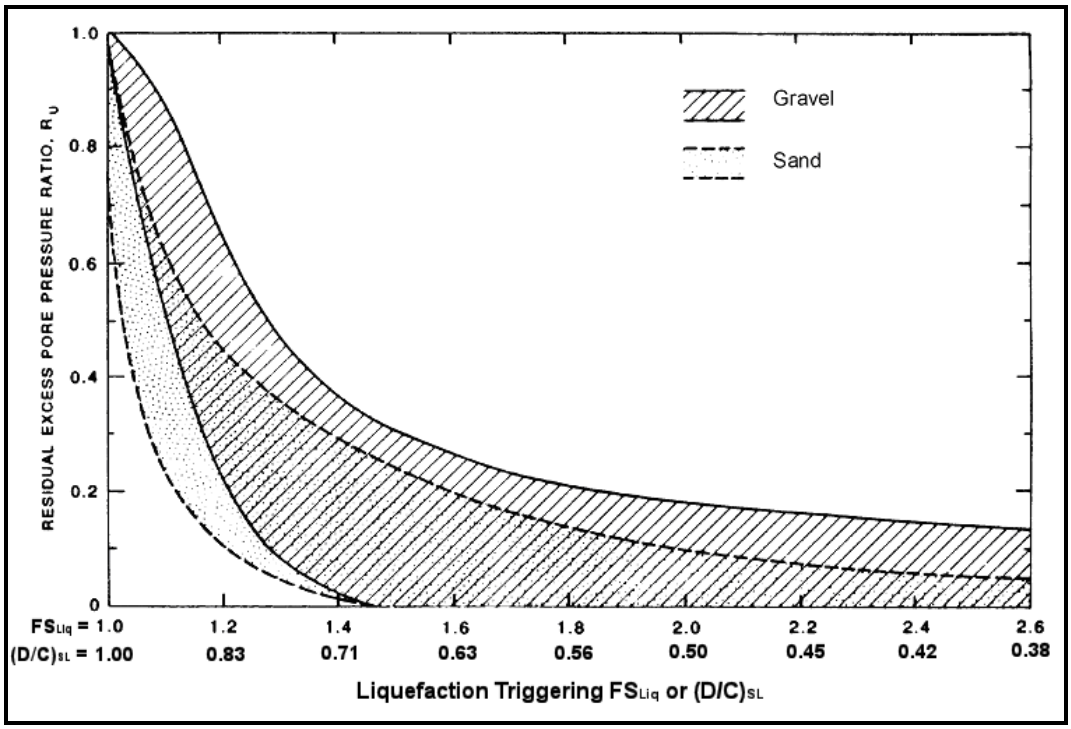

Figure 13-35, Excess Pore Pressure Ratio - Liquefaction Triggering (Modified Marcuson et al., 1990)

The excess pore pressure ratio, $R_u = \Delta u/\sigma'_{vo}$ is the ratio of excess pore water pressure (Δu) divided by the effective overburden stress (σ'_{vo}). The liquefaction triggering resistance ratio $(D/C)_{SL}$ of Sand-Like soils can be defined based on the excess pore pressure ratio generated as either Full Liquefaction, Limited Liquefaction, or No Liquefaction. The Limited Liquefaction potential represents a transition zone between the triggering resistance factor for the onset of liquefaction ($\varphi_{SL\text{-}Sand}$) and the no soil SSL resistance factor, $\varphi_{NLS\text{-}Sand}$ for Sand-Like Soils as indicated in Figure 13-32. The resistance factors (φ) indicated in Figure 13-32 are for illustration purposes. Resistance factors used for design shall be those presented in Chapter 9.

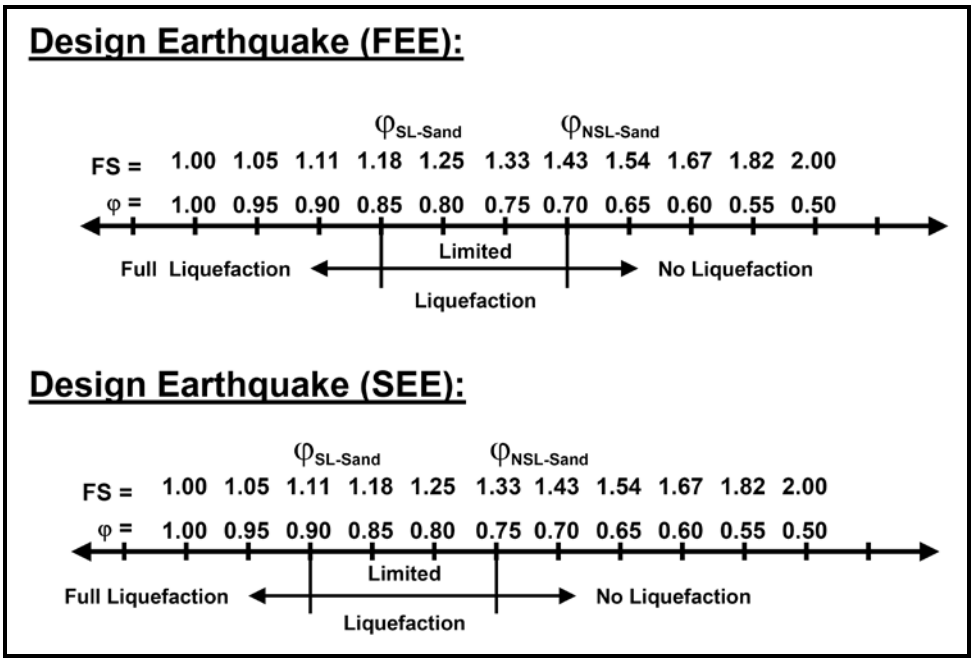

Figure 13-36, Shear Strength of Sand-Like Soils

The Limited Liquefaction case represents partial pore pressure generation and the shear strength for this case can be computed based on the following equation.

$$\tau_{rl-\lim} = \sigma'_{vo}(1 - R_u)\tan(\phi_{rl}) \qquad \text{Equation 13-70}$$

Where,

R_u = Excess pore pressure ratio

ϕ_{rl} = Internal friction angle for cyclic liquefaction

The equivalent limited liquefaction internal friction angle $\phi'_{rl\text{-}lim}$ can be approximated by reducing the internal friction angle (ϕ_{rl}) as a function of the excess pore water pressure ratio using the following equation.

$$\phi'_{rl-\lim} = \tan^{-1}\left[(1 - R_u)\left(\frac{\tau_{rl}}{\sigma'_{vo}}\right)\right] = \tan^{-1}[(1 - R_u)\tan(\phi_{rl})] \qquad \text{Equation 13-71}$$

Guidelines for determining the shear strength of Sand-Like soils are provided in Table 13-5.

Table 13-5, Sand-Like Shear Strengths

Liquefaction Potential	Liquefaction Triggering Criteria	Soil Shear Strength
Full Liquefaction	$(D/C)_{SL\text{-}Sand} < \varphi_{SL\text{-}Sand}$ $(R_u \approx 1.0)$	Use Idriss and Boulanger (2008) residual shear strength of liquefied soils (τ_{rl}) correlations. Section 13.12.2.3 Equation 13-72 $\phi_{rl} = \tan^{-1}\left(\frac{\tau_{rl}}{\sigma'_{vo}}\right)$
Limited Liquefaction	$\varphi_{SL\text{-}Sand} \le (D/C)_{SL\text{-}Sand} < \varphi_{NSL\text{-}Sand}$ $(0.20 \le R_u < 1.0)$	Use $\phi_{rl\text{-}lim}$ based on partial pore pressure generation using a $R_u = 0.4$ Equation 13-73 $\phi'_{rl-lim} = \tan^{-1}\left[\left(1-R_u\right)\left(\frac{\tau_{rl}}{\sigma'_{vo}}\right)\right] = \tan^{-1}\left[\left(1-R_u\right)\tan\left(\phi_{rl}\right)\right]$
No Liquefaction	$(D/C)_{SL\text{-}Sand} \le \varphi_{NSL\text{-}Sand}$ $(R_u < 0.20)$	Drained shear strength (τ') or residual shear strength (τ'_r) based on strain level. See Chapter 7.

13.12.2 Sand-Like Soil Cyclic Liquefaction Shear Strength

The following three methods are currently used to estimate the residual shear strength of liquefied Sand-Like soils.

1. SPT - Seed and Harder (1990)
2. SPT and CPT - Olson and Stark (2002, 2003)
3. SPT and CPT – Idriss and Boulanger (2008)

The Idriss and Boulanger (2008) method is the preferred method because it incorporates case histories from Seed (1987), Seed and Harder (1990), and Olson and Stark (2002). The Idriss and Boulanger (2008) method is also more advanced in that it uses residual shear strength ratios and allows residual shear strengths to be evaluated for void redistribution effects. All three methods are presented below to provide the designer with the appropriate background to evaluate the appropriate residual shear strength for liquefied Sand-Like soils.

13.12.2.1 Seed and Harder (1990) – Liquefied Residual Shear Strength

The Seed and Harder (1990) chart has been one of the most widely used methods to estimate the upper and lower bound relationship between $N^*_{1,60,cs}$ and residual shear strength of liquefied

soils (τ_{rl}). The Seed and Harder (1990) correlation is shown in Figure 13-33. Typically the lower one-third (1/3) design boundary shown in Figure 13-33 has been used to compute the residual shear strength of liquefied soils.

The Seed and Harder (1990) correlation uses a corrected fines content SPT blow count, $N^*_{1,60,cs}$, computed as shown in Equation 13-67. Standardized and normalized SPT blow counts, $N^*_{1,60}$, should be computed in accordance with Chapter 7. Values for N_{Corr} can be found in Figure 13-33.

$$N^*_{1,60,CS} = N^*_{1,60} + N_{Corr} \qquad \text{Equation 13-74}$$

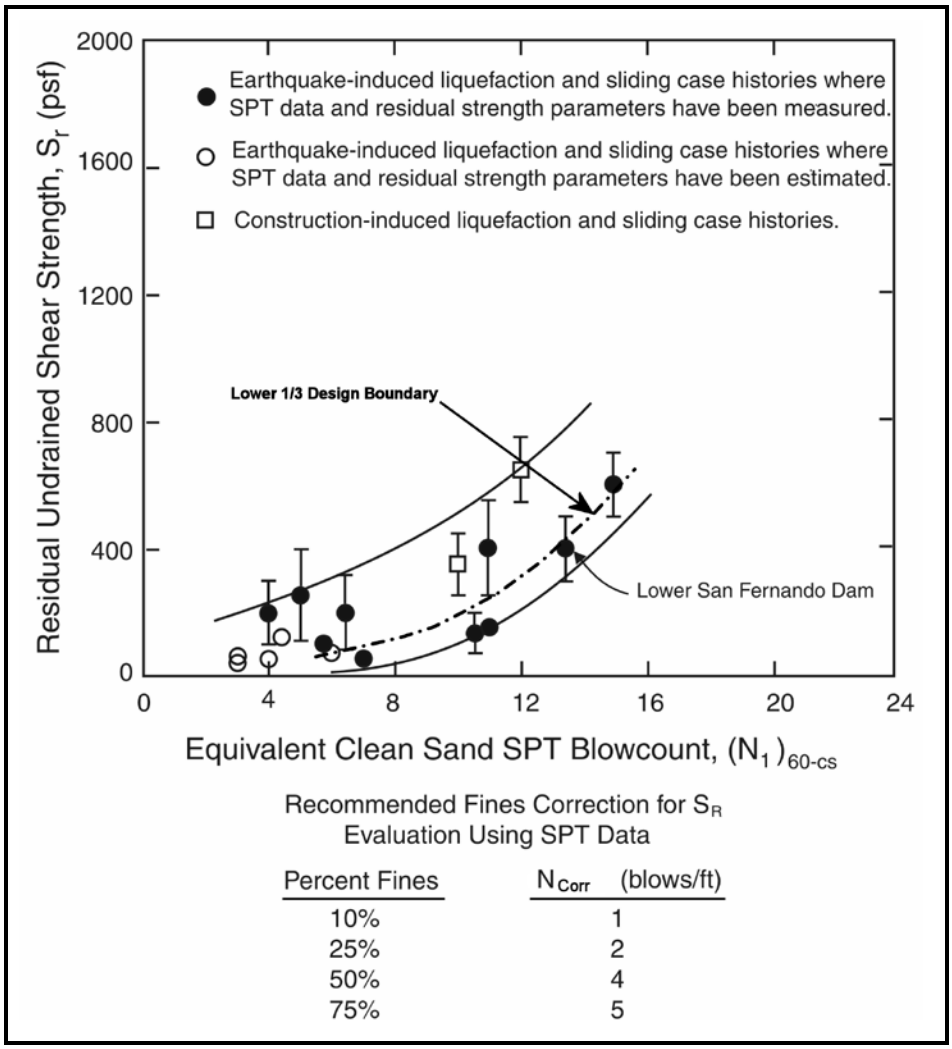

Recommended Fines Correction for S_R Evaluation Using SPT Data

Percent Fines	N_{Corr} (blows/ft)
10%	1
25%	2
50%	4
75%	5

Figure 13-37, Residual Shear Strength ($\tau_{rl} = S_{rl}$) vs. Corrected Clean Sand SPT (Modified Seed and Harder, 1990)

13.12.2.2 Olson and Stark (2002, 2003) – Liquefied Residual Shear Strength

The Olson and Stark (2002, 2003) methods allow for the computation of the liquefaction shear strength ratio (τ_{rl}/σ'_{vo}), which is the ratio of liquefied shear strength (τ_{rl}) to effective overburden stress (σ'_{vo}). The relationship between liquefaction shear strength ratio and the normalized SPT blow count ($N^*_{1,60}$) is provided in Figure 13-34. The average trend line for Figure 13-34 can be computed using the following equation.

$$\left(\frac{\tau_{rl}}{\sigma'_{vo}}\right) = 0.03 + 0.0075\left(N^*_{1,60}\right) \pm 0.03 \qquad \text{Equation 13-75}$$

Where,

$N^*_{1,60}$ = Normalized SPT blow count and values of $N^*_{1,60} \leq 12$ blows per foot.

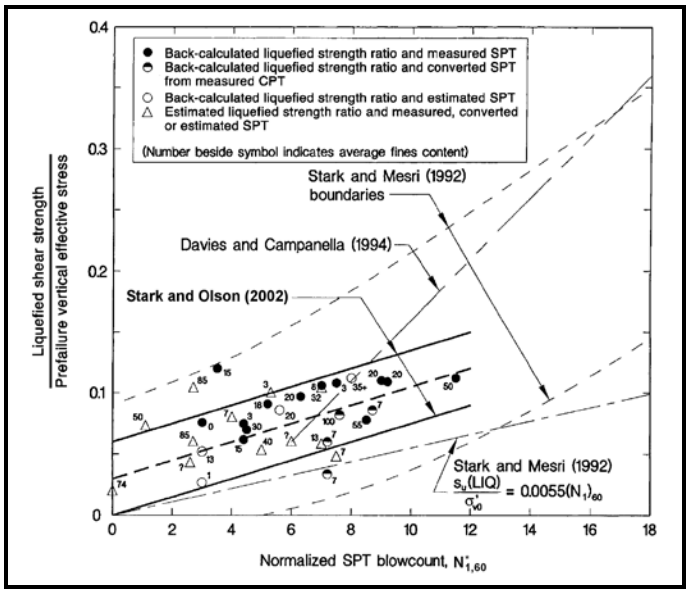

Figure 13-38, Liquefied Shear Strength Ratio - SPT Blow Count (Olson and Stark, 2002, 2003 with permission from ASCE)

The relationship between liquefaction shear strength ratio and the normalized CPT tip resistance ($q_{c,1}$) is provided Figure 13-35. The average trend line for Figure 13-35 can be computed using the following equation.

$$\left(\frac{\tau_{rl}}{\sigma'_{vo}}\right) = \mathbf{0.03} + \mathbf{0.0143}\left(q_{c,1}\right) \pm \mathbf{0.03} \qquad \text{Equation 13-76}$$

Where,

$q_{c,1}$ = Normalized CPT tip resistance (in units of MPa) for values $q_{c,1} \leq 6.5$ MPa (approximately 68 tsf) .

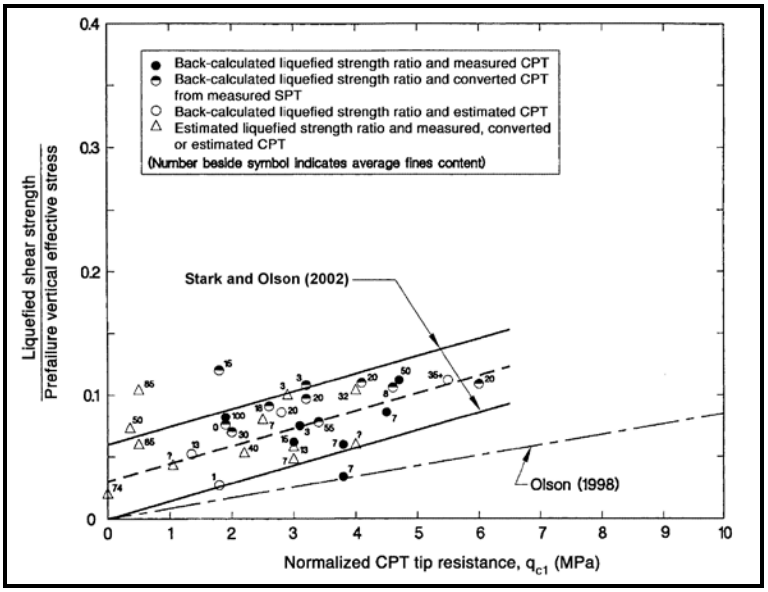

Figure 13-39, Liquefied Shear Strength Ratio - CPT Tip Resistance (Olson and Stark, 2002, 2003 with permission from ASCE)

13.12.2.3 Idriss and Boulanger (2008) – Liquefied Residual Shear Strength

The Idriss and Boulanger (2008) method allows for the computation of the liquefaction residual shear strength ratio (τ_{rl} / σ'_{vo}), which is the ratio of liquefied residual shear strength ($\tau_{rl} = S_{rl}$) to effective overburden stress (σ'_{vo}). The liquefaction residual shear strength ratio (τ_{rl} / σ'_{vo}) has been correlated to SPT and CPT in-situ testing.

The Idriss and Boulanger (2008) relationship for liquefaction residual shear strength ratio (τ_{rl} / σ'_{vo}) for SPT and CPT in-situ testing includes the following:

Case 1: Condition in which the effects of void redistribution can be confidently judged to be negligible. This condition occurs at sites where the site stratigraphy would not impede dissipation of excess pore water pressure and the dissipation of excess pore water pressure would be accompanied by densification of the soils.

Case 2: Condition in which the effects of void redistribution can be significant. This condition occurs at sites where the site stratigraphy would impede dissipation of excess pore water pressure. Sites that meet this condition include sites with relatively thick layers of liquefiable soils that are overlain by lower permeability soils that would impede the dissipation of excess pore water pressure by trapping the upwardly seeping pore water beneath the lower permeability soil. This condition would lead to localized loosening, strength loss, and possibly even the formation of water film beneath the lower permeability soil.

The SPT correlation uses a corrected fines content SPT blow count, $N^*_{1,60,cs}$, computed as shown in Equation 13-70. Corrected and normalized SPT blow counts, $N^*_{1,60}$, should be computed in accordance with Section 13.11.1.3. Values for $\Delta N_{1,60\text{-}rl}$ can be found in Table 13-6.

$$N^*_{1,60,CS} = N^*_{1,60} + \Delta N_{1,60-rl}$$ Equation 13-77

Table 13-6, Values of $\Delta N_{1,60\text{-}rl}$ (Seed, 1987)

Fines Content, FC (% passing No. 200 sieve)	$\Delta N_{1,60\text{-}rl}$
10	1
25	2
50	4
75	5

The liquefaction residual shear strength ratio (τ_{rl} / σ'_{vo}) for SPT can be determined for Case 1 and Case 2 using Figure 13-36. Note in Figure 13-36 τ_{rl} is equivalent to S_r.

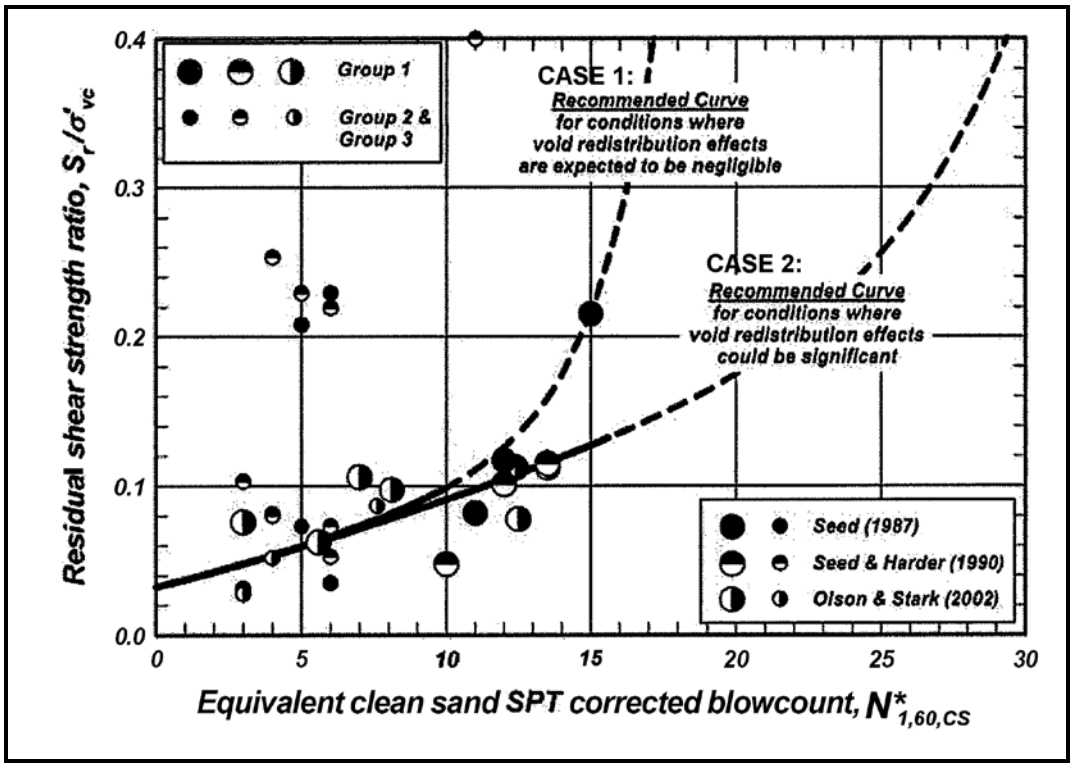

Figure 13-40, Liquefied Shear Strength Ratio - SPT (Idriss and Boulanger, 2008)

In lieu of using Figure 13-36, the liquefaction residual shear strength ratio (τ_{rl} / σ'_{vo}) for SPT can be determined for Case 1 and Case 2 by using the following equations.

Case 1:

Equation 13-78

$$\left(\frac{\tau_{rl}}{\sigma'_{vo}}\right) = \exp\left[\left(\frac{N^*_{1,60,CS}}{16}\right) + \left(\frac{N^*_{1,60,CS} - 16}{21.2}\right)^3 - 3.0\right] \times \left(1 + \exp\left[\frac{N^*_{1,60,CS}}{2.4} - 6.6\right]\right) \leq \tan\phi'$$

Case 2:

Equation 13-79

$$\left(\frac{\tau_{rl}}{\sigma'_{vo}}\right) = \exp\left[\frac{N^*_{1,60,CS}}{16} + \left(\frac{N^*_{1,60,CS} - 16}{21.2}\right)^3 - 3.0\right] \leq \tan\phi'$$

The CPT correlation uses a corrected normalized and adjusted for fines content CPT tip resistance, $q_{c,1,N,CS}$, computed as shown in Equation 13-73. Corrected and normalized blow counts, $q_{c,1,N}$, should be computed in accordance with Section 13.11.1.4. Values for $\Delta q_{c,1,N\text{-}rl}$ can be found in Table 13-7.

Equation 13-80

$$q_{c,1N,CS} = q_{c,1N} + \Delta q_{c,1N-rl}$$

Table 13-7, Values of $\Delta q_{c,1,N,\text{-}rl}$
(Idriss and Boulanger, 2008)

Fines Content, FC (% passing No. 200 sieve)	$\Delta q_{c,1,N\text{-}rl}$
10	10
25	25
50	45
75	55

The liquefaction residual shear strength ratio (τ_{rl} / σ'_{vo}) for CPT can be determined for Case 1 and Case 2 using Figure 13-37.

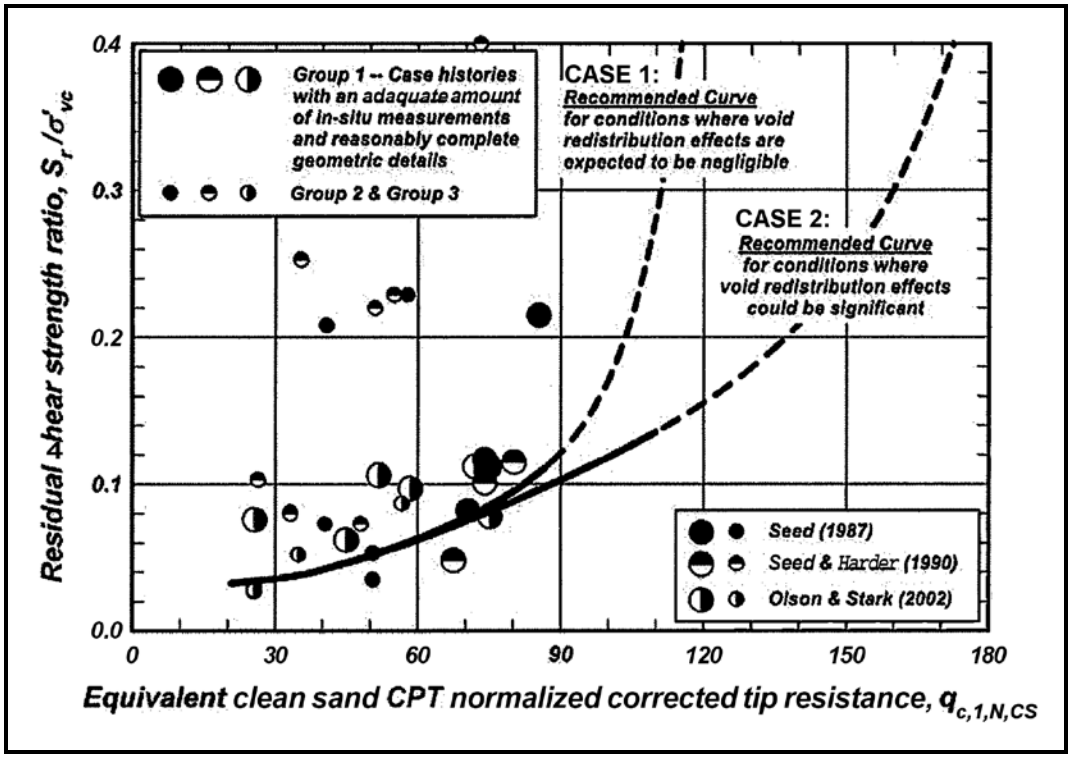

Figure 13-41, Liquefied Shear Strength Ratio - CPT Tip Resistance (Idriss and Boulanger, 2008)

In lieu of using Figure 13-37, the liquefaction residual shear strength ratio (τ_{rl} / σ'_{vo}) for CPT can be determined for Case 1 and Case 2 by using the following equations.

Case 1:

Equation 13-81

$$\left(\frac{\tau_{rl}}{\sigma'_{vo}}\right) = \exp\left[\left(\frac{q_{c,1N,CS}}{24.5}\right) - \left(\frac{q_{c,1N,CS}}{61.7}\right)^2 + \left(\frac{q_{c,1N,CS}}{106}\right)^3 - 4.42\right] \leq \tan\phi'$$

Case 2:

Equation 13-82

$$\left(\frac{\tau_{rl}}{\sigma'_{vo}}\right) = \exp\left[\left(\frac{q_{c,1N,CS}}{24.5}\right) - \left(\frac{q_{c,1N,CS}}{61.7}\right)^2 + \left(\frac{q_{c,1N,CS}}{106}\right)^3 - 4.42\right] \times \left(1 + \exp\left[\left(\frac{q_{c,1N,CS}}{11.1}\right) - 9.82\right]\right) \leq \tan\phi'$$

13.12.3 Clay-Like Soil Cyclic Shear Strength Triggering

NS Clay-Like soils with soil SSL triggering resistance ratio $(D/C)_{SL}$ greater than the Clay-Like soil SSL triggering resistance factor ($\varphi_{SL\text{-}Clay}$) will be subject to soil SSL approximately equal to the cyclic softening residual shear strength, τ_{rs}. The resistance factor (φ) indicated in Figure 13-38 are for illustration purposes. Resistance factors used for design shall be those presented in Chapter 9.

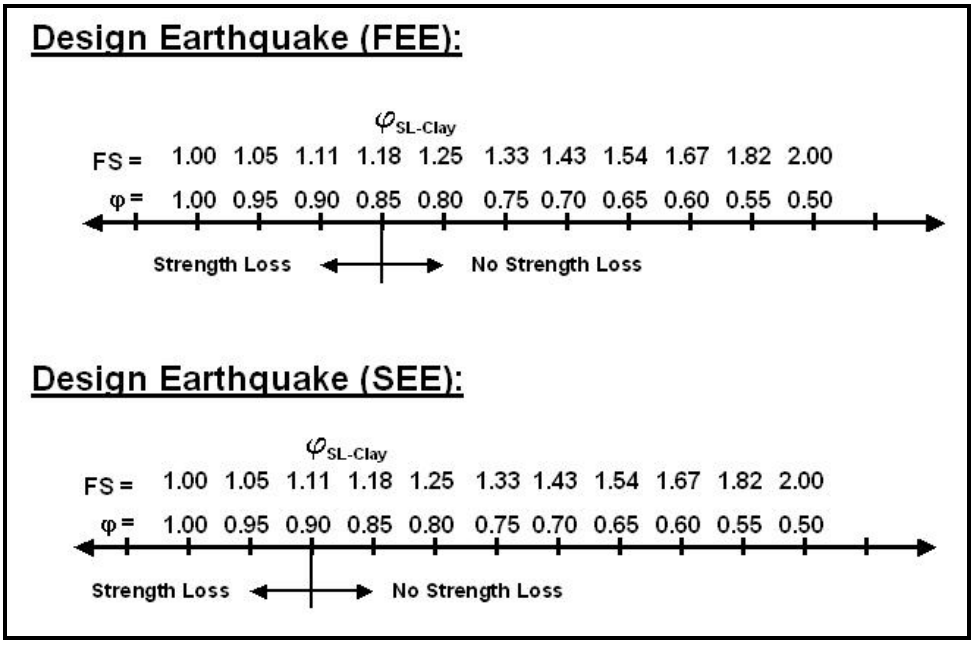

Figure 13-42, Shear Strength of Clay-Like Soils

13.12.4 Clay-Like Soil Cyclic Softening Shear Strength

NS Clay-Like soils below the water table having low sensitivity ($S_t < 5$) and subjected to modest cyclic shear stresses can produce significant permanent strains that can lead to stresses near the soil's yield stress. The residual cyclic softening shear strength, τ_{rs}, of cohesive soils can be estimated by reducing the soil's undrained shear strength ($\tau_{Peak} = S_u$) using the following equation.

$$\tau_{rs} = 0.8\tau_{Peak} \qquad \text{Equation 13-83}$$

Highly sensitive Clay-Like soils having sensitivity ratio, $S_t \geq 5$ that are subject to modest cyclic shear stresses can experience moderate to significant loss in soil shear strengths. The reduced shear strength can be estimated by determining the remolded soil shear strength ($\tau_{remolded}$) as indicated in Chapter 7.

13.12.5 Seismic Soil Shear Strength Selection

The use of drained/undrained soil shear strengths is dependent on the type of soil and the shear strain level the soil is experiencing. Large variations in shear strain levels can occur during a seismic event from small strains during cyclic loadings to large strains during soil failures. The Extreme Event I limit state is used to perform geotechnical analyses for earthquake loadings (Design Earthquake Events FEE and SEE). Because performance limits for the Extreme Event I limit state allow for deformations, the selected shear strength will depend on the strain level that the soil will experience and its potential for soil SSL.

Soil shear strength selection for seismic analyses should be made based on laboratory testing and soil strain level anticipated from analyses. Table 13-8 provides a summary of "general" soil behavior (shear stress vs. strain) observed from published soil stress-strain curves from Holtz and Kovacs (1981), Terzaghi, Peck, and Mesri (1996), and Duncan and Wright (2005). Table 13-8 should be used for "general" guidance on the selection of seismic shear strengths based on soil type and soil strain level anticipated from analyses.

Table 13-8, Seismic Soil Shear Strength Selection

Sand-Like Soils (Undrained)	**Strain Level at Failure [(1)]**			
	Cyclic Strains	**±5% Strains**	**15–20% Strains**	**Large Strains >20%**
Med. To Dense Sand	τ_{Peak}	τ_{Peak}	τ_r	τ_r
Non-Liquefying Loose Sands	τ_{Peak}	τ_{Peak}	τ_{Peak}	τ_{Peak}
Liquefied Soils	τ_{rl}	τ_{rl}	τ_{rl}	τ_{rl}
NS Clay-Like Soils (Undrained)	**Strain Level at Failure [(1)]**			
	Cyclic Strains	**±2% Strains**	**10–15% Strains**	**Large Strains >15%**
OCR =1, $S_t < 5$	τ_{rs}	τ_{Peak}	τ_{Peak}	τ_{Peak}
OCR >1, $S_t < 5$	τ_{rs}	τ_{Peak}	τ_r	τ_r
HS Clay-Like Soils (Undrained)	**Strain Level at Failure [(1)]**			
	Typically Failure < 3%			
Highly Sensitive ($S_t \geq 5$)	$\tau_{remolded}$			

Shear Strength Nomenclature:

τ_{Peak} = Peak Soil Shear Strength

τ_r = Residual Soil Shear Strength

$\tau_{remolded}$ = Remolded Soil Shear Strength

τ_{rl} = Cyclic Liquefaction Residual Shear Strength

τ_{rs} = Cyclic Softening Residual Shear Strength

[(1)] Strain levels indicated are generalizations and are dependent on the stress-strain characteristics of the soil and should be verified by laboratory testing.

13.13 FLOW SLIDE FAILURE

Flow liquefaction failure occurs when the soils exhibit strain softening and gravitational shear stresses are larger than the cyclic liquefaction residual soil shear strength. The strain softening can be a result of monotonic or cyclic undrained loading. Flow liquefaction failures typically occur rapidly and are usually catastrophic. Earthquake-induced flow liquefaction tends to occur after the cyclic loading ceases due to the progressive nature of the load redistribution; however, if the soils are sufficiently loose and the static shear stresses are sufficiently large, the earthquake loading may trigger essentially "spontaneous liquefaction" within the first few cycles of loading.

Flow failures are the most destructive form of liquefaction-induced ground failure. A flow failure is characterized by substantial masses of surficial soils undergoing large translational or rotational deformations and typically occurs after the earthquake shaking has ceased. The surficial soils undergo deformations when static driving forces exceed the average soil shearing stress along the critical failure surface. The soil shearing stress along the critical shear surface is significantly reduced due to the strain softening of underlying granular loose deposits that occurs during flow liquefaction. Because flow liquefaction tends to occur after the cyclic loading ceases, the effects of earthquake ground motions (inertial forces due to the earthquake shaking) are not included in the analyses.

The evaluation of the onset of a flow failure proceeds as follows:

1. Use steeply sloped ground site conditions to evaluate the potential for flow failure

2. If flow failure potential exists, perform a SSL Triggering analysis to determine which soils are susceptible to SSL.

3. Assign appropriate soil shear strengths to Sand-Like, NS Clay-Like, and HS Clay-Like soils susceptible to SSL and undrained/drained shear strengths to soils not susceptible to SSL.

4. Perform a conventional static slope stability analysis (no seismic acceleration coefficient). Determine the static resistance to flow failure $(D/C)_{Flow}$ and the required resistance factor against flow failure, φ_{Flow}. If the static resistance to flow failure $(D/C)_{Flow} > \varphi_{Flow}$, flow failure potential exists at the site. The LRFD equation for use in determining the onset of flow failure is shown below.

$$\left(\frac{D}{C}\right)_{Flow} \leq \varphi_{Flow} \qquad \text{Equation 13-84}$$

The magnitude of flow failure deformations is typically in excess of 25 feet, depending on the geometry of the flowing ground, extent of strain softening of the subsurface soils, and the soil stratification. Estimation of lateral flow deformation is very complex and there are currently no accepted methods for evaluating this type of deformation. Since flow failure deformations can not be reliably estimated, it is assumed that the soils will undergo unlimited deformation and as

a result exert soil pressure loads on any structures that are affected by the flow failure movements.

13.14 LATERAL SPREAD

Lateral spreading is the horizontal displacement that occurs on mostly level ground or gentle slopes (< 5 degrees) as a result of cyclic liquefaction of shallow Sand-Like soil deposits. The soil can slide as intact blocks down the slope towards a free face such as an incised river channel. Case studies have reported displacements as great as 30 feet with smaller associated settlements.

Lateral spread occurs as a result of the static and dynamic (earthquake shaking) driving forces applied to surficial soils that have experienced or undergone significant reduction in soil shear strength due to a liquefaction of a loose sand layer typically located within the upper 10 feet. The main distinction between lateral spread and general seismic slope instability is that lateral spread typically occurs on level ground sites not susceptible to flow slide failure and soil SSL along the failure surface are generally greater than 20% when compared to the shear strengths along the failure surface prior to the soil SSL. As a result of the slope instability, a failure surface resembling a sliding block typically develops along the liquefied soils and is subject to lateral displacements until equilibrium is restored. In addition to lateral spread deformations, the ground is also susceptible to seismic settlement. A liquefaction potential assessment in accordance with Sections 13.6 and 13.7 should first be made to determine if screening and triggering of lateral spread is possible. Since cyclic soil strength degradation or liquefaction may occur during the earthquake shaking, the effects of earthquake ground motions (inertial forces) and residual shear strengths (liquefied soils and non-liquefied soils) shall be used during the evaluation of the potential for lateral spread.

The lateral spread displacement evaluation process is as follows:

Step 1. Perform a SSL Triggering analysis for level ground sites to determine which soils are susceptible to SSL.

Step 2. Assign appropriate soil shear strengths to Sand-Like, NS Clay-Like, and HS Clay-Like soils susceptible to SSL and undrained/drained shear strengths to soils not susceptible to SSL.

Step 3. Perform a conventional pseudo-static slope stability analysis with average horizontal acceleration coefficient with adjustments for wave scattering (k_h). Determine the static resistance ratio to lateral spread $(D/C)_{Spread}$ and the required resistance factor against lateral spread, φ_{Spread}. If the static resistance ratio to lateral spread $(D/C)_{Spread} > \varphi_{Spread}$, lateral spread potential exists at the site. The LRFD equation used in determining the onset of lateral spread is shown below.

$$\left(\frac{D}{C}\right)_{Spread} \leq \varphi_{Spread} \qquad \text{Equation 13-85}$$

Step 4. Perform empirical or semi-empirical deformation analyses as described in this Section. If the computed deformations multiplied by a factor of "2" is less than the performance limit requirements in Chapter 10 (2 x deformation computed $\leq$ required performance limits) then no deformation analysis is required. A factor of "2" times the displacements computed has been selected because of the associated uncertainty inherent in the empirical or semi-empirical deformation analytical methods.

Step 5. If the displacements computed in Step 4 exceed the performance limits, additional displacement calculations should be performed using all of the empirical and semi-empirical methods for computing lateral spread deformations that are presented in this section. The Newmark displacement methods may be used with caution provided that the requirements stated below are adhered to.

Step 6. From the displacement computations performed in Steps 4 and 5, the designer will need to evaluate if there are any trends in the displacements computed. It should be noted that these displacement methods have been shown by various case histories to be very unreliable with just as many under predictions as over predictions, up to a factor of "2" as was used in Step 4.

Empirical/semi-empirical methods have been developed based on case history databases for specific types of failure modes, earthquake characteristics, site geometry, and subsurface soils. Methods indicated as semi-empirical are based on some numerical basis to estimate residual shear strains in the soils after liquefaction. Empirical and semi-empirical methods are only used for screening purposes because of the low reliability of the predictions. The following empirical and semi-empirical methods have been developed specifically to evaluate lateral spread:

- Youd et al., 2002 – Multilinear Regression Equations for Prediction of Lateral Spread Displacements
- Rauch and Martin, 2000- EPOLLS Model for Predicting Average Displacements on Lateral Spreads
- Zhang et al., 2004 – SPT or CPT Liquefaction-Induced Lateral Displacements

Newmark methods of displacement analysis are typically not appropriate for evaluation of lateral spreads when soil SSL are greater than 50% when compared to the shear strengths prior to the SSL. If it can be shown that the shear failure surface as a whole has not lost more than 50% of the shear failure resistance prior to the soils SSL, the Newmark method may be used. The Newmark method may also be used without adjusting soil shear strengths to obtain a lower bound displacement. If the lower bound displacement exceeds the performance limits mitigation of the hazard will be required. Newmark methods described in Section 13.17 should be used with caution.

13.14.1 Multilinear Regression of Lateral Spread Displacements

Youd et al. (2002) revised the multilinear regression empirical equations previously developed by Bartlett and Youd (1992, 1995) for prediction of lateral spread displacement. This method used a large database of lateral spread case histories from past earthquakes. A review of the Bartlett and Youd, 1992, case history database reveals measured displacements that range

from less than one inch to as much as 30 feet. The predicted displacements vary from one-half of the measured value to twice the measured value. Because of the high uncertainty associated with lateral displacement values computed with this method it is only used for screening of potential for lateral spread displacements. It should be noted that the following equations are valid when liquefaction occurs over a widespread area, and not just isolated pockets. Liquefiable soils layers must be identified as indicated in Sections 13.6 and 13.7. Guidance for specific input of each of the parameters in the following equations is provided by Youd, et al. (2002).

For ground slope condition (Figure 13-40: Case 1):

Equation 13-86

$$\log D_H = -16.213 + 1.532 M_w - 1.406 \log(R^{*}) - 0.012R + 0.338 \log(S) + 0.540 \log T_{15} + 3.413 \log (100 - F_{15}) - 0.795 \log (D50_{15} + 0.1 \text{ mm})$$

For free-face condition (Figure 13-40 Case 2):

Equation 13-87

$$\log D_H = -16.713 + 1.532 M_w - 1.406 \log(R^{*}) - 0.012R + 0.592 \log(W) + 0.540 \log(T_{15}) + 3.413 \log (100 - F_{15}) - 0.795 \log (D50_{15} + 0.1 \text{ mm})$$

Where:

D_H = Estimated lateral ground displacement in meters

T_{15} = Cumulative thickness of saturated granular layers with corrected blow counts, $(N_1)_{60}$, less than or equal to 15, in meters.

$D50_{15}$ = Average mean grain size in granular layer included in T_{15} in mm.

F_{15} = Average fines content (passing #200 sieve) for granular layers included in T_{15} in percent.

M_w = Design earthquake magnitude (moment magnitude).

R = Site-to-source distance, in kilometers.

R_o = Distance factor that is a function of earthquake magnitude, M_w and is computed using the following equation.

$$R_o = 10^{(0.89M_w - 5.64)}$$ Equation 13-88

R^{*} = Modified source distance and is computed using the following equation.

$$R^{*} = R + R_o$$ Equation 13-89

S = Ground slope, in percent.

W = Ratio of the height (H) of the free face to the distance (L) from the base of the free face to the point in question, in percent (i.e.,100H/L).

The design earthquake moment magnitude, M_w, and the site-to-source distance, R, shall be those determined for the design earthquake under evaluation as required in Chapter 12.

13.14.2 EPOLLS – Average Horizontal Lateral Spread Displacements

Rauch and Martin (2000) developed the EPOLLS (Empirical Prediction Of Liquefaction-induced Lateral Spreading) model to predict the average horizontal ground surface displacements due to liquefaction-induced lateral spread. The liquefaction accounts only for the SSL of Sand-Like soils. This method does not account for SSL in NS Clay-Like soils or HS Clay-Like soils. The EPOLLS model was developed from a multiple regression analysis of data from 71 lateral spread case studies with 15 earthquakes in western North America and eastern Asia (mostly California, Alaska, and Japan). The maximum average horizontal displacements in the database is approximately 16 feet (4.8 m) with approximately 1/3 of the cases having an average horizontal displacement less than 8.5 feet (2.5 m). The EPOLLS model uses seismic input, site topography, and subsurface conditions to predict horizontal ground surface displacements.

The EPOLLS model predicts the average displacement across the surface of a lateral spread. The EPOLLS model was developed based on three components: Regional, Site, and Geotechnical. The Regional component (R-EPOLLS) accounts for earthquake source factors affecting the magnitude of the lateral spread such as the earthquake magnitude, distance to fault rupture, peak horizontal acceleration, and duration of strong shaking. The Site component (S-EPOLLS) accounts for site factors affecting the magnitude of the lateral spread such as the length of sliding area, slope of the ground surface, and height of free-face. The Geotechnical component (G-EPOLLS) accounts for geotechnical factors affecting the magnitude of the lateral spread such as depth of liquefaction zone and depth to the top of the liquefied soils. It should be noted that the following equations are valid when cyclic liquefaction of Sand-Like soils occurs over a widespread area, and not just isolated pockets. Liquefiable soils layers must be identified as indicated in Sections 13.6 and 13.7. Guidance for specific input of each of the parameters in the following equations is provided by Rauch and Martin (2000).

R-EPOLLS (Regional Component):

$$D_R = (613M_W - 13.9R - 2420A_{max} - 11.4D_{5\text{-}95})/1000 \qquad \text{Equation 13-90}$$

$$\text{R-EPOLLS Avg. Displacement} = (D_R - 2.21)^2 + 0.149 \qquad \text{Equation 13-91}$$

S-EPOLLS (Site Component):

$$D_S = 0.523L_{slide} + 42.3S_{top} + 31.3H_{face})/1000 \qquad \text{Equation 13-92}$$

$$\text{S-EPOLLS Avg. Displacement} = (D_R + D_S - 2.44)^2 + 0.111 \qquad \text{Equation 13-93}$$

G-EPOLLS (Geotechnical Component):

$$D_G = (50.6Z_{Bottom} - 86.1Z_{Top})/1000 \qquad \text{Equation 13-94}$$

$$\text{G-EPOLLS Avg. Displacement} = (D_R + D_S + D_G - 2.49)^2 + 0.124 \qquad \text{Equation 13-95}$$

Where:

M_w = Design earthquake moment magnitude

R = Site-to-source, in kilometers

A_{max} = Peak horizontal acceleration, units of g (gravity)

D_{5-95} = Duration of strong shaking, units of seconds

L_{Slide} = Length of sliding area, in meters

S_{Top} = Slope of ground surface, in units of percent (%)

H_{Face} = Height of free-face, in units meters

Z_{Bottom} = Depth to bottom of liquefied layer from ground surface, in units of meters.

Z_{Top} = Depth to top of liquefied layer from ground surface, in units of meters.

The design earthquake moment magnitude (M_w), source to site distance (R), peak horizontal acceleration (A_{max} = PGA), and the duration of strong shaking (D_{5-95}) are determined for the design earthquake under evaluation as indicated in Chapter 12.

The model parameters used in the equation should be checked to ensure that a prediction is within the limits of the data indicated in Table 13-9 that was used to develop the model.

The G-EPOLLS Avg. Displacement results should be used in Step 4 (Section 13.14) of the lateral spread displacement evaluation process.

Table 13-9, Limiting Range of EPOLLS Model Parameters (Rauch and Martin, 2000 with permission from ASCE)

Variables	Minimum Value	Maximum Value	Units
M_w	6.5	9.2	---
R	0	119	Km
A_{max}	.16	0.52	G
D_{5-95}	4	88	Sec
L_{Slide}	20	1,360	m
S_{Top}	-0.7	5.2	%
H_{Face}	0	9.0	m
Z_{Bottom}	2.4	12.4	m
Z_{Top}	0.9	7.3	m

A check to ensure that parameter combinations do not exceed the limits of the database should be made by computing D_R, (D_R + D_S), and (D_R + D_S + D_G) are within the limits of Table 13-10. Note that the average horizontal lateral spread displacement computed using G-EPOLLS ranges from 0.23 to 4.29 meters.

Table 13-10, Limiting Range of EPOLLS Variables
(Rauch and Martin, 2000 with permission from ASCE)

Variables	Minimum Value	Maximum Value	Units
D_R	6.5	9.2	m
$(D_R + D_S)$	0	119	m
$(D_R + D_S + D_G)$	.16	0.52	m
R-EPOLLS Avg. Displacement	4	88	m
S-EPOLLS Avg. Displacement	20	1,360	m
G-EPOLLS Avg. Displacement	-0.7	5.2	m

13.14.3 SPT/CPT Liquefaction-Induced Lateral Displacements

Liquefaction-induced lateral spread displacements can be estimated by either SPT or CPT in-situ testing results using the method proposed by Zhang et al., 2004. The SPT and CPT normalized values of $N^*_{1,60,cs}$ and $q_{c,1,N,cs}$ are computed in accordance with Sections 13.11.2 and 13.11.3, respectively. The relationship between the maximum cyclic shear strain, γ_{max}, and the liquefaction triggering resistance ratio, $(D/C)_{SL}$, for soils with different relative densities, D_r, is provided in Figure 13-39. The liquefaction triggering resistance ratio, $(D/C)_{SL}$, is obtained from the soil SSL triggering analysis for level ground sites in Section 13.7.

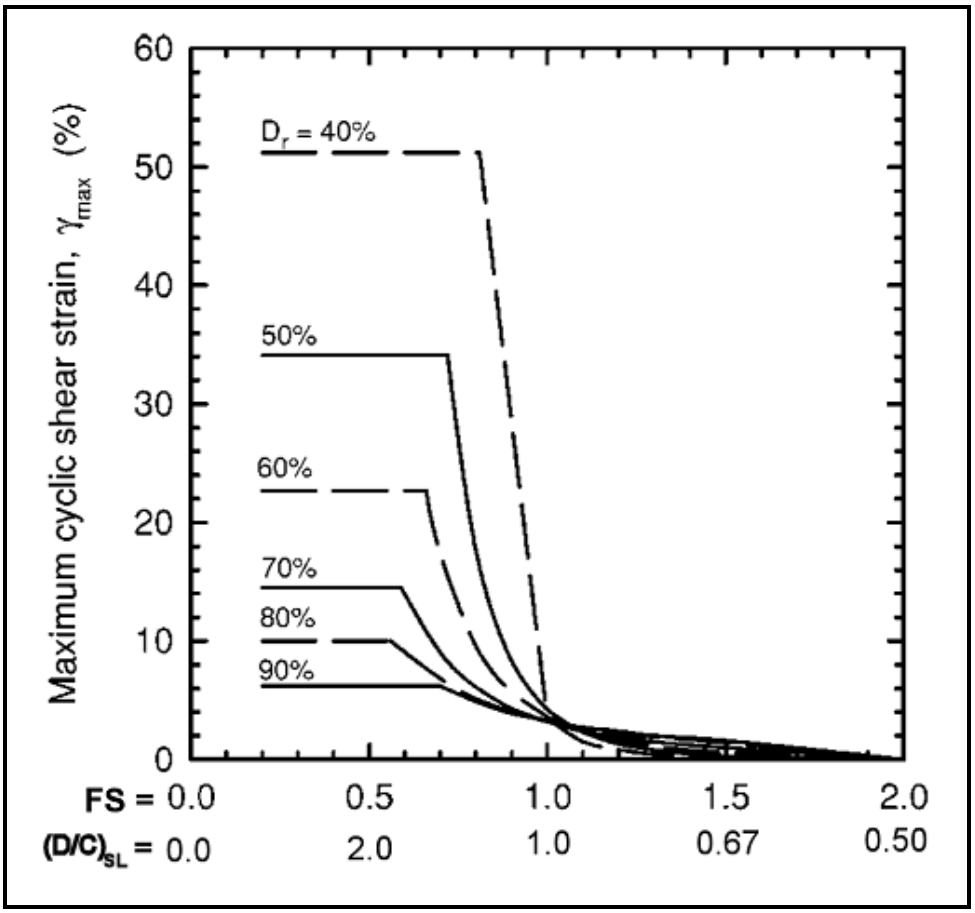

Figure 13-43, Relationship Between Maximum Cyclic Shear Strain and φ
(Zhang et al., 2004 with permission from ASCE)

The SPT and CPT equivalent clean sand normalized values of $N^{*}_{1,60,cs}$ and $q_{c,1,N,cs}$ can be used to estimate the relative density, D_r, of the potentially liquefiable soils. The relative density, D_r, can be estimated from SPT blow counts ($N^{*}_{1,60,cs}$ in units of blows/foot) using the following equation.

Equation 13-96

$$D_r = 14 \cdot \sqrt{N^{*}_{1,60,cs}} \qquad \left[N^{*}_{1,60,cs} \leq 42 \; blows/foot\right]$$

The relative density, D_r, can be estimated from CPT tip resistance ($q_{1,c,mod}$ in units of kPa) using the following equation.

Equation 13-97

$$D_r = -85 + 76 \log\left(q_{c,1N,cs}\right) \qquad \left[q_{c,1N,cs} \leq 200\right]$$

In lieu of using Figure 13-39 to estimate the maximum cyclic shear strain, γ_{max}, the equations listed in Table 13-11 can be used.

Table 13-11, Relationship Between Maximum Cyclic Shear Strain and φ[1]
(Zhang et al., 2004 – data from Ishihara and Yoshimine, 1992 and Seed, 1979)

$$\textit{If } D_r = 90\%, \quad \gamma_{max} = 3.26\left(\frac{1}{\varphi}\right)^{-1.80} \quad \textit{for } 0.70 \le \left(\frac{1}{\varphi}\right) \le 2.00$$

$$\textit{If } D_r = 90\%, \quad \gamma_{max} = 6.2 \quad \textit{for } \left(\frac{1}{\varphi}\right) \le 0.70$$

$$\textit{If } D_r = 80\%, \quad \gamma_{max} = 3.22\left(\frac{1}{\varphi}\right)^{-2.08} \quad \textit{for } 0.56 \le \left(\frac{1}{\varphi}\right) \le 2.00$$

$$\textit{If } D_r = 80\%, \quad \gamma_{max} = 10.0 \quad \textit{for } \left(\frac{1}{\varphi}\right) \le 0.56$$

$$\textit{If } D_r = 70\%, \quad \gamma_{max} = 3.20\left(\frac{1}{\varphi}\right)^{-2.89} \quad \textit{for } 0.59 \le \left(\frac{1}{\varphi}\right) \le 2.00$$

$$\textit{If } D_r = 70\%, \quad \gamma_{max} = 14.5 \quad \textit{for } \left(\frac{1}{\varphi}\right) \le 0.59$$

$$\textit{If } D_r = 60\%, \quad \gamma_{max} = 3.58\left(\frac{1}{\varphi}\right)^{-4.42} \quad \textit{for } 0.66 \le \left(\frac{1}{\varphi}\right) \le 2.00$$

$$\textit{If } D_r = 60\%, \quad \gamma_{max} = 22.7 \quad \textit{for } \left(\frac{1}{\varphi}\right) \le 0.66$$

$$\textit{If } D_r = 50\%, \quad \gamma_{max} = 4.22\left(\frac{1}{\varphi}\right)^{-6.39} \quad \textit{for } 0.72 \le \left(\frac{1}{\varphi}\right) \le 2.00$$

$$\textit{If } D_r = 50\%, \quad \gamma_{max} = 34.1 \quad \textit{for } \left(\frac{1}{\varphi}\right) \le 0.72$$

$$\textit{If } D_r = 40\%, \quad \gamma_{max} = 3.31\left(\frac{1}{\varphi}\right)^{-7.97} \quad \textit{for } 1.00 \le \left(\frac{1}{\varphi}\right) \le 2.00$$

$$\textit{If } D_r = 40\%, \quad \gamma_{max} = 250\left(1.0 - \left(\frac{1}{\varphi}\right)\right) + 3.5 \quad \textit{for } 0.81 \le \left(\frac{1}{\varphi}\right) \le 1.00$$

$$\textit{If } D_r = 40\%, \quad \gamma_{max} = 51.2 \quad \textit{for } \left(\frac{1}{\varphi}\right) \le 0.81$$

[1] $\varphi = (D/C)_{SL}$

A Lateral Displacement Index (LDI) has been developed in order to quantify the potential for lateral displacements for a given soil profile, soil properties, and earthquake characteristics. The LDI is computed by integrating the calculated maximum cyclic shear strain, γ_{max}, over the maximum depth of all potential liquefiable layers. The LDI can be computed as indicated in the following equation.

$$LDI = \int_0^{z_{max}} \gamma_{max} dz \qquad \text{Equation 13-98}$$

Where Z_{max} is the maximum depth below all the potential liquefiable layers with a calculated liquefaction resistance ratio, $(D/C)_{SL} < 0.50$.

The magnitude of lateral displacement, LD, is dependent on the LDI and the geometric parameters characterizing ground geometry. The following ground geometry cases are used in these analyses.

Case 1. Gently sloping ground without a free face

Case 2. Nearly level ground with a free face

Case 3. Gently sloping ground with a free face

The ground geometry parameters used to define the above cases are described below and illustrated in Figure 13-40.

S = Ground Slope (%)

H = Free Face Height (Units consistent with units of L)

L = Distance to Free Face (Units consistent with units of H)

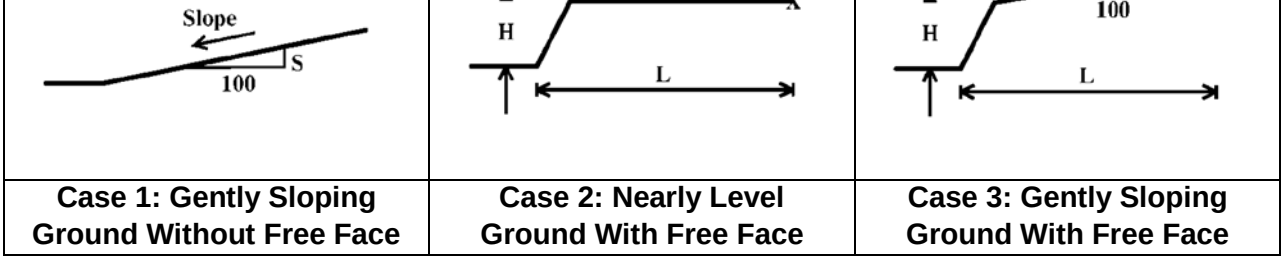

Case 1: Gently Sloping Ground Without Free Face	Case 2: Nearly Level Ground With Free Face	Case 3: Gently Sloping Ground With Free Face

Figure 13-44, Ground Geometry Cases
(Zhang et al., 2004 with permission from ASCE)

Once the ground geometry has been defined, the lateral displacements, LD, can be computed as indicated below:

Case 1: Gently Sloping Ground Without Free Face

$$LD = LDI(S + 0.2) \qquad [0.20\% < S < 3.5\%] \qquad \text{Equation 13-99}$$

Cases 2 or 3: Nearly Level Ground to Gently Sloping Ground With Free Face

Equation 13-100

$$LD = 6 \cdot LDI\left(L/H\right)^{-0.8} \qquad \left[4 < \left(L/H\right) < 40\right]$$

Since this method is a semi-empirical method, it should be limited to the ranges of earthquake properties and ground conditions included within the case history database as indicated below.

- Moment Magnitude, M_w: $6.4 \leq M_w \leq 9.2$
- Peak Horizontal Ground Acceleration, a_{max}: $0.19g \leq a_{max} \leq 0.60g$
- Free Face Height, H: H < 60 feet

13.15 SEISMIC GLOBAL STABILITY

Earthquake-induced global instability can occur at bridge abutments, roadway embankments, bridge approach fills, natural cut slopes, and at ERSs. This geotechnical seismic hazard occurs as a coherent sliding soil mass that moves along a critical shear failure surface. The global slope instability is typically slow moving and generally consists of a deep-seated failure surface that is either circular or sliding block shape. The triggering mechanism for these types of slope instabilities is the earthquake horizontal accelerations that induce inertial driving forces in addition to the initial static driving stresses that already exist. As a consequence of the cyclic shear stress induced by the earthquake, some soils may experience strain softening which results in a reduced soil shearing resistance. The reduction in soil shear strength must not be greater than 20%. If this threshold is exceeded, then the geotechnical seismic hazard is considered a lateral spread. The combination of the inertial driving forces and the reduced soil shear strength can result in instability of the earthen slopes. This situation could lead to significant deformations that can affect adjacent transportation structures such as bridges, roadways, and ERSs.

The standard-of-practice for evaluating seismic global instabilities consists of performing pseudo-static slope stability analyses. The pseudo-static slope stability analysis is a modified conventional slope stability analysis that allows the inclusion of inertial driving forces generated by the earthquake as equivalent static horizontal force acting on the potential sliding mass. The pseudo-static slope stability method uses the average horizontal acceleration coefficients adjusted for wave scattering (k_h) as indicated in Section 13.16 to compute the inertial loadings in the seismic global stability analysis. If the seismic slope stability ratio $(D/C)_{EQ\text{-}Stability} \leq \varphi_{EQ\text{-}Stability}$, then the Extreme Event I (EEI) limit state stability requirements and performance limits (no deformations) have been satisfied. If the seismic slope stability ratio $(D/C)_{EQ\text{-}Stability} > \varphi_{EQ\text{-}Stability}$, then a Newmark sliding block analysis is performed to estimate the displacements and determine if they meet the performance limits in Chapter 10. A reduction in the horizontal seismic coefficient (k_h) due to displacements is dependent on the yield acceleration, the average horizontal acceleration coefficients adjusted for wave scattering (k_h), peak horizontal ground acceleration (PGA) at the ground surface, and the peak ground velocity (PGV or V_{Peak}).

The overall seismic slope stability evaluation process is shown in Figure 13-41. The evaluation of the onset of seismic global instability proceeds as follows:

1. Determine earthquake parameters (PGA, S_{D1}, and PGV) from Chapter 12.

2. Determine wave scattering scaling factor (α_w) from Section 13.16.

3. Compute average horizontal seismic coefficient, k_h, in accordance with Section 13.16.

4. Perform a conventional pseudo-static slope stability analysis conforming to the requirements of Chapter 17 with average horizontal acceleration coefficient with adjustments for wave scattering (k_h). The vertical acceleration coefficient (k_v) is assumed to equal zero. Assign appropriate soil shear strengths based on soil SSL triggering to Sand-Like soils, NS Clay-Like soils, and HS Clay-Like soils that are susceptible to soil SSL. Use fully mobilized undrained/drained shear strengths for soils not susceptible to soil SSL.

5. Evaluate the critical slope failure surfaces to determine if any critical failure surfaces intersect soils with potential SSL. If the failure surfaces intersect these soil layers, compute the shear failure surface resistance as a "whole" and compare it to the shear failure resistance prior to the soils SSL. If it can be shown that the shear failure surface as a "whole" has not lost more than 20% strength, then hazard analysis can be continued as a seismic instability; otherwise, analyze the site as a lateral spread geotechnical seismic hazard.

6. Determine the seismic stability resistance ratio $(D/C)_{EQ\text{-}Stability}$. Obtain the required seismic slope instability resistance factor ($\varphi_{EQ\text{-}Stability}$) from Chapter 9. The LRFD equation used to determine the onset of lateral spread is shown below.

$$\left(\frac{D}{C}\right)_{EQ-Stability} \leq \varphi_{EQ-Stability} \qquad \text{Equation 13-101}$$

If the seismic instability ratio $(D/C)_{EQ\text{-}Stability} \leq \varphi_{EQ\text{-}Stability}$, then there is no potential for seismic slope instability hazard and the analysis can be terminated.

If the seismic instability ratio $(D/C)_{EQ\text{-}Stability} > \varphi_{EQ\text{-}Stability}$, seismic instability potential exists at the site, the evaluation process should continue to Step 7 to evaluate the displacements.

7. Compute the horizontal yield acceleration (k_y) by varying the horizontal acceleration until the seismic instability ratio $(D/C)_{EQ\text{-}Stability} = 1$.

8. Compute the deformations (ΔL) of the seismic slope instability using Newmark sliding block method described in Section 13.17.

9. If the displacements are within the acceptable performance limits, the seismic slope stability hazard is acceptable with respect to the Extreme Event I limit state

and the performance, limits. If the deformations computed exceed the performance limits then develop methods to mitigate this hazard as indicated in Chapter 14 and then evaluate the seismic global stability hazard again (Step 4).

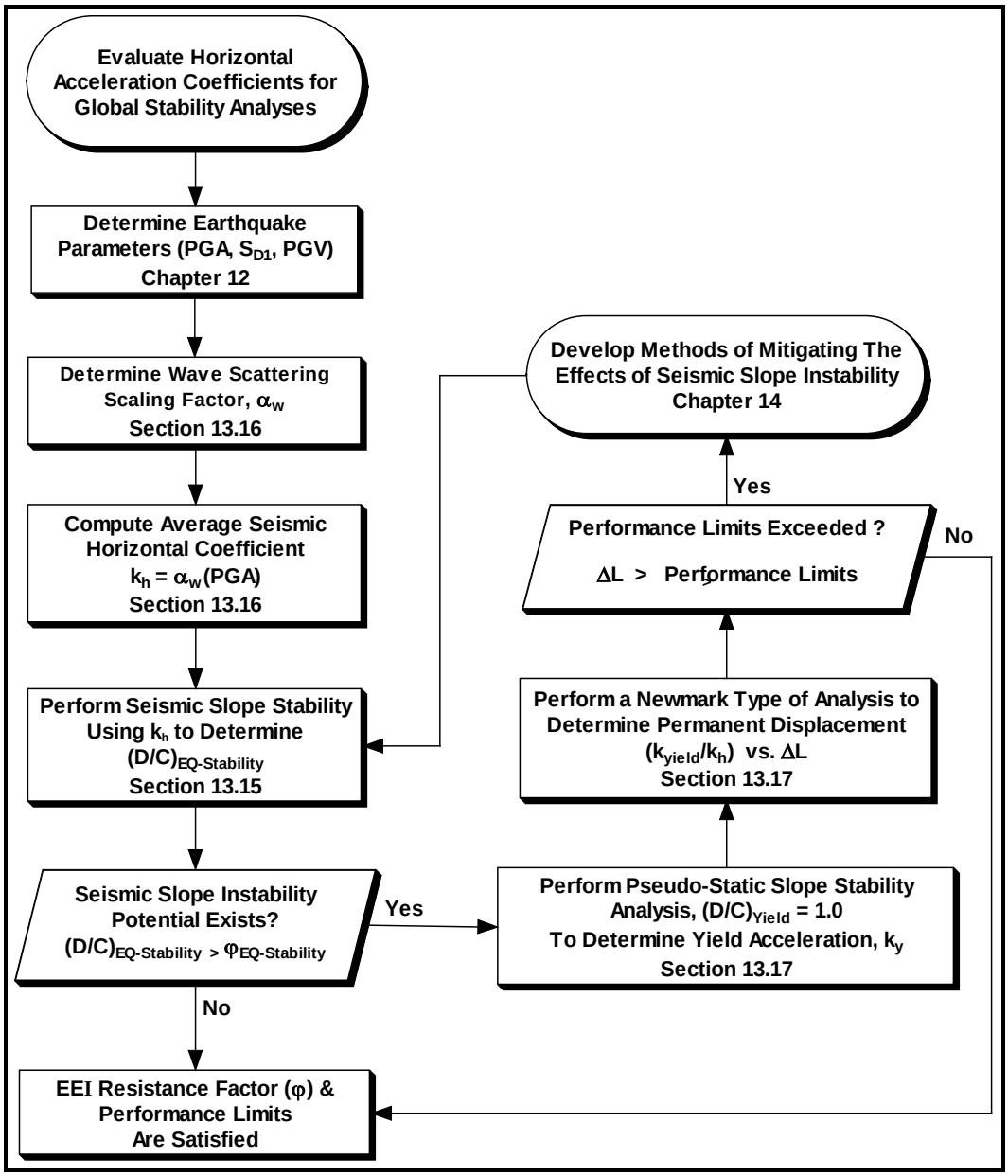

Figure 13-45, Seismic Slope Stability Evaluation Process

Sites that meet any of the following requirements are considered complex sites that may require a site-specific two-dimensional dynamic response analysis to estimate peak ground acceleration at the base of the failure surface, k_{max}. The PCS/GDS should be consulted when a complex site is identified.

- Sites that require a site-specific response analysis
- Geometries such as compound slopes, broken back slopes, etc.
- Soil properties such as sensitive soils, significant liquefaction potential, etc.
- Transportation facilities impacted significantly by failures or deformations

13.16 SEISMIC ACCELERATION COEFFICIENTS

The magnitude of earthquake inertial forces and seismic loading (active / passive pressures) that are used in pseudo-static stability analyses or limit-equilibrium analyses of ERSs are based on computing average horizontal acceleration coefficients adjusted for wave scattering (k_h). The horizontal acceleration coefficient (k_h) is computed by using the peak horizontal acceleration at the ground surface (PGA = a_{max}, etc.) with adjustments that typically reduce the acceleration by taking into account wave scattering of the horizontal ground accelerations and displacements of a yielding structure. The wave scattering scaling factor (α_w) is dependent on the design pseudo-spectral acceleration at 1 second (S_{D1}) from the ADRS curve and the height of the embankment, slope, or ERS.

Seismic inertial loadings are typically estimated by pseudo-static analytical methods that consist of multiplying the average horizontal seismic coefficient (k_h) and average vertical seismic coefficient (k_v) by the mass of the soil or structure that is being accelerated due to the earthquake shaking. The vertical seismic coefficient (k_v) is typically neglected ($k_v = 0$) by the fact that the higher frequency vertical accelerations will be out of phase with the horizontal accelerations and will have positive and negative contributions to the seismic loadings that on average will tend to cancel itself and therefore, have little, if any effect, on the seismic loading. The horizontal seismic coefficient (k_h) is used to compute a constant horizontal force in global seismic stability of slopes and ERSs. The horizontal seismic coefficient (k_h) has typically been assigned some fraction (0.3 to 0.7) of the peak horizontal ground acceleration (PGA). Reductions in PGA are typically attributable to either wave scattering or stress relief associated with displacements. The displacement dependent stress relief reduction of the horizontal seismic coefficient is computed using the Newmark displacement method as shown in Section 13.17.

Wave scattering is a term used to account for the seismic wave incoherence or variations behind a wall or slope. NCHRP 12-70 (2007) developed a relationship utilizing a scale factor, α_w, (reduction factor) to account for wave scattering as indicated by the following equation.

$$\boldsymbol{k_h} = \boldsymbol{k_{avg}} = \boldsymbol{\alpha_w k}_{\max} \qquad \text{Equation 13-102}$$

Where,

k_h = Average seismic horizontal coefficient due to wave scattering

α_w = Wave scattering scaling factor (reduction factor)

k_{max} = Peak ground acceleration coefficient (PGA) for the design event

The wave scattering scaling factor (α_w) was found to be dependent on the ground motion and the height of the wall or slope as shown in Figure 13-42. For wall or slope heights less than or equal to 20 feet α_w is 1.0. For wall or slope heights greater than 70 feet a numerical analysis is required.

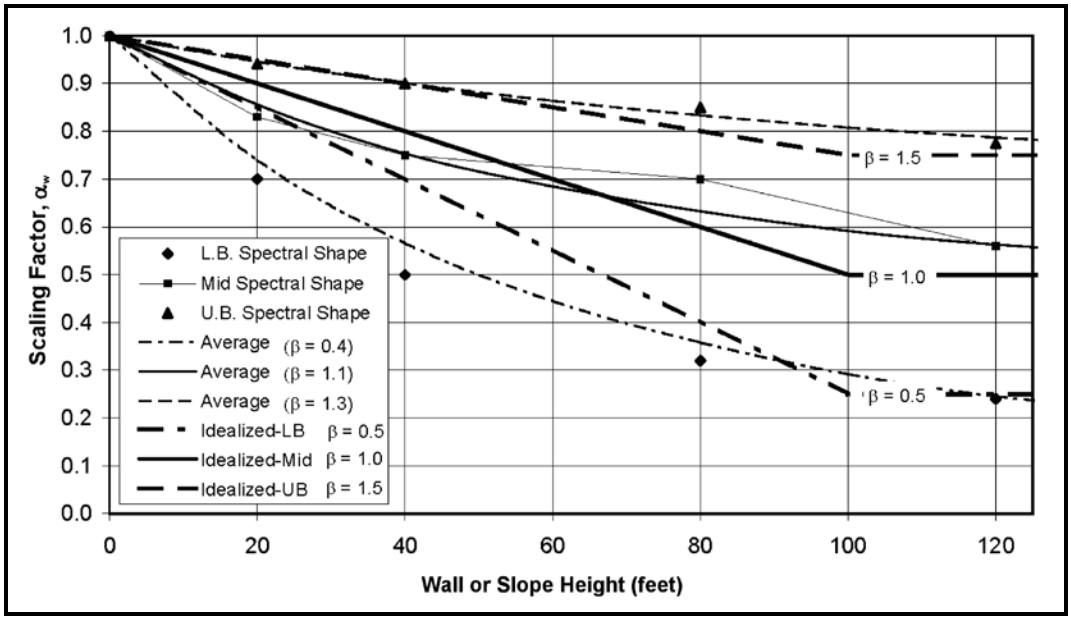

Figure 13-46, Simplified Wave Scattering Scaling Factor (NCHRP 12-70, 2007)

For wall or slope heights greater than 20 feet and less than or equal to 70 feet, α_w shall be determined by the following equation.

$$\alpha_w = 1 + 0.01H[(0.5\beta) - 1] \leq 1.0 \qquad \text{Equation 13-103}$$

Where,

H = Height of wall or slope (feet)

β = Ground motion index that is used to characterized shape of the ADRS.

The ground motion index, β, is applicable to a range of $0.5 \leq \beta \leq 1.5$ and is computed using the following equation.

$$\beta = \frac{S_{D1}}{PGA} \qquad \text{Equation 13-104}$$

Where,

S_{D1} = Peak ADRS spectral acceleration at 1 second (Chapter 12)
$PSA_{1\text{-}secB\text{-}C}$ = Mapped pseudo spectral acceleration at 1 second (Chapter 11)
PGA = Peak horizontal acceleration at ground surface (Chapter 12)
$PGA_{B\text{-}C}$ = Mapped PGA at B/C boundary (Chapter 11)

The wave scattering scaling factor (α_w) is applicable to soil Site Classes C, D, and E. If the Site Class is A or B, the wave scattering scaling factor (α_w) should be increased by 20 percent without exceeding a wave scattering factor of α_w = 1.0 (Use α_w = 1.0 for walls or slopes less than 20 feet in height when founded on Site Class A or B soils).

13.17 NEWMARK SEISMIC DISPLACEMENT METHODS

The Newmark sliding block model is used to evaluate displacements that occur as a result of an imbalance between driving forces (static and seismic) and loss in resisting forces (strain softening of soils) acting on the displaced soil mass. The models that have been developed based on Newmark rigid sliding block assume that the deformation takes place on a well-defined failure surface, the yield acceleration remains constant during shaking, and the soil is perfectly plastic. The displacements are computed based on the cumulative displacements of the sliding mass generated when accelerations exceed the yield acceleration that defines the point of impending displacement. Newmark type methods for computing deformations are typically associated with an improved reliability when compared to the empirical methods because it is a numerical method that permits modeling of the site response for the design earthquake being investigated.

The state-of-practice is that the assumptions used in the Newmark sliding block model provide reasonable results when the shear failure surface as a whole has not lost more than 50% of the shear resistance prior to the soils SSL. These assumptions are applicable to seismic slope instability and to lateral seismic deformation of gravity ERSs that are not significantly affected by cyclic liquefaction. Bardet et al. (1999) observed that when cyclic liquefaction occurs in a lateral spread, the assumptions of the Newmark sliding block model requirements are not met because (1) the shear strain in liquefied soil does not concentrate within a well defined surface, (2) the shear strength and yield acceleration of saturated soils varies during cyclic loading as pore pressure varies, and (3) soils are generally not perfectly plastic materials, but commonly harden and/or soften.

Several analytical methods based on the Newmark sliding block model have been developed to estimate deformations induced by earthquake cyclic loadings. The Newmark type methods typically fall into one of the following categories:

- Newmark Time History Analyses
- Simplified Newmark Charts

The Newmark displacement method can be performed using the design earthquake's time history acceleration record if a site-specific seismic response is performed in accordance with Chapter 12. Alternatively, Simplified Newmark charts can be used when a site-specific seismic response is not performed. The Simplified Newmark charts are based on a large database of earthquake records and the Newmark Time History Analysis method to develop charts that relate the ratio of acceleration to yield acceleration occurring at the base of the sliding mass to ground displacement.

If a site-specific response analysis is performed in accordance with Chapter 12, then the Newmark Time History Analyses should be performed in combination with the Simplified Newmark evaluation to validate deformation analyses performed using the Newmark Time History analyses. If a simplified site response method is used (i.e. three-point ADRS curves) to evaluate the local response site effects, then the Simplified Newmark charts should be used. The Newmark time history method and the Simplified Newmark charts are described in the following Sections.

13.17.1 Newmark Time History Analyses

The Newmark "sliding block" method for analyzing ground displacements along a shear plane was developed by Newmark (1965). Newmark's method has been applied to seismic slope stability performance of dams, embankments, natural slopes, and retaining walls (Newmark, 1965, Makdisi and Seed, 1978, Yegian et al., 1991, Jibson, 1994, and Richard and Elms, 1979). This method is typically incorporated into computer programs as described by Houston et al. (1987).

Randall W. Jibson and Matthew W. Jibson have developed a computer program to model slope performance during earthquakes. The Java program uses a modification of Newmark's method where a decoupled analysis is performed that allows modeling landslides that are not assumed to be rigid blocks. The software and more information can be obtained at the USGS website http://earthquake.usgs.gov/resources/software/slope_perf.php.

Ebeling, et al., (2007) have developed a computer program for the US Army Corps of Engineers that estimates the translational response of retaining walls to earthquake ground motions called $C_{orps}W_{all}$Slip (CWSlip) that could be used to estimate lateral displacements for gravity ERSs.

In this method, the deformations are assumed to occur along a well-defined plane and the sliding mass is assumed to be a rigid block as shown in Figure 13-43. When the earthquake accelerations exceed a yield acceleration threshold, the sliding mass displaces as indicated in Figure 13-44. The displacement accumulates over a time span ($t_3 - t_1$) where the acceleration exceeds the yield acceleration (k_y) at time t_1 to when the induced velocity drops to zero at time t_2. The displacements are computed by double integrating the accelerogram over the time span ($t_3 - t_1$) cumulative over each cycle for the duration of the earthquake as indicated in Figure 13-44. The total displacement is computed as the cumulative displacement that occurs during the earthquake shaking.

Note that the yield acceleration, k_y, in Figure 13-44 varies with the level of acceleration as a result of the cyclic soil strength degradation or liquefaction. Soils that are subject to significant strain softening will develop lower yield acceleration, k_y, thresholds as the earthquake-induced cyclic soil strength degradation progresses. The yield acceleration, k_y, is generally maintained constant because of the conservative approach used to determine the yield acceleration, k_y.

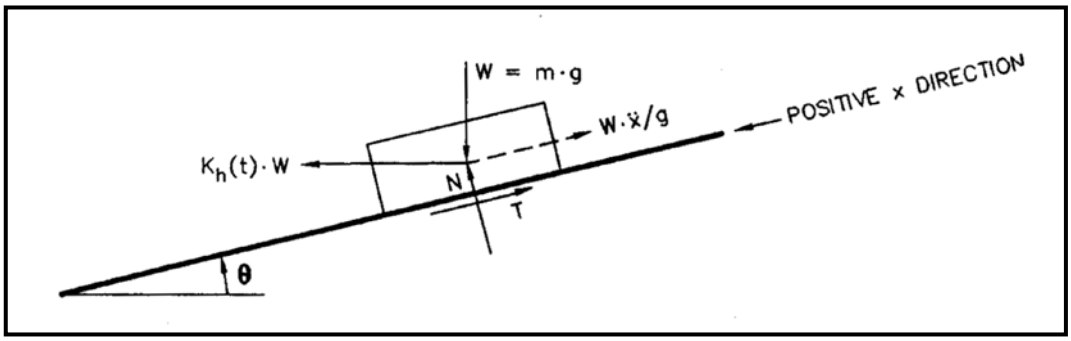

Figure 13-47, Newmark Sliding Block Method (Matasovic, Kavazanjian, and Giroud 1998)

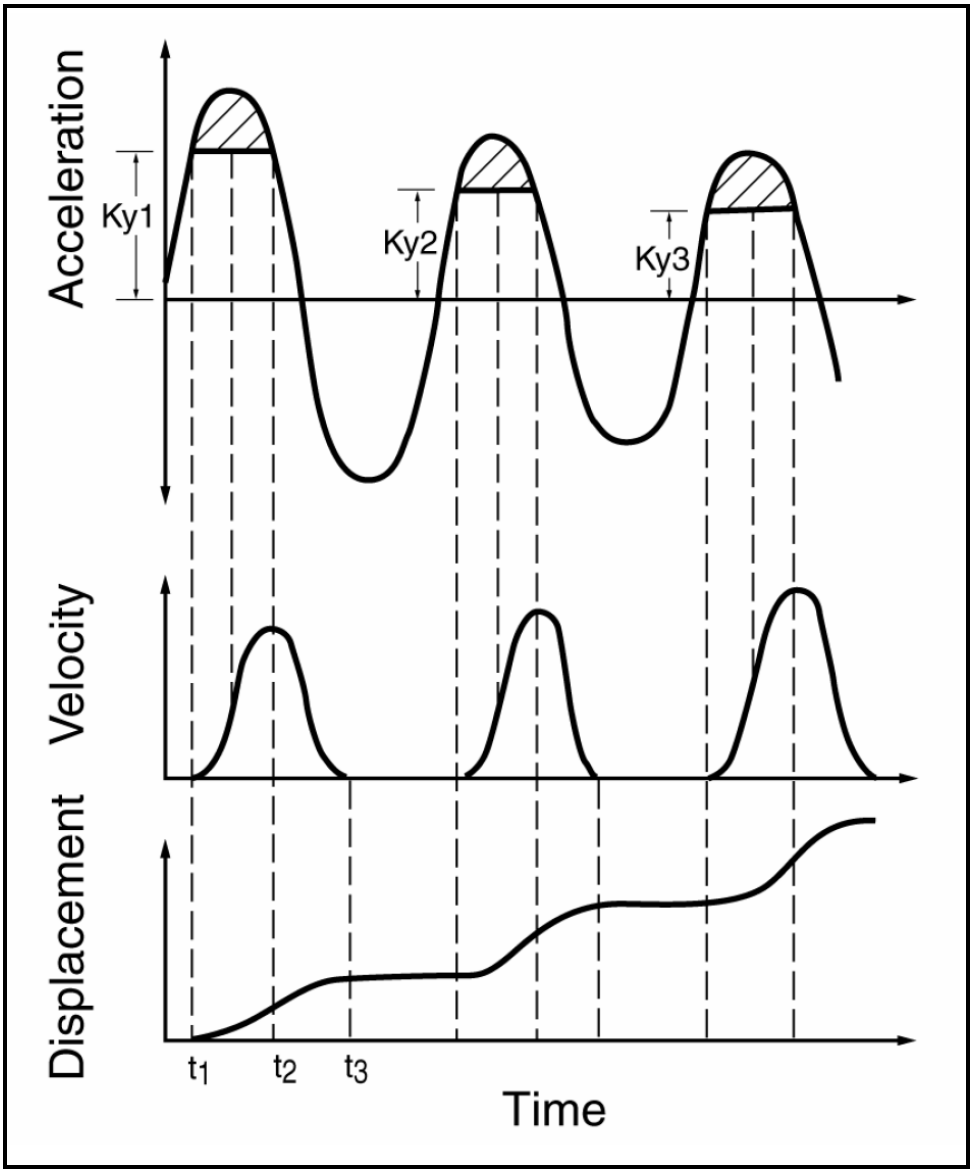

Figure 13-48, Newmark Time History Analysis
(Goodman and Seed, 1966 with permission from ASCE)

The earthquake shaking that triggers the displacement is characterized by an acceleration record at the base of the sliding mass for the design earthquake being evaluated. A minimum of twelve independent earthquake records should be selected from a catalogue of earthquake records that are representative of the source mechanism, magnitude (M_w), and site-to-source distance (R). A sensitivity analysis of the input parameters used in the site-specific response analysis should be performed to evaluate its effect on the magnitude of the displacement computed.

A pseudo-static slope stability analysis is performed to determine the threshold yield acceleration, k_y, where displacements begin to occur for a specific critical failure surface. The pseudo-static slope stability analysis should be performed with cyclic residual shear strength (Section 13.12) assigned to soils with the potential for soil SSL. The yield acceleration, k_y, is the

acceleration that corresponds to a pseudo-static slope stability analysis for a critical failure surface with a seismic stability resistance ratio of $(D/C)_{EQ\text{-}Stability} = 1.0$ (1/FS = 1.0).

The following are sources of uncertainty that are inherent when using the Newmark Time History method to compute displacements in the CEUS:

- Lack of strong motion time history records in the CEUS
- Earthquake source mechanism is not well understood
- Site-to-source distance, *R*, not well defined in the CEUS
- Infrequency of earthquake events in the last 10,000 years (Holocene Period)
- Point in the time history when cyclic strength degradation or liquefaction is triggered
- Magnitude of the apparent post-liquefaction residual resistance
- Influence of the thickness of liquefied soil on displacement
- Changes in values of yield acceleration, k_y, as deformation accumulates
- Influence of non-rigid sliding mass
- Influence of ground motion incoherence over the length of the sliding mass

Because of the uncertainties involved in the selection of the time history acceleration records in the CEUS, results of the Newmark Time History Analyses must be compared with the results obtained using Simplified Newmark Charts discussed in Section 13.17.2.

13.17.2 Simplified Newmark Charts

Simplified Newmark displacement charts were developed as a result of the NCHRP 12-70 (2007) study based on Newmark's Time History Analyses discussed in Section 13.17.1. These Simplified Newmark displacement charts are based on the earthquake database published by Hynes and Franklin (1984). The database of earthquake records used for this study was limited to earthquakes with moment magnitudes of $6.0 \leq M_w \leq 7.5$.

These charts have been developed as a function of a ratio (k_y / k_{max}) or yield acceleration (k_y) to max acceleration (k_{max}), peak ground velocity (V_{Peak} = PGV = V), peak ground acceleration, (PGA = A), and by region of the United States (WUS and CEUS) for either rock or soil site conditions. The charts shown in Figures 13-45 and 13-46 are based on an earthquake moment magnitude of $6.0 \leq M_w \leq 7.5$ in the CEUS. Figure 13-45 is appropriate for a stiff site with a peak ground velocity of $V_{Peak} = 30\ k_{max}$ in/sec ($V_{Peak} = 760\ k_{max}$ mm/sec). Figure 13-46 is appropriate for a soft soil site with a peak ground velocity of $V_{Peak} = 60\ k_{max}$ in/sec ($V_{Peak} = 1520\ k_{max}$ mm/sec).

For embankments and ERSs classified as ROC= I or II, the displacements computed using the simplified charts should be multiplied by 2 in order to obtain an 84% confidence level. For embankments and ERSs classified as ROC= III, do not multiply by any factor. The computed displacements should be compared with the required Performance Limits established in Chapter 10.

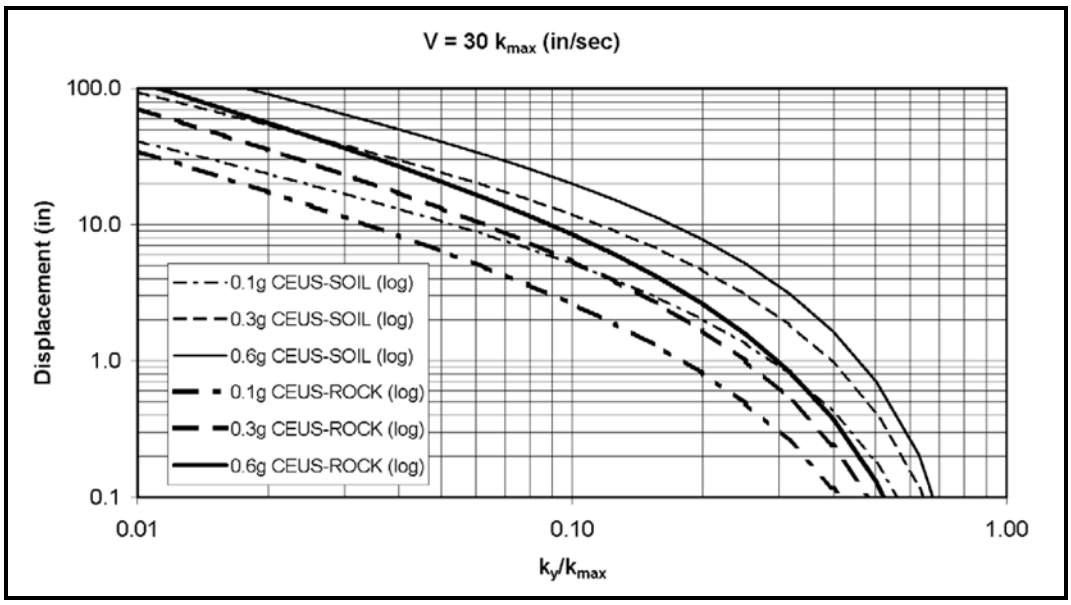

Figure 13-49, Simplified Newmark Chart (V = 30 k_{max} in/sec) (NCHRP 12-70, 2007)

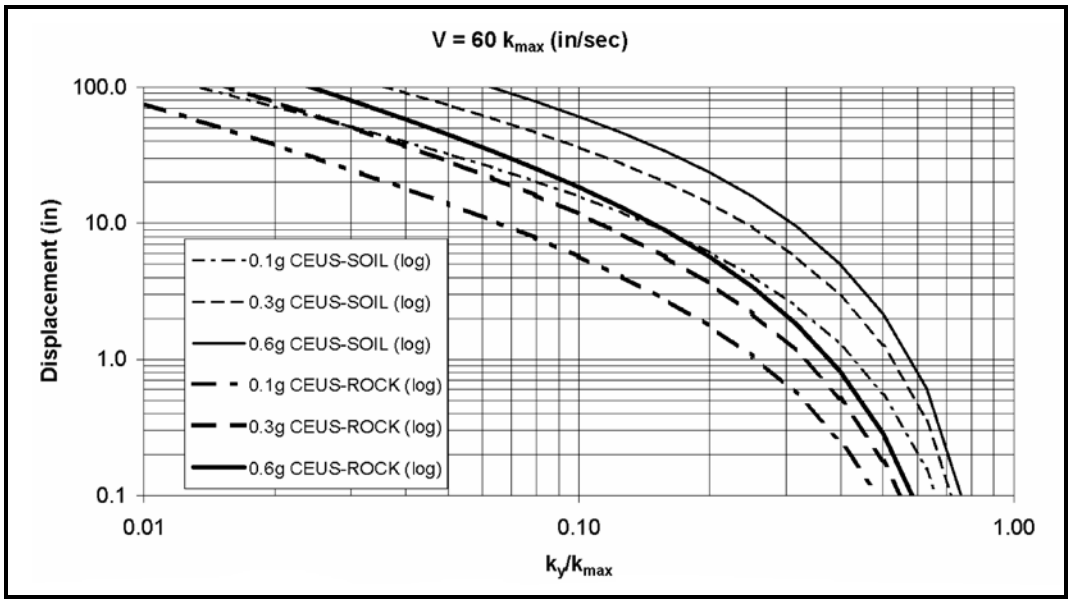

Figure 13-50, Simplified Newmark Chart (V = 60 k_{max} in/sec) (NCHRP 12-70, 2007)

In lieu of using charts in Figures 13-45 and 13-46 to compute the residual displacement, d, and having more flexibility in selecting the appropriate site factors (A and V_{Peak}), the following equations may be used.

CEUS-Rock (Standard Error of 0.31 $\log_{10}$ units):

Equation 13-105

$$\log(d) = -1.31 - 0.93\log\left(\frac{k_y}{k_{max}}\right) + 4.52\log\left[1 - \left(\frac{k_y}{k_{max}}\right)\right] - 0.46\log\left(k_{max}\right) + 1.12\log\left(V_{Peak}\right)$$

CEUS-Soil (Standard Error of 0.23 $\log_{10}$ units):

Equation 13-106

$$\log(d) = -1.49 - 0.75\log\left(\frac{k_y}{k_{max}}\right) + 3.62\log\left[1-\left(\frac{k_y}{k_{max}}\right)\right] - 0.85\log\left(k_{max}\right) + 1.61\log\left(V_{Peak}\right)$$

Where,

k_y = Yield Acceleration in units of g (Sections 13.15 and 13.17.1)

k_{max} = Peak ground acceleration (PGA) at the base of the failure surface in units of g

V_{Peak} = Peak ground velocity (PGV) in units of inches/sec. Correlations of peak ground velocity are found in Section 12.9.

13.18 SEISMIC SOIL SETTLEMENT

Ground settlements due to the effects of earthquake shaking (seismic induced) are one of the potential geotechnical seismic hazards that must be evaluated. Seismic induced ground settlements that are not due to flow failure or lateral spreading are typically the result of ground shaking caused densification of the underlying soils. Densification or seismic compression of soils has been observed in unsaturated sands, silts, and clayey sands above the water table. Densification of saturated loose sands subject to cyclic liquefaction has also been observed below the water table. Seismic settlements for depths greater than 80 feet, do not need to be computed unless the settlements are being computed to evaluate the effects of downdrag on deep foundations.

Soil settlements computed for unsaturated soils and saturated soils are additive as indicated by the following equation.

$$S_{TS} = S_{us} + S_{sat}$$ Equation 13-107

Where,

S_{TS} = Total seismic settlement in units of inches.

S_{us} = Total seismic settlement of unsaturated soils in units of inches (Section 13.18.3)

S_{sat} = Total seismic settlement of saturated soils in units of inches (Section 13.18.4)

The procedures presented in the following Sections for computing settlements are only applicable to level ground site conditions and in the absence of lateral flow or spreading. Soils susceptible to ground settlements that are located below sloping ground or adjacent to a free-face may be subject to static driving shear stresses oriented towards down-slope or free-face direction. The presence of static driving shear stresses for these site conditions will tend to increase vertical settlements and lateral displacements. Since the simplified methods presented to analyze settlements do not account for static driving shear stresses, the geotechnical engineer should be aware that settlements may be on the order of 10% to 20% greater for steeply sloped sites (Wu, 2002). This increase in settlement may be disregarded if the steeply sloped ground site has the potential for flow slide or seismic slope instability since these failure mechanisms will likely exceed the performance limits that have been established in Chapter 10.

13.18.1 Soil Characterization

The corrected SPT driving resistance ($N^*_{1,60}$) will be computed in accordance with Section 13.11.1.3. For soils with fines content (FC) greater than 5 percent, the SPT driving resistance must be adjusted for fines content to obtain an equivalent corrected clean sand SPT resistance ($N^*_{1,60,cs}$) in accordance with Section 13.11.2.

The normalized corrected CPT tip resistance ($q_{c,1,N}$) will be computed in accordance with Section 13.11.1.4. For soils with fines content (FC) greater than 5 percent, the normalized corrected CPT tip resistance must be adjusted for fines content to obtain an equivalent normalized corrected clean sand tip resistance ($q_{c,1,N,CS}$) in accordance with Section 13.11.3.

For seismic settlement methods that require an equivalent normalized corrected clean sand SPT resistance ($N^*_{1,60,cs}$) and only CPT in-situ testing data is available to compute seismic settlements, the normalized cone tip resistance, $q_{c,1,N}$, (Section 13.11.1.4) needs to be correlated to corrected SPT $N^*_{1,60}$ values in accordance with Section 13.11.1.1. The correlated SPT blow count ($N^*_{1,60}$) should then be adjusted for fines content (FC) greater than 5 percent, in accordance with Section 13.11.2.

13.18.2 Cyclic Shear Strain (γ)

The cyclic shear strain, γ, induced during earthquake shaking at various depths below the ground surface is the primary factor that controls the magnitude of the settlement of unsaturated sands. The effective shear strain, γ_{eff}, (or average shear strain, γ) is used to estimate seismic settlement by using the following equation.

$$\gamma_{eff} = \frac{\tau_{avg}}{G_{eff}} = \frac{\tau_{avg}}{G_{\max}\left(\frac{G_{eff}}{G_{\max}}\right)} \qquad \text{Equation 13-108}$$

Where,

τ_{avg} = Average cyclic shear stress

G_{eff} = Effective shear modulus at the induced strain level. The ratio of the effective shear modulus (G_{eff}) to initial small strain shear modulus (G_{max}) is a hypothetical effective shear stress factor (G_{eff}/G_{max}). The effective shear strain, γ_{eff}, can be computed as a function of γ_{eff} (G_{eff}/G_{max}) using the following equation.

$$\gamma_{eff}\left(\frac{G_{eff}}{G_{\max}}\right) = \frac{\tau_{avg}}{G_{\max}} \qquad \text{Equation 13-109}$$

The *Simplified Procedure* (Section 13.10.1.1) for determining the maximum earthquake induced stress (τ_{max}) should be used for the upper 80 feet. For depths greater than 80 feet the

maximum earthquake induced stress (τ_{max}) should be computed using site specific response analyses in accordance with Section 13.10.1.2.

The average cyclic shear stress, τ_{avg}, is computed by taking 65% of the maximum earthquake induced stress (τ_{max}) as shown in the following equation.

$$\tau_{avg} = 0.65\tau_{max} \qquad \text{Equation 13-110}$$

The initial small strain shear modulus, G_{max}, or soil stiffness can be determined based on the mass density, ρ, of the soil and the shear wave velocity, V_s, of the soil as indicated in Chapter 12.

The γ_{eff} (G_{eff}/G_{max}) variable is then computed using Equation 13-102. The effective shear strain, ($\gamma_{eff} = \gamma$) can be estimated using the relationships developed by Darendeli and Stokoe (2001), Vucetic and Dobry (1991), and Iwasaki et al. (1978) for modulus reduction curves shown in Figure 13-47.

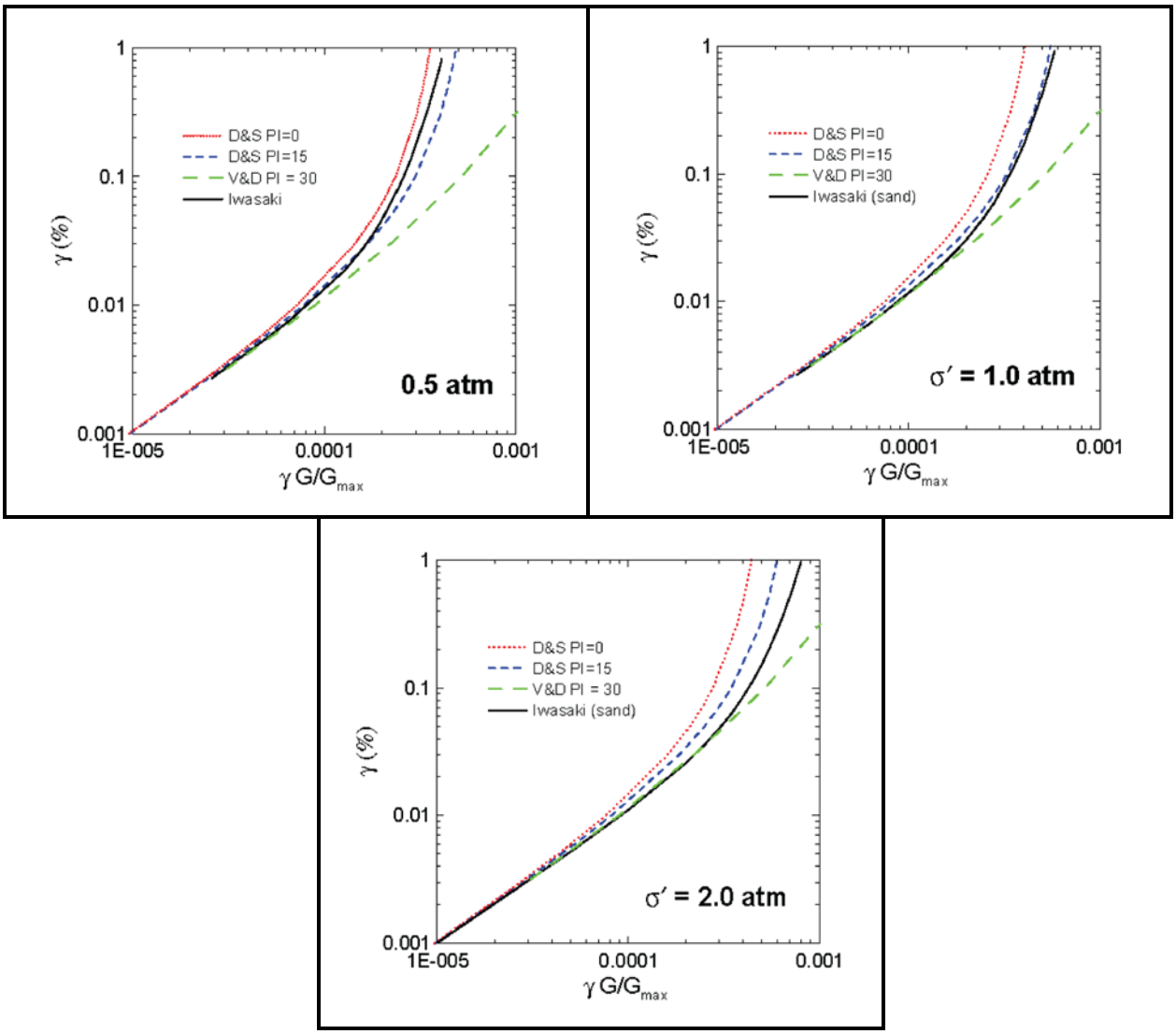

Figure 13-51, Modulus Reduction Curves (presented by Stewart et al., 2004)

The effective shear strain ($\gamma_{eff} = \gamma$) relationships presented in Figure 13-47 for a plasticity index, PI = 0, 15, and 30 and effective overburden stress, σ'_v = 0.5atm, 1.0 atm, 2.0 atm can be computed by the using the following equation. For soils with (0 < PI < 15) or (15 < PI < 30) the shear strains (γ) can be linearly interpolated using the following equation.

$$\gamma = \frac{\left(1+\left(g_1 e^{(g_2 \cdot P)}\right)\right)}{1+g_1} P \cdot 100 \qquad \text{Equation 13-111}$$

Where,

PI ≈ 0:

$g_1 = 0.199(\sigma'_m/p_a)^{0.231}$

$g_2 = 10850(\sigma'_m/p_a)^{-0.410}$

PI ≈ 15:

$g_1 = 0.194(\sigma'_m/p_a)^{0.265}$

$g_2 = 7490(\sigma'_m/p_a)^{-0.418}$

PI ≈ 30:

$g_1 = 4.0$

$g_2 = 1400$

p_a = Atmospheric pressure: pa = 1.0 atm = 101.3 kPa = 1.0 tsf

σ'_m = Mean effective stress. An approximation of mean normal effective stress, $\sigma'_m \approx 0.65\sigma'_v$ would apply to a sand layer with an approximate internal friction angle, ϕ, of 32 degrees. σ'_m can be computed by the following equation:

$$\sigma'_m = \left[\frac{1+2K_o}{3}\right]\sigma'_v \approx 0.65\sigma'_v \qquad \text{Equation 13-112}$$

K_o = Coefficient of lateral earth pressure at-rest (Chapter 12)

σ'_v = Effective vertical overburden stress. In units of tons per square foot (tsf)

p_a = Atmospheric pressure

P = $\gamma_{eff}\left(\frac{G_{eff}}{G_{max}}\right)$ (See Equation 13-102)

13.18.3 Unsaturated (Dry) Sand Settlement

Settlement of unsaturated loose sand (above the water table) typically occurs during the earthquake shaking under conditions of constant effective vertical stress (depending on the degree of saturation). Sands that are above the water table are typically referred to as unsaturated, even though these soils typically have some degree of saturation particularly near the water table. Settlement potential of unsaturated sands is computed using the same methodology given by Tokimatsu and Seed (1987) except that volumetric strain models developed by Stewart et al. (2004) are used. The total unsaturated soil settlement, S_{us}, is computed as the sum of the individual settlement of the unsaturated soil settlement layers, δ_{us}, as indicated in the following equation.

$$S_{us} = 2 \cdot \sum_{n=1}^{n=i_{us}} \delta_{us} = 2 \cdot \sum_{n=1}^{n=i_{us}} \varepsilon_c C_{VN} \cdot H_{us} \qquad \text{Equation 13-113}$$

Where,

δ_{us} = Settlement of Unsaturated Sand layer in units of inches

ε_c = Volumetric Strain of the in-place soil (or compacted fill) in units of (%)

C_{VN} = Volumetric strain correction factor

H_{us} = Layer Thickness of Unsaturated Sand layer in units of inches

i_{us} = total number (n) of unsaturated sand layers

Note that a factor of two is included in Equation 13-106 to correct for multidirectional shaking effect as recommended by Pyke et al. (1975).

13.18.3.1 Volumetric Strain Soil Models

The cyclic shear strain, γ_c, at each soil layer can be approximated by the effective shear strain, $\gamma_{eff,}$ ($\gamma_c \approx \gamma_{eff} = \gamma$) as computed in Section 13.18.2. The volumetric strain of the unsaturated soil, ε_c, for an earthquake of equivalent number of uniform strain cycles of n = 15 can be determined from volumetric strain material models based on laboratory simple shear testing. Volumetric strain material models are provided for clean sand, soil with non-plastic fines, and soils with variable plastic fines in Sections 13.18.3.3, 13.18.3.4, and 13.18.3.5, respectively.

The volumetric soil models provided for clean sands uses relative density, D_r = 45%, 60%, and 80%, as an indicator for selecting model coefficients. For in place soils, the relative density can be estimated based on the in-situ testing correlations provided in Section 13.11.1.1. For compacted fill embankments, a relative density, D_r = 60% can be used.

The volumetric soil models for soils with non-plastic fines and variable plastic fines use a relative compaction (RC) based on the Modified Proctor test and the degree of saturation parameter, S. Since the SCDOT standard construction specifications use the Standard Proctor test for field control, it is necessary to estimate the equivalent RC based on the Modified Proctor test for the various soil models. The degree of saturation, S, for in-place soils shall be computed from laboratory testing. The degree of saturation, S, for compacted soils will need to be estimated. Table 13-12 provides approximate relationships between the Standard and Modified Proctor value and approximate degree of saturation, S, for the maximum dry density of various soil types. The values in Table 13-12 are estimates based on accepted industry practice and shall be used unless specific testing has been performed. The Proctor test values shall be determined using the testing methods provided in Chapter 5.

Table 13-12, Relationships for Relative Compaction and Saturation

Soil Types	Description	Standard Proctor	Modified Proctor (1)	Degree of Saturation
Soils With NP Fines	50 % Sand / 50% Silt	95%	85%	55%
		100%	90%	66%
Soils with Variable Plasticity Fines	Low Plasticity Fine Grained Soil (PI = 2)	95%	85%	58%
		100%	90%	66%
	Moderate Plasticity Fine Grained Soil (PI = 15)	95%	78%	67%
		100%	82%	75%
	High Plasticity Fine Grained Soil (PI = 27)	95%	76%	75%
		100%	80%	83%

(1) The equivalent Standard Proctor RC is based on the following:
90% of the Standard Proctor for Silty Soils
82% of the Standard Proctor for Moderately Plastic Clay Soils
80% of the Standard Proctor for Highly Plastic Clay Soils

The ratio between the volumetric strain of the in-place soils (ε_c) and the equivalent volumetric strain ($\varepsilon_{c\text{-}15}$) of the soil for a number of uniform strain cycles, N = 15 is defined as the volumetric strain correction factor. The equivalent number of uniform strain cycles (N) can be estimated from Section 13.18.3.2. The volumetric correction ratio is provided for each volumetric strain material model in the following Sections.

13.18.3.2 Equivalent Number of Uniform Strain Cycles (N)

The equivalent number of uniform strain cycles (N) is used to normalize the effects of earthquakes of different Moment Magnitudes (M_W = m) and site-to-source distances (R = r). The relationship shown in Figure 13-48 was developed by Liu et al. (2001) to estimate the equivalent number of uniform strain cycles (N). Also shown in Figure 13-48 is Seed et al. (1975) recommendations.

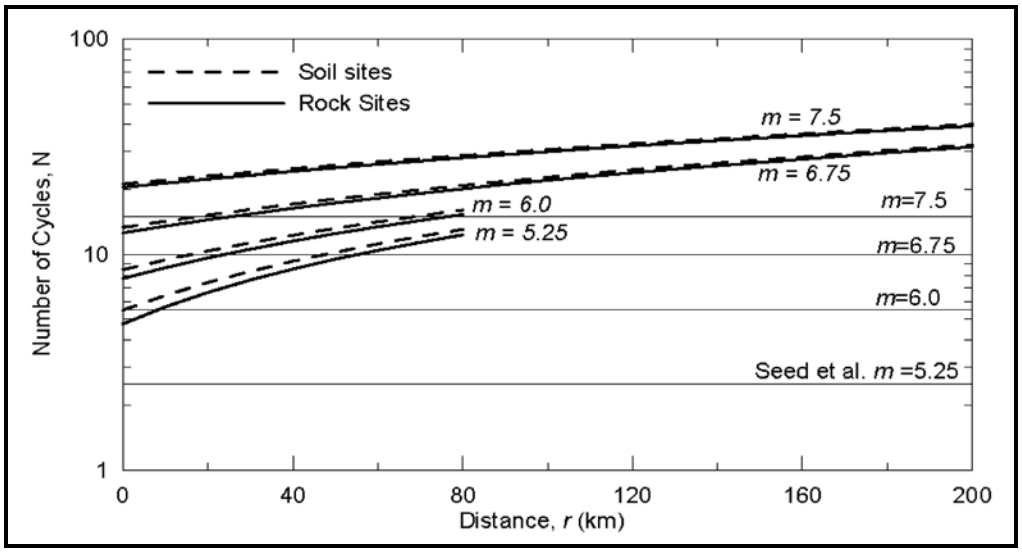

Figure 13-52, Number of Cycles with Distance and Moment Magnitude (Liu et al., 2001 and Seed et al., 1975 with permission from ASCE)

The Liu et al. (2001) relationship for the equivalent number of uniform strain cycles (N) can be computed using the following equation.

$$N = \frac{\left(\exp\left(b_1 + b_2\left(M_W - m^*\right)\right)\right)^{\left(\frac{1}{3}\right)}}{4.9 \times 10^6 \beta} + Sc_1 + Rc_2 \qquad \text{Equation 13-114}$$

Where,

b_1 = 1.53 (Coefficient)
b_2 = 1.51 (Coefficient)
c_1 = 0.750 (Coefficient)
c_2 = 0.095 (Coefficient)
β = *3.2* (Coefficient)
M_W = Earthquake moment magnitude
m^* = 5.8

S = Site Parameter: *S* = 0 (Rock Site or Soil < 20 m)
or *S* = 1 (Soil Site > 20 m)
R = Site-Source Distance in units of kilometers (km)

13.18.3.3 Clean Sand

Clean sand is typically defined as a cohesionless material with fines content, FC, less than 5 percent. The volumetric strain model for Clean Sand proposed by Stewart et al. (2004) with relative density (D_r) of 45%, 60%, and 80% is shown in Figure 13-49.

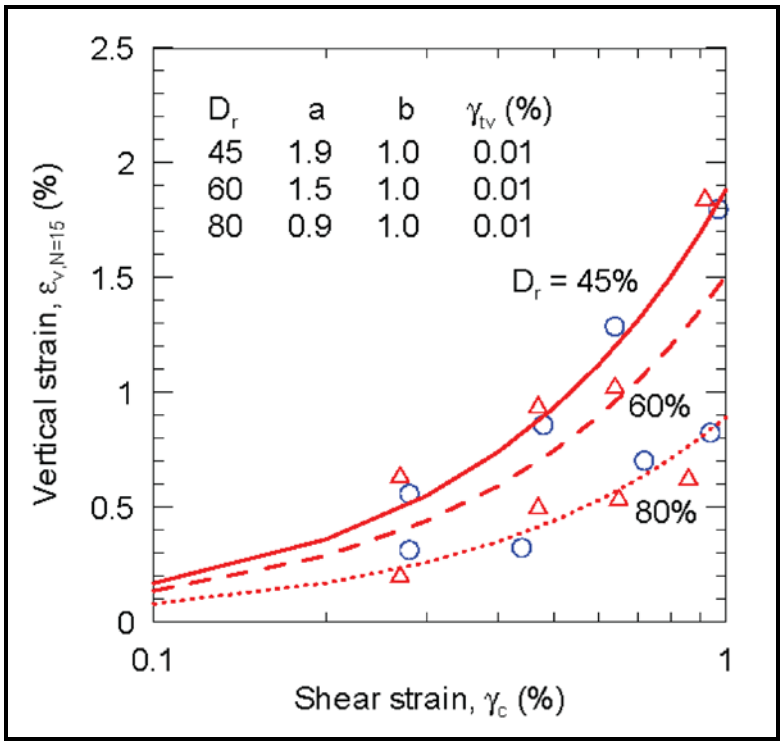

Figure 13-53, Volumetric Strain Model – Clean Sand (Stewart et al., 2004)

The volumetric strain model for Clean Sand proposed by Stewart et al. (2004) can be computed by the following equations. Note that these correlations are applicable to cyclic strains less than 1.0 percent (γ_c < 1.0%).

$$\gamma_c > \gamma_{tv}: \quad \varepsilon_{v,N=15} = a(\gamma_c - \gamma_{tv})^b \qquad \text{Equation 13-115}$$

$$\gamma_c < \gamma_{tv}: \quad \varepsilon_{v,N=15} = 0 \qquad \text{Equation 13-116}$$

Where,

$\varepsilon_{v,N=15}$ = Volumetric strain of unsaturated soils in units of percentage (%)
$\gamma = \gamma_c$ = Cyclic strain in units of percentage (%) (Equation 13-104)
γ_{tv} = Thresholds shear strain in units of percentage (%) – See Table 13-13
a = Coefficient – See Table 13-13
b = Coefficient – See Table 13-13

Table 13-13, Volumetric Strain Clean Sand Model Coefficients

D_r (%)	a	b	γ_{tv} (%)
45	1.9	1.0	0.01
60	1.5	1.0	0.01
80	0.9	1.0	0.01

The volumetric strain correction factor, C_{VN}, adjusts the volumetric strain for N=15 cycles, $\varepsilon_{v,N=15}$, obtained from the volumetric soil model to the equivalent number of uniform strain cycles (*N*) of the design earthquake (FEE or SEE) being evaluated. The equivalent number of uniform strain cycles (N) is computed using the moment magnitude (M_W = m) and site-to-source distances (R) as indicated in Section 13.18.3.2. The volumetric strain correction factor, C_{VN}, for Clean Sands is computed using the following equation.

$$C_{VN} = 0.33\ln(N) + 0.1063 \qquad \text{Equation 13-117}$$

13.18.3.4 Soils With Non-Plastic Fines

Soils with non-plastic fines are defined as a cohesionless material with 50% Sand / 50% Silt by weight. The volumetric strain model for soils with non-plastic fines proposed by Stewart et al. (2004) with Relative Compaction (RC) based on the Modified Proctor of RC= 87% and 92% with corresponding degree of saturation of S = 30% and 0, ≥60% for each RC are shown in Figure 13-50.

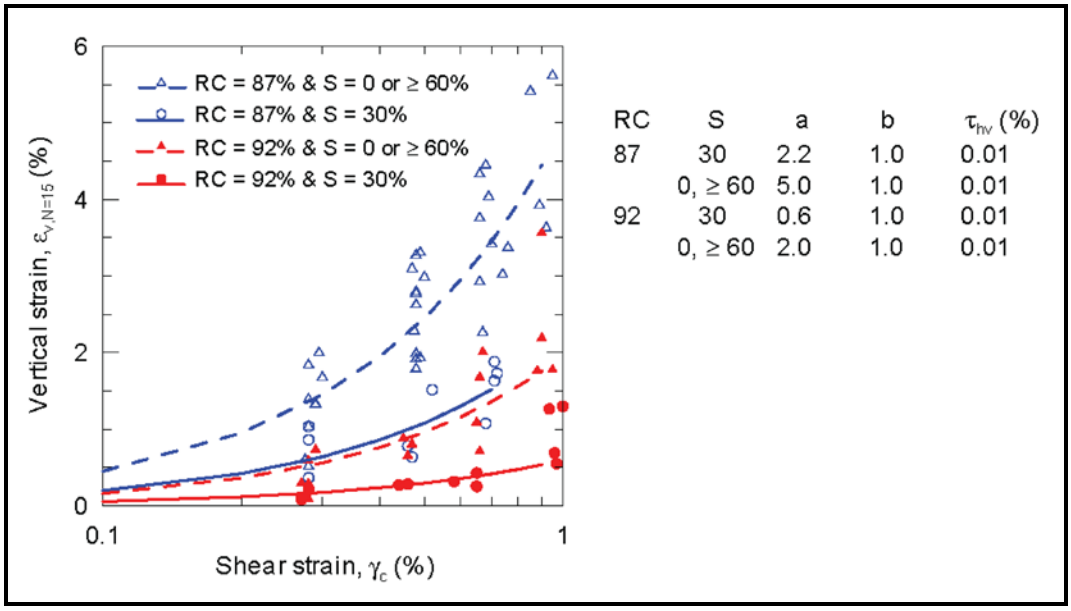

Figure 13-54, Volumetric Strain Model - Soils With Non-plastic Fines (Stewart et al., 2004)

The volumetric strain model for soils with non-plastic fines proposed by Stewart et al. (2004) can be computed by the following equations. Note that these correlations are applicable to cyclic strains less than 1.0 percent (γ_c < 1.0%).

$$\gamma_c > \gamma_{tv} : \quad \varepsilon_{v,N=15} = a\left(\gamma_c - \gamma_{tv}\right)^b \qquad \text{Equation 13-118}$$

$$\gamma_c < \gamma_{tv} : \quad \varepsilon_{v,N=15} = 0 \qquad \text{Equation 13-119}$$

Where,

$\varepsilon_{v,N=15}$ = Volumetric strain of unsaturated soils in units of percentage (%)

$\gamma = \gamma_c$ = Cyclic strain in units of percentage (%) (Equation 13-104)

γ_{tv} = Thresholds shear strain in units of percentage (%) – See Table 13-14

a = Coefficient – See Table 13-14

b = Coefficient – See Table 13-14

Table 13-14, Volumetric Strain Soils With Non-Plastic Fines Model Coefficients

RC (%)	S (%)	a	b	γ_{tv} (%)
87	30	2.2	1.0	0.01
87	0, >60	5.0	1.0	0.01
92	30	0.60	1.0	0.01
92	0, >60	2.0	1.0	0.01

For soils with fines content (Silt) between 0 and 50%, the volumetric strain for these types of soils should be interpolated between the results of this model (soils with non-plastic fines) and the results of the volumetric strain model for clean sand (Section 13.18.3.3).

The volumetric strain correction factor, C_{VN}, adjusts the volumetric strain for N=15 cycles, $\varepsilon_{v,N=15}$, obtained from the volumetric soil model to the equivalent number of uniform strain cycles (N) of the design earthquake (FEE or SEE) being evaluated. The equivalent number of uniform strain cycles (N) is computed using the moment magnitude (M_W = m) and site-to-source distances (R) as indicated in Section 13.18.3.2. The volumetric strain correction factor, C_{VN}, for soils with non-plastic fines is computed using the following equation.

$$C_{VN} = 0.36\ln(N) + 0.0251 \qquad \text{Equation 13-120}$$

13.18.3.5 Soils With Variable Plastic Fines

Soil with variable plastic fines is defined as a fine-grained soil with fine contents, FC > 50% and a range of Plasticity Index of $2 \le PI \le 27$. These soils have been divided into Low Plasticity Soil, Moderate Plasticity Soil, and High Plasticity Soil as indicated below.

Low Plasticity Soils: A volumetric strain model for Low Plasticity Soils ($2 \le PI \le 10$, LL=27) was proposed by Stewart et al. (2004) with Relative Compaction (RC) based on the Modified Proctor of RC = 90-92% and 93-95% and variation in degree of saturation, S=55-80 and S=80-99% for each RC range as are shown in Figure 13-51. The overall strain level for Low Plasticity Soils was significantly less than those for clean sand and soils with non-plastic fines (Silts).

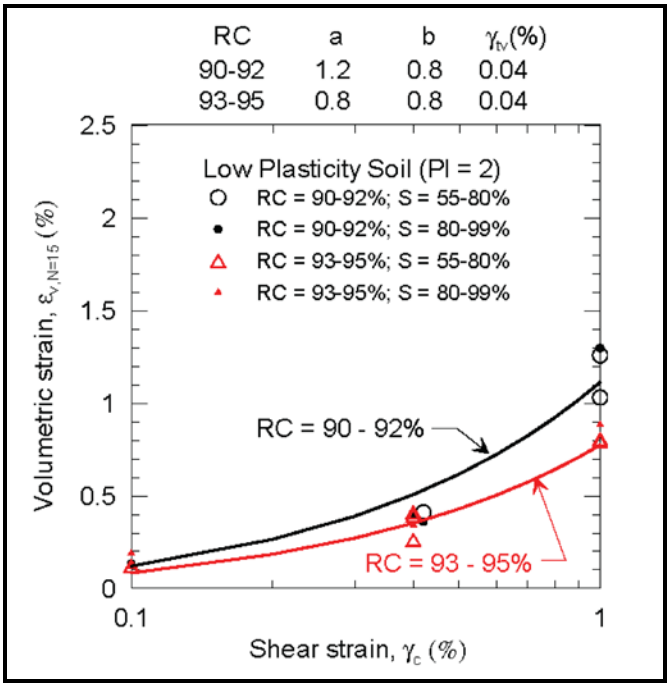

Figure 13-55, Volumetric Strain Model – Low Plasticity Soil (Stewart et al., 2004)

The volumetric strain model for Low Plasticity Soil proposed by Stewart et al. (2004) can be computed by the following equations. Note that these correlations are applicable to cyclic strains less than 1.0 percent (γ_c < 1.0%).

$$\gamma_c > \gamma_{tv}: \quad \varepsilon_{v,N=15} = a(\gamma_c - \gamma_{tv})^b \qquad \text{Equation 13-121}$$

$$\gamma_c < \gamma_{tv}: \quad \varepsilon_{v,N=15} = 0 \qquad \text{Equation 13-122}$$

Where,

$\varepsilon_{v,N=15}$ = Volumetric strain of unsaturated soils in units of percentage (%)

$\gamma = \gamma_c$ = Cyclic strain in units of percentage (%) (Equation 13-104)

γ_{tv} = Thresholds shear strain in units of percentage (%) – See Table 13-15

a = Coefficient – See Table 13-15

b = Coefficient – See Table 13-15

Table 13-15, Volumetric Strain Low Plasticity Soil Model Coefficients

RC (%)	a	b	γ_{tv} (%)
90 - 92	1.2	0.8	0.04
93 - 95	0.8	0.8	0.04

The volumetric strain correction factor, C_{VN}, adjusts the volumetric strain for N=15 cycles, $\varepsilon_{v,N=15}$, obtained from the volumetric soil model to the equivalent number of uniform strain cycles (N) of the design earthquake (FEE or SEE) being evaluated. The equivalent number of uniform strain cycles (N) is computed using the moment magnitude (M_W = m) and site-to-source distances (R)

as indicated in Section 13.18.3.2. The volumetric strain correction factor, C_{VN}, for Low Plasticity Soil is computed using the following equation.

$$C_{VN} = 0.32\ln(N) + 0.1334 \qquad \text{Equation 13-123}$$

Moderate Plasticity Soils: A volumetric strain model for Moderate Plasticity Soil ($11 \le PI \le 20$, LL=33) was proposed by Stewart et al. (2004) with Relative Compaction (RC) based on the Modified Proctor of RC= 84%, 88%, 88%, 92%, and 92% with corresponding degree of saturation, S = Any, 60%, 90%, 70%, and 90% was developed as are shown in Figure 13-52. It was observed that volumetric strain decreases with increasing RC and S.

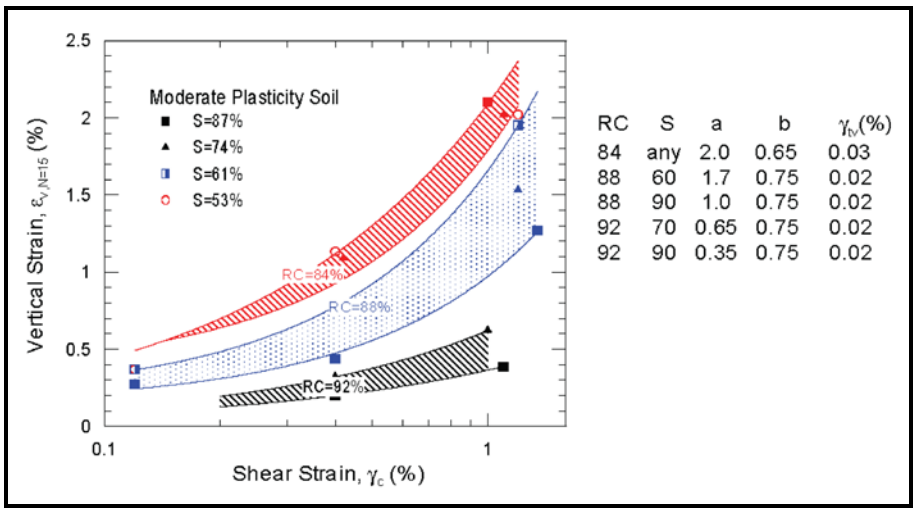

RC	S	a	b	γ_{tv}(%)
84	any	2.0	0.65	0.03
88	60	1.7	0.75	0.02
88	90	1.0	0.75	0.02
92	70	0.65	0.75	0.02
92	90	0.35	0.75	0.02

Figure 13-56, Volumetric Strain Model – Moderate Plasticity Soil (Stewart et al., 2004)

The volumetric strain model for Moderate Plasticity Soil proposed by Stewart et al. (2004) can be computed by the following equations. Note that these correlations are applicable to cyclic strains less than 1.0 percent ($\gamma_c < 1.0\%$).

$$\gamma_c > \gamma_{tv}: \quad \varepsilon_{v,N=15} = a(\gamma_c - \gamma_{tv})^b \qquad \text{Equation 13-124}$$

$$\gamma_c < \gamma_{tv}: \quad \varepsilon_{v,N=15} = 0 \qquad \text{Equation 13-125}$$

Where,

$\varepsilon_{v,N=15}$ = Volumetric strain of unsaturated soils in units of percentage (%)

$\gamma = \gamma_c$ = Cyclic strain in units of percentage (%) (Equation 13-104)

γ_{tv} = Thresholds shear strain in units of percentage (%) – See Table 13-16

a = Coefficient – See Table 13-16

b = Coefficient – See Table 13-16

Table 13-16, Volumetric Strain Moderate Plasticity Soil Model Coefficients

RC (%)	S (%)	a	b	γ_{tv} (%)
84	Any	2.00	0.65	0.03
88	60	1.70	0.75	0.02
88	90	1.00	0.75	0.02
92	70	0.65	0.75	0.02
92	90	0.35	0.75	0.02

The volumetric strain correction factor, C_{VN}, adjusts the volumetric strain for N=15 cycles, $\varepsilon_{v,N=15}$, obtained from the volumetric soil model to the equivalent number of uniform strain cycles (*N*) of the design earthquake (FEE or SEE) being evaluated. The equivalent number of uniform strain cycles (N) is computed using the moment magnitude (M_W = m) and site-to-source distances (R) as indicated in Section 13.18.3.2. The volumetric strain correction factor, C_{VN}, for Moderate Plasticity Soil is computed using the following equation.

$$C_{VN} = \mathbf{0.34}\ln(N) + \mathbf{0.0793} \qquad \text{Equation 13-126}$$

High PlasticitySoils: A volumetric strain model for High Plasticity Soil (21 ≤ PI ≤ 27, LL=47) was proposed by Stewart et al. (2004) with Relative Compaction (RC) based on the Modified Proctor of RC= 87% with corresponding degree of saturation, S = 60%, 90%, and RC= 92% any saturation, was developed as are shown in Figure 13-53. It was observed that volumetric strain showed dependency on saturation at low RC = 87% and relatively no dependency on saturation high at RC =92%. These soils resulted in volumetric strains that were about half of the Moderate Plastic soils. For soils with PIs greater than 27, no volumetric strain is anticipated.

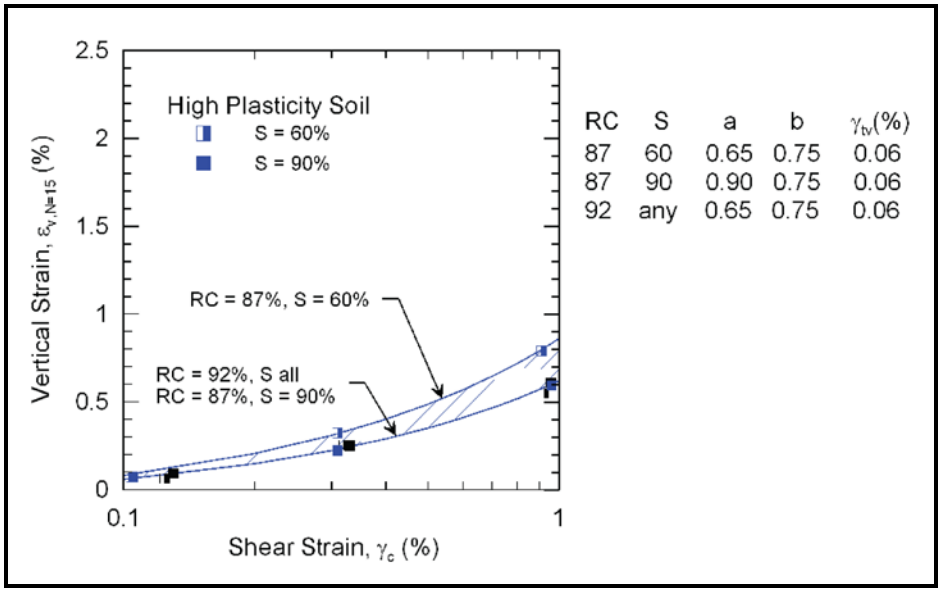

Figure 13-57, Volumetric Strain Model – High Plasticity Soil (Stewart et al., 2004)

The volumetric strain model for High Plasticity Soils proposed by Stewart et al. (2004) can be computed by the following equations. Note that these correlations are applicable to cyclic strains less than 1.0 percent (γ_c < 1.0%).

$$\gamma_c > \gamma_{tv} : \quad \varepsilon_{v,N=15} = a(\gamma_c - \gamma_{tv})^b \qquad \text{Equation 13-127}$$

$$\gamma_c < \gamma_{tv} : \quad \varepsilon_{v,N=15} = 0 \qquad \text{Equation 13-128}$$

Where,

$\varepsilon_{v,N=15}$ = Volumetric strain of unsaturated soils in units of percentage (%)
$\gamma = \gamma_c$ = Cyclic strain in units of percentage (%) (Equation 13-104)
γ_{tv} = Thresholds shear strain in units of percentage (%) – See Table 13-17
a = Coefficient – See Table 13-17
b = Coefficient – See Table 13-17

Table 13-17, Volumetric Strain High Plasticity Soil Model Coefficients

RC (%)	S (%)	a	b	γ_{tv} (%)
87	60	0.65	0.75	0.06
87	90	0.90	0.75	0.06
92	Any	0.65	0.75	0.06

The volumetric strain correction factor, C_{VN}, adjusts the volumetric strain for N=15 cycles, $\varepsilon_{v,N=15}$, obtained from the volumetric soil model to the equivalent number of uniform strain cycles (N) of the design earthquake (FEE or SEE) being evaluated. The equivalent number of uniform strain cycles (N) is computed using the moment magnitude (M_W = m) and site-to-source distances (R) as indicated in Section 13.18.3.2. The volumetric strain correction factor, C_{VN}, for High Plasticity Soil is computed using the following equation.

$$C_{VN} = 0.25\ln(N) + 0.3230 \qquad \text{Equation 13-129}$$

13.18.4 Saturated Sand Settlement

Settlement of saturated sands occurs when Sand-Like soils have the potential to experience cyclic liquefaction due to dissipation of excess pore water pressure generated during the earthquake shaking. These soils experience a reconsolidation as the pore water pressure dissipates and the sand particles rearrange into a more compact state causing settlement of these soil layers. Seismic induced settlements of Sand-Like soils that have the potential to experience cyclic liquefaction are typically larger than compaction settlements that result from unsaturated sands. Several methods to evaluate the magnitude of seismic settlement of saturated sands have been proposed by Tokimatsu and Seed (1987), Ishihara and Yoshimine (1992), Shamoto et al. (1998), and Wu et al. (2003). These methods all use the reconsolidation volumetric strain due to cyclic liquefaction (ε_v). The total settlement, S_{sat}, of Sand-Like Soils with the potential to experience cyclic liquefaction is computed using the following equation.

$$S_{sat} = \sum_{n=1}^{n=i_{sat}} \delta_{sat} = \sum_{n=1}^{n=i_{sat}} \varepsilon_v \cdot H_{sat} \qquad \text{Equation 13-130}$$

Where,

δ_{sat} = Post-Liquefaction Settlement of Saturated Sand layer in units of inches

ε_v = Reconsolidation Volumetric Strain due to Liquefaction in units of percentage (%)

H_{sat} = Layer Thickness of Saturated Sand layer in units of inches

i_{sat} = Total number (n) of Potentially Liquefiable sand layers

The most referenced method used to compute the settlement potential of saturated liquefiable clean sands was proposed by Tokimatsu and Seed (1987). Several other relationships (Ishihara and Yoshimine, 1992; Shamoto et al, 1998 and Wu et al., 2002) have been proposed that address some of the deficiencies found with Tokimatsu and Seed, (1987) with respect to soils that have higher fines content. Idriss and Boulanger (2008) compared these three alternate methods as shown in Figure 13-54.

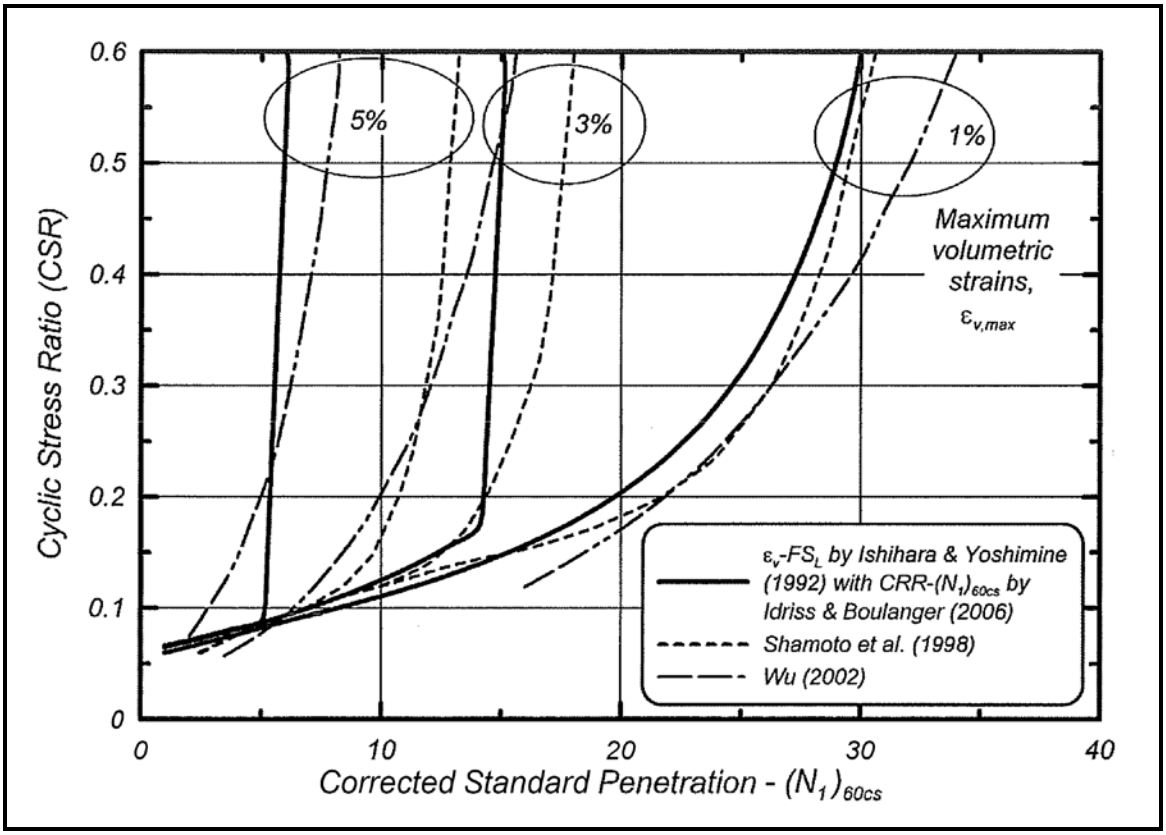

Figure 13-58, Volumetric Strain Relationship Comparison - M_w=7.5; σ'_{vc} = 1 atm (Idriss and Boulanger, 2008)

The settlement of saturated sands that are potentially liquefiable will be computed based on Idriss and Boulanger (2008) recommended reconsolidation volumetric strain, ε_v, relationship based on Ishihara and Yoshimine (1992) shown in Figure 13-55. Reconsolidation volumetric strain, ε_v, relationships for SPT and CPT results in Figure 13-55 have been developed to be compatible by using the correlations for relative density from SPT and CPT in Section 13.11.1.1. The CSR^*_{eq}, is computed based on Section 13.10. The normalized SPT driving resistance, $N^*_{1,60,cs}$, is computed based on Section 13.11.2. The normalized corrected CPT tip resistance, $q_{c,1,N,CS}$, is computed based on Section 13.11.3.

The use of reconsolidation volumetric strain, ε_v, relationship based on Shamoto et al. (1998), or Wu et al. (20032) will require approval from the PCS/GDS. If CPT testing data is used with these relationships, the correlations for relative density from SPT and CPT in Section 13.11.1.1 shall be used in order to maintain compatibility between testing methods.

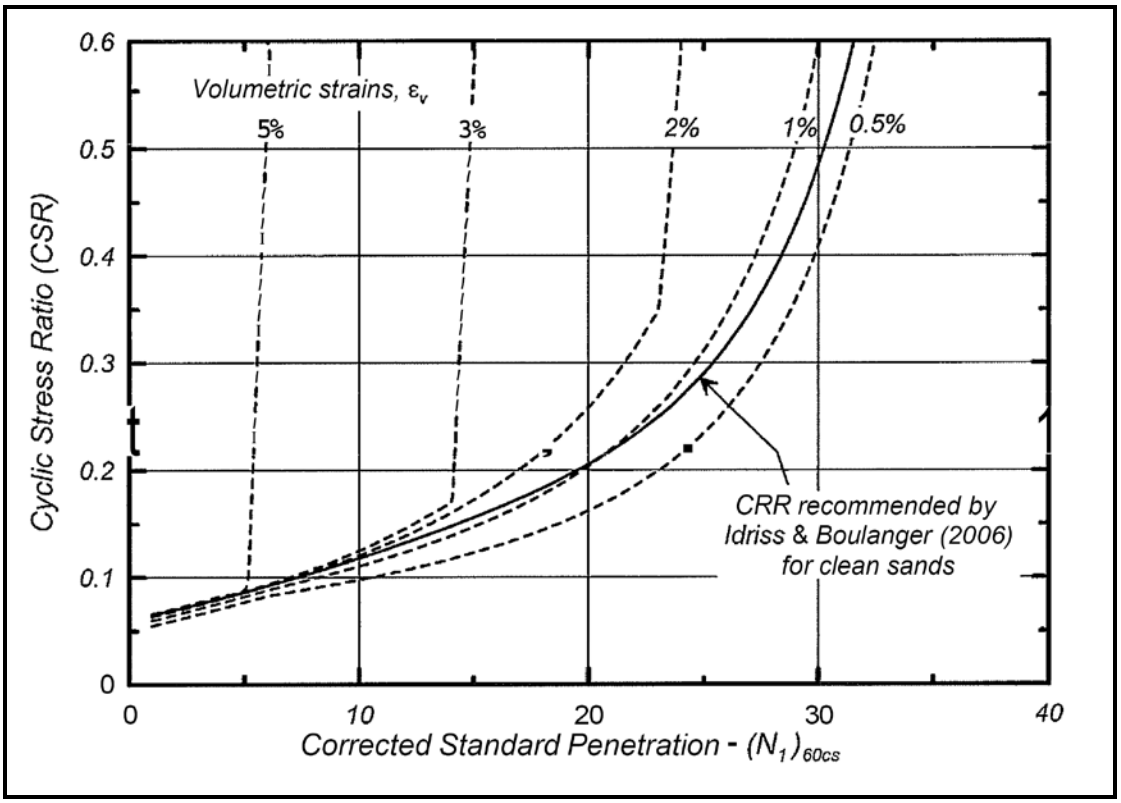

(A) SPT Based Correlation ($N^{*}_{1,60,cs}$)

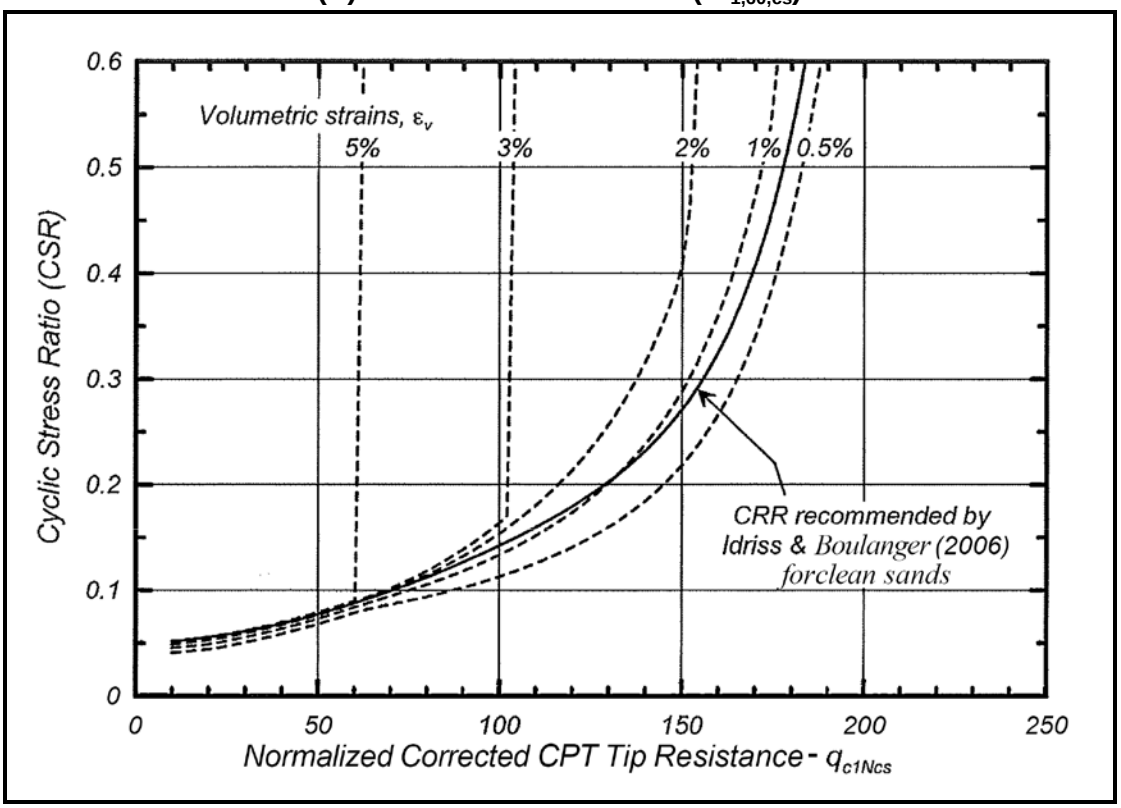

(B) CPT Based Correlation ($q_{c,1,N,cs}$)

Figure 13-59, Volumetric Strain Relationship - M_w=7.5; σ'_{vc} = 1 atm (Ishihara and Yoshimine, 1992; modified by Idriss and Boulanger, 2008)

When soils are stratified and potentially cyclic liquefiable layers are located between non-liquefiable soil layers, there is a possibility of under-predicting or over-predicting excess pore water developed depending on the location of the soil layers within the stratified system (Polito and Martin, 2001). Polito and Martin (2001) have shown that thin layers of dense sand (non-liquefiable soil) could liquefy if sandwiched between liquefiable soil layers. Ishihara (1985) proposed the method shown in Figure 13-56 to determine the thickness, H_2, of the liquefiable soil layer. H_1 is the thickness of the non-liquefiable soil layer above the liquefiable soil layer, H_2. The thickness of the liquefiable soil layer, H_2, is dependent on criteria indicated in Figure 13-56. In addition to the criteria indicated in Figure 13-56, the following criteria must also be satisfied:

1. Thickness of the non-liquefiable layer (H_b) is less than or equal to 5 feet ($H_b \leq 5$ feet).

2. Non-liquefiable soil layer "B" has a normalized and corrected SPT $N^*_{1,60,cs} < 30$ blows/foot or a normalized corrected CPT tip resistance $q_{1,c,N,cs} < 170$.

3. Non-liquefiable soil layer "B" is a sand or silty sand with fines content, $FC \leq 35$.

4. Moment magnitude of design earthquake, $M_w \geq 7.0$.

This procedure to evaluate thickness, H_2, of liquefiable soil layers is used for all subsequent soil layers that have the potential to liquefy in the stratified soil system.

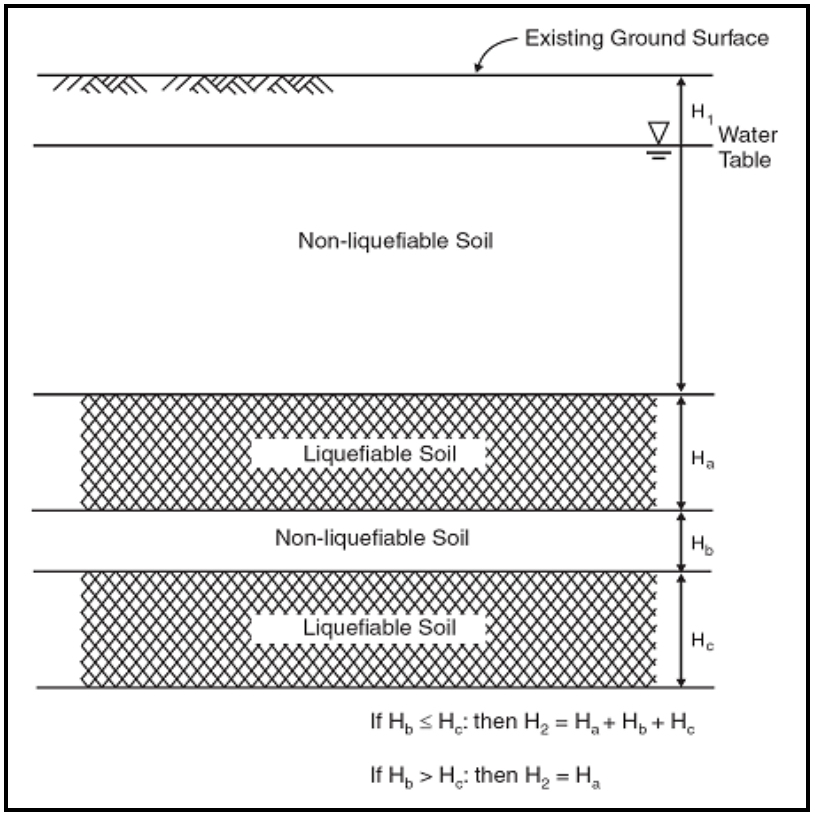

Figure 13-60, Liquefiable Soil Layer Thickness in Stratified Soils (Ishihara, 1985)

13.19 REFERENCES

The geotechnical design specifications contained in this Manual must be used in conjunction with the *AASHTO* LRFD Bridge Design Specifications (latest edition). The SCDOT Seismic Design Specifications for Highway Bridges will take precedence over AASHTO Seismic Guidelines.

Andrus, R. D., Hayati, H., and Mohanan, N. P. (2009). “Correcting Liquefaction Resistance for Aged Sands Using Measured to Estimated Velocity Ratio.” Journal of Geotechnical and Geoenvironmental Engineering, ASCE, v. 135, Issue 6.

Bardet, J.P., Mace, N. and Tobita, T. (1999). "Liquefaction-induced Ground Deformation and Failure." Report to PEER/PG&E, Task 4A - Phase 1, University of Southern California, Los Angeles.

Bartlett, S.F. and Youd, T.L., (1992). "Empirical Analysis of Horizontal Ground Displacement Generated by Liquefaction Induced Lateral Spreads.” Technical Report NCEER 92-0021, National Center for Earthquake Engineering Research, University at Buffalo.

Bartlett, S.F. and Youd, T.L., (1995). "Empirical Prediction of Liquefaction-induced Lateral Spread.” Journal of Geotechnical Engineering, ASCE, v. 121, Issue 4.

Boulanger, R. W. (2003a). "High Overburden Stress Effects in Liquefaction Analyses." Journal of Geotechnical and Geoenvironmental Engineering, ASCE, v. 129, Issue 12.

Boulanger, R. W. (2003b). "Relating Ka to a Relative State Parameter Index." Journal of Geotechnical and Geoenvironmental Engineering, ASCE, v. 129, Issue 8.

Boulanger, R. W., and Idriss, I. M. (2004a). “Evaluating the Potential for Liquefaction or Cyclic Failure of Silts and Clays.” Report UCD/CGM-04/01, Center for Geotechnical Modeling, University of California, Davis, CA.

Boulanger, R. W., and Idriss, I. M. (2004b). "State Normalization of Penetration Resistances and the Effect of Overburden Stress on Liquefaction Resistance." Proc., 11th International Conference on Soil Dynamics and Earthquake Engineering, and 3rd International Conference on Earthquake Geotechnical Engineering, D. Doolin et al., eds., Stallion Press, Vol. 2.

Boulanger, R. W., and Idriss, I. M. (2006). "Liquefaction Susceptibility Criteria for Silts and Clays." Journal of Geotechnical and Geoenvironmental Engineering, ASCE, v. 132, Issue 11.

Boulanger, R. W., and Idriss, I. M. (2007). "Evaluation of Cyclic Softening in Silts and Clays." Journal of Geotechnical and Geoenvironmental Engineering, ASCE, v. 133, Issue 6.

Bray, J.D., and Sancio R.B. (2006). "Assessment of the Liquefaction Susceptibility of Fine-Grained Soils." Journal of Geotechnical and Geoenvironmental Engineering, v. 132, Issue 9.

Cetin, K. O., Seed, R. B., Der Kiureghian, A., Tokimatsu, K., Harder, L. F. Jr, Kayen, R. E., and Moss, R. E. S. (2004). “Standard Penetration Test-Based Probabilistic and Deterministic

Assessment of Seismic Soil Liquefaction Potential." Journal of Geotechnical and Geoenvironmental Engineering, ASCE, v. 130, Issue 12.

Darendeli M. B. and Stokoe, K. H. (2001). "Development of a New Family of Normalized Modulus Reduction and Material Damping Curves." Geotechnical Engineering Report GDOI-I, University of Texas, Department of Civil Engineering. Geoenvironmental Engineering, ASCE, v. 131, Issue 8.

Duncan, J.M., and Wright, S.G., (2005), "Soil Strength and Slope Stability." John Wiley & Sons, Inc., Hoboken, New Jersey.

Ebeling, R. M., Chase, A., White, B. C., (2007). "Translational Response of Toe-Restrained Retaining Walls to Earthquake Ground Motions Using $C_{orps}W_{all}$Slip (CWSLIP)." Technical Report ERDC/ITL TR-07-01. Vicksburg, Mississippi: Corps of Engineers Waterways Experiment Station, June 2007.

Fear, C. E., and Robertson, P. K. (1995). ''Estimating the undrained strength of sand: A theoretical framework.'' Can. Geotech. J., 32(4), 859–870.

Golesorkhi, R. (1989). "Factors Influencing the Computational Determination of Earthquake-Induced Shear Stresses in Sandy Soils." Ph. D. Thesis, University of California, Berkeley.

Goodman, R.E., and Seed, H.B. (1966). "Earthquake–induced Displacements in Sand Embankments." Journal of the Soil Mechanics and Foundations Division, ASCE, v. 92, Issue 2.

Goulois, A. M., Whitman, R. V. and Hoeg,K., (1985). "Effects of Sustained Shear Stresses on the Cyclic Degradation of Clay," Strength Testing of Marine Sediments: Laboratory and In-Situ Strength Measurements, ASTM STP 883, R. C. Chaney and K. R. Demars, eds., ASTM, Philadelphia, pp. 336-351, 1985.

Harder, L. F., and Boulanger, R. W. (1997). "Application of K-alpha and K-sigma Correction Factors." Proceedings of the NCEER.

Hayati, H. and Andrus, R. D., (2008). "Liquefaction Potential Map of Charleston, South Carolina Based on the 1886 Earthquake." Journal of Geotechnical and Geoenvironmental Engineering, ASCE, v. 134, Issue 6.

Holtz, R. D., and Kovacs, W.D., (1981), "An Introduction to Geotechnical Engineering." Prentice-Hall, Inc., Englewood Cliffs, New Jersey.

Houston, S. L., Houston, W. N., and Padilla, J. M. (1987). ''Microcomputer-aided Evaluation of Earthquake-induced Permanent Slope Deformations.'' Microcomputers in Civil Engineering.

Hynes, M.E. and Franklin, A.G., (1984). "Rationalizing the Seismic Coefficient Method." Miscellaneous Paper GL-84-13, *U.S. Army Waterways Experiment Stations*, Vicksburg, MS, July,.

Idriss, I. M. (1999). “An Update to the Seed-Idriss Simplified Procedure for Evaluating Liquefaction Potential.” Proceedings, TRB Workshop on New Approaches to Liquefaction, Publication No. FHWA-RD-99-165, FHWA, U.S. Department of Transportation.

Idriss, I. M. and Boulanger, R. W. (2004). “Semi-empirical Procedures for Evaluating Liquefaction Potential During Earthquakes.” Proceedings, 11th International Conference on Soil Dynamics and Earthquake Engineering and 3rd International Conference on Earthquake Geotechnical Engineering, D. Doolin et. al., eds., Stallion Press, Vol. 1.

Idriss, I.M. and Boulanger, R.W., (2008) “Soil Liquefaction During Earthquakes.” Earthquake Engineering Research Institute (EERI), EERI Monograph MNO-12.

Ishihara, K., (1985). “Stability of Natural Deposits During Earthquakes.” Proceedings, 11th International Conference on Soil Mechanics and Foundation Engineering, San Francisco, CA, Volume 1,.

Ishihara, K. and Yoshimine, M. (1992). “Evaluation of Settlements in Sand Deposits Following Liquefaction During Earthquakes.” Soils and Foundations, 32 (1).

Iwasaki, I., Tatsuoka, F., and Takagi, Y. (1978). “Shear Modulus of Sands Under Cyclic Torsional Shear Loading.” Soils and Foundations, 18 (1).

Jibson, R., (1994). "Predicting Earthquake-induced Landslide Displacement Using Newmark's Sliding Block Analysis." Transportation Research Record 1411, Transportation Research Board, Washington, D.C.

Kramer, S.L. (1996). *Geotechnical Earthquake Engineering*, Prentice-Hall, Upper Saddle River, NJ

Kramer, S.L. and Elgamal, A.-W. (2001). “Modeling Soil Liquefaction Hazards for Performance-Based Earthquake Engineering.” State-of-the-Art Report, Pacific Earthquake Engineering Research Center, in preparation.

Ladd, C., and Foott. R. ,(1974). "New Design Procedure for Stability of Soft Clays." Journal of the Geotechnical Engineering Division, (July 1974): 763-786.

Ladd, C. C., Foot, R., Ishihara, K., Schlosser, F., and Poulos, H. G. (1977). “Stress Deformation and Strength Characteristics.” Proc., 9th Int. Conf. on Soil Mech. and Found. Engrg., Vol. 2, Tokyo, Japan.

Leon, E., Gassman, S. L., and Talwani, P., (2006). "Accounting for Soil Aging When Assessing Liquefaction Potential.” Journal of Geotechnical and Geoenvironmental Engineering, ASCE, v. 132, Issue 3.

Lewis, M. R., Arango, I., and McHood, M. D., (2007). ‘‘Geotechnical Engineering at the Savannah River Site and Bechtel.’’ Report No. WSRC-STI-2007-00373, Contract No. DE-AC09--96SR18500, U. S. Department of Energy, July 17, 2007.

Liu A. H., Stewart J. P., Abrahamson N. A. and Moriwaki, Y. (2001). "Equivalent Number of Uniform Stress Cycles for Soil Liquefaction Analysis." Journal of Geotechnical and Geoenvironmental Engineering, ASCE, v. 127, Issue 121.

Makdisi, F. T., and H. B. Seed. 1978. “Simplified Procedure for Estimating Dam and Embankment Earthquake-Induced Deformations.” Journal of Geotechnical Engineering, ASCE, v. 104, Issue 7.

Marcuson, W. F. III, Hynes, M. E., and Franklin, A. G. (1990). “Evaluation and Use of Residual Strength in Seismic Safety Analysis of Embankments.” Earthquake Spectra, Vol 6, No. 3.

Matasovic, N., Kavazanjian, E., and Giroud, J. P. (1998). “Newmark Seismic Deformation Analysis for Geosynthetic Covers.” Geosynthetics International, International Geosynthetics Society.

McGee W. J. , Sloan E., Manigault, G. E., Newcomb, S., Peters, K. E., and Herrmann, R. B. eds., (1986). "First-hand Observations of the Charleston Earthquake of August 31, 1886, and Other Earthquake Materials." Reports of Bulletin 41, South Carolina Geological Survey.

Newmark, N.M. (1965). ”Effects of Earthquakes on Dams and Embankments.” *Geotechnique*, London, England v.5, no.2.

NCHRP 12-70 (2007), “Seismic Analysis and Design of Retaining Walls, Buried Structures, Slopes, and Embankments.” NCHRP, CH2M HILL, November 2007.

Olson, S. M., and Stark, T. D., (2002), “Liquefied Strength Ratio from Liquefaction Flow Failure Case Histories.” Canadian Geotechnical Journal, 39.

Olson, S. M., and Stark, T. D., (2003), “Yield Strength Ratio and Liquefaction Analysis of Slopes and Embankments,” Journal of Geotechnical and Geoenvironmental Engineering, ASCE v. 129, Issue 8.

Polito, C.P., and Martin, J.R. (2001). "Effects of Nonplastic Fines on the Liquefaction Resistance of Sands." Journal of Geotechnical and Geoenvironmental Engineering, ASCE, v. 127, Issue 51.

Pyke, R., Seed, H.B., Chan, C.K. (1975). "Settlement of Sands Under Multi-directional Shearing." Journal of Geotechnical Engineering, ASCE, v. 101, Issue 41.

Rauch, A. F., and Martin, J. R., Jr. (2000). “EPOLLS Model for Predicting Average Displacements on Lateral Spreads.” *Journal of Geotechnical and Geoenvironmental Engineering*, ASCE, v. 126, Issue 4.

Richards, R. and Elms, D. G., (1979). “Seismic Behavior of Gravity Retaining Walls.” Journal of Geotechnical Engineering., ASCE, v.105, Issue 4.

Robertson, P.K., and Wride, C.E. (1997) “Cyclic Liquefaction and its Evaluation Based on SPT and CPT.” Proceedings NCEER Workshop on Evaluation of Liquefaction Resistance of Soils.

Schneider, J.A., and Mayne, P.W. (1999). “Soil Liquefaction Response in Mid-America Evaluated by Seismic Piezocone Tests.” Report MAE-GT-3A, Mid America Earthquake Center, October, 253 pp.

Seed, H. B. (1979). ‘‘Soil Liquefaction and Cyclic Mobility Evaluation for Level Ground During Earthquakes.’’ Journal of Geotechnical Engineering, ASCE, v. 105 Issue 2.

Seed, H. B. (1986). ‘‘Design Problems in Soil Liquefaction.’’ University of California, Earthquake Engineering Research Center (UCB/EERC), UBC/EERC-86/02, February.

Seed, H. B. (1987)., “Design Problems in Soil Liquefaction.” Journal of Geotechnical Engineering., ASCE, v.113, Issue 8.

Seed, R.B., Cetin, K.O., Moss, R.E.S., Kammerer, A., Wu, J., Pestana, J. and Riemer, M., Sancio, R.B., Bray, J.D., Kayen, R.E., and Faris, A. (2003). "Recent Advances in Soil Liquefaction Engineering: A Unified and Consistent Framework.” EERC-2003–06, Earthquake Engineering Research Institute, Berkeley, Calif.

Seed, R.B. and Harder, L.F., Jr., (1990). “SPT-Based Analysis of Cyclic Pore Pressure Generation and Undrained Residual Strength.” Proceedings, H. Bolton Seed Memorial Symposium, BiTech Publishers, Ltd.

Seed, H.B., and Idriss, I.M., (1971), “Simplified Procedure or Evaluating Soil Liquefaction Potential.” Journal of the Soil Mechanics and Foundations Division, ASCE, v. 97, Number SM9.

Seed, H. B., Idriss, I. M., Makdisi, F., and Banerjee, N. (1975). “Representation of Irregular Stress Time Histories by Equivalent Uniform Stress Series in Liquefaction Analysis.” Report No. EERC 75-29, Earthquake Engineering Research Center, University of California, Berkeley.

Shamoto, Y., Zhang, J., and Tokimatsu, K. (1998). “New charts for predicting large residual post-liquefaction ground deformations.” *Soil dynamics and earthquake engineering*, Vol. 17, Elsevier, New York.

Spencer, E. (1967). "A Method of Analysis of the Stability of Embankments Assuming Parallel Inter-Slice Forces." Geotechnique, Great Britain, Vol. 17, No. 1, March,.

Stewart, J.P., Whang, D.H., Moyneur, M., and Duku, P. (2004). “Seismic Compaction of As-Compacted Fill Soils With Variable Levels of Fines Content and Fines Plasticity.” Department of Civil and Environmental Engineering, University of California, Los Angeles, Consortium of Universities for Research in Earthquake Engineering (CUREE), CUREE Publication No. EDA-05, July 2004.

Talwani, P., and Schaeffer, W. T. (2001). “Recurrence rates of large earthquakes in the South Carolina Coastal Plain based on paleoliquefaction data.” Journal of Geophyiscal Research, 106(B4), 6621–6642.

Terzaghi, K., Peck, R.B., and Mesri, G., (1996), "Soil Mechanics in Engineering Practice." John Wiley & Sons, Inc., 605 Third Avenue, New York, NY.

Tokimatsu, K., and H. B. Seed. 1987. "Evaluation of Settlements in Sands Due to Earthquake Shaking." Journal of Geotechnical Engineering, ASCE, v. 113 Issue 8.

U.S. Geological Survey, http://earthquake.usgs.gov/regional/qfaults/eusa/char.php.

U.S. Geological Survey, http://earthquake.usgs.gov/resources/software/slope_prep.php.

Vucetic, M. and Dobry, R. (1991). "Effect of Soil Plasticity on Cyclic Response." Journal of Geotechnical Engineering, ASCE, Vol. 117, No. 1.

Weems, R. E., Lemon, E. M., Jr., and Chirico, P. (1997). "Digital Geology and Topography of the Charleston Quadrangle, Charleston and Berkeley Counties, South Carolina." USGS Open-File Report Number 97-531, U.S. Geological Survey, Reston, Va.

Willoughby, R. H., Nystrom, P. J., Campbell, L. D., Katuna, M. P. (1999). "Cenozoic Stratigraphic Column of the Coastal Plain of South Carolina." South Carolina Department of Natural Resources, Geological Survey, Columbia, SC

Wu, J. (2002). "Liquefaction triggering and Post-liquefaction Deformations of Monterey 0/30 Sand Under Uni-directional Cyclic Simple Shear Loading." Ph.D. thesis, University of California, Berkeley.

Wu, J., Seed, R.B., and Pestana, J.M. (2003). "Liquefaction Triggering and Post Liquefaction Deformations of Monterey 0/30 Sand Under Unidirectional Cyclic Simple Shear Loading." Geotechnical Engineering Repost No. UCB/GE-2003/01, April 2003, University of California, Berkeley, CA.

Yegian, M.K. Marciano, E., and Ghahraman, V.G. (1991). "Earthquake-induced permanent deformations: probabilistic approach." Journal of Geotechnical Engineering, ASCE, Vol. 117, No. 1.

Youd, T. L., and Carter, B.L., (2005). "Influence of Soil Softening and Liquefaction on Spectral Acceleration." Journal of Geotechnical and Geoenvironmental Engineering Division, ASCE, v. 131, Issue 7.

Youd, T.L., Hansen, C.M., and Bartlett, S.F., (2002). "Revised Multilinear Repression Equations for Prediction of Lateral Spread Displacement." Journal of Geotechnical and Geoenvironmental Engineering, ASCE, v. 128, Issue 12.

Youd, T. L., and Idriss, I. M., eds. (1997). Technical Report NCEER-97-0022 Proceedings, *NCEER Workshop on Evaluation of Liquefaction Resistance of Soils*, National Center for Earthquake Engineering Research, State Univ. of New York at Buffalo.

Youd, T.L., Idriss, I.M., Andrus, R.D., Arango, I., Castro, G., Christian, J.T., Dobry, R., Finn, W., D.L. Harder, L.F., Jr., Hynes, M.E., Ishihara, K., Koester, J.P., Liao, S.S.C., Marcuson, W. F., III, Martin, G.R. Mitchell, J.K., Moriwaki, Y., Power, M.S., Robertson, P.K., Seed, R.B., and Stokoe,

K.H., II, (2001). “Liquefaction resistance of soils: Summary Report from the 1996 NCEER and 1998 NCEER/NSF Workshops on Evaluation of Liquefaction Resistance of Soils.” Journal of Geotechnical and Geoenvironmental Engineering, ASCE, v. 127, Issue 10.

Youd, T.L. and Perkins, D.M., (1978). “Mapping of Liquefaction-Induced Ground Failure Potential.” Journal of the Geotechnical Engineering Division, ASCE, v. 104, Issue 4.

Zhang, G., Roberson, P. K., and Brachman, R. W. I. (2004). ‘‘Estimating Liquefaction-Induced Lateral Displacements Using the Standard Penetration Test or Cone Penetration Test.’’ Journal of Geotechnical and Geoenvironmental Engineering, ASCE, v. 130, Issue 8.